

Interval-censored Hawkes processes

Marian-Andrei RizoIU

University of Technology Sydney

Ultimo NSW 2007, Australia

Alexander Soen

The Australian National University

Canberra ACT 2601, Australia

Shidi Li

The Australian National University

Canberra ACT 2601, Australia

Leanne J. Dong

Concordia University

Montréal, Canada

Aditya Krishna Menon

Google Research

Lexing Xie

The Australian National University

Canberra ACT 2601, Australia

MARIAN-ANDREI.RIZOIU@UTS.EDU.AU

ALEXANDER.SOEN@ANU.EDU.AU

SHIDI.LI@ANU.EDU.AU

LEANNE.DONG@CONCORDIA.CA

ADITYAKMENON@GOOGLE.COM

LEXING.XIE@ANU.EDU.AU

Editor:

Abstract

Hawkes processes are a popular means of modeling the event times of self-exciting phenomena, such as earthquake strikes or tweets on a topical subject. Classically, these models are fit to historical event time data via likelihood maximization. However, in many scenarios, the exact times of historical events are not recorded for either privacy (e.g., patient admittance to hospitals) or technical limitations (e.g., most transport data records the volume of vehicles passing loop detectors but not the individual times). The *interval-censored* setting denotes when only the aggregate *counts* of events at specific time intervals are observed. Fitting the parameters of *interval-censored* Hawkes processes requires designing new training objectives that do not rely on the exact event times.

In this paper, we propose a model to estimate the parameters of a Hawkes process in interval-censored settings. Our model builds upon the existing Hawkes Intensity Process (HIP) of RizoIU et al. (2017b) in several important directions. First, we observe that while HIP is formulated in terms of expected intensities, it is more natural to work instead with expected *counts*; further, one can express the latter as the solution to an integral equation closely related to the defining equation of HIP. Second, we show how a non-homogeneous Poisson approximation to the Hawkes process admits a tractable likelihood in the interval-censored setting; this approximation recovers the original HIP objective as a special case, and allows for the use of a broader class of Bregman divergences as loss function. Third, we explicate how to compute a tighter approximation to the ground truth in the likelihood. Finally, we show how our model can incorporate information about varying interval lengths. Experiments on synthetic and real-world data confirm our HIPPer model outperforms HIP and several other baselines on the task of interval-censored inference.

Keywords: Hawkes process, Interval-censored

1. HIP and beyond: interval-censored Hawkes processes

Temporal point processes model the times at which events of interest occur, such as tweets on a topic or the impact times of an earthquake (Cox and Isham, 1980; Daley and Vere-Jones, 2003). The *Hawkes process* (Hawkes, 1971; Laub et al., 2015) is a point process which can model *self-excitation*, wherein the occurrence of one event increases the likelihood of further events. The ubiquity of this phenomenon has seen the process applied in fields ranging from seismology (Ogata, 1988), finance (Bowsher, 2007; Hardiman et al., 2013), and social media (Crane and Sornette, 2008; Zhou et al., 2013; RizoIU et al., 2017b).

Given a dataset of historical event times, e.g., tweets about a topic for the past month, the standard way to fit a Hawkes process is to maximize its log-likelihood (Ozaki, 1979). However, in many scenarios one does not know the exact historical event times, but rather only the counts of the *number* of events in specific time intervals. This can be due to data availability — say, for epidemics when the exact infection time of each individual is unknown, and the observed data is the number of hospital admissions per day — or due to data privacy — e.g., YouTube does not expose individual viewing sessions for its online videos, but it shows the number of views per day for each video. This *interval-censored* learning requires designing new training objectives that do not rely on exact event times.

Recently, RizoIU et al. (2017b) proposed the *Hawkes Intensity Process (HIP)* to tackle this problem. The HIP objective is to minimize the squared error of the observed counts to the theoretical *expected intensity* of the process. The key insight is that this expected intensity can be expressed as the solution to a particular integral equation, which may be approximately solved by exploiting again the observed counts. Despite its empirical success, the HIP model has several conceptual limitations. First, there is a mismatch between the objective and the observed data; the observations are of event *counts*, while the objective measures closeness to the event *rates*. Second, the HIP objective is not derived as the likelihood of a particular process, raising uncertainty as to precisely what sense it approximates the Hawkes likelihood. Last, the HIP training relies on an approximation to the underlying integral equation, which is of unclear quality, and cannot handle intervals of unequal length.

In this paper, we introduce a new point process — the Mean Behavior Poisson (MBP) — and a set of tools that allow fitting Hawkes processes observed in either point process or discrete time (i.e. interval-censored). The MBP is a non-homogeneous Poisson process, with a deterministic intensity function equal to the *expectation* of a Hawkes process intensity, taken over all possible process realizations. There is a one-to-one parameter equivalence between MBP and the Hawkes process. We propose the interval-censored log-likelihood (IC-LL) for MBP, which allows one to fit the process on interval-censored data — i.e. on discrete time intervals. We show that MBP allows one to retrieve the Hawkes model parameters for interval-censored scenarios, as well as for event time data. Fig. 1 illustrates the relation between Hawkes and MBP. When the process is observed as event times, both Hawkes and MBP can successfully fit the model — despite MBP using a deterministic intensity function (shown as a red line in Fig. 1) — using a *point process likelihood* (PP-LL). When the same

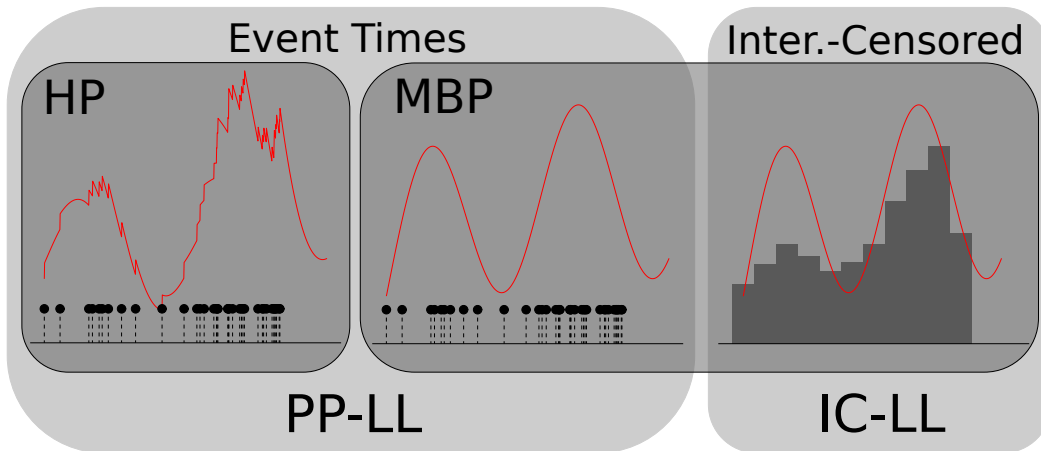


Figure 1: Illustration of the applicability of the Hawkes process and MBP process in event time and interval censored settings. The Hawkes process is only applicable when the data given is in event time format, which can then be fitted using the standard point process log-likelihood (PP-LL). On the other hand, the MBP process can be used in both the event time and interval-censored data settings by switching between PP-LL and the proposed interval-censored log-likelihood (IC-LL).

realization is observed interval-censored, only MBP can be used to retrieve the original parameters using the *interval-censored likelihood* (IC-LL).

We also study scenarios in which the exogenous events are observed directly – either as event times or interval-censored – rather than having their arrival governed by a given exogenous intensity functions. This is often the case in real-world applications, such as our popularity prediction exercise in Section 8 where the shares and tweets driving the views of YouTube videos are observed separate from the views process. With respect to prior literature, we address the shortcomings of the interval-censored model HIP (Rizoiu et al., 2017b) and we show for the first time – as far as we are aware – the link between continuous and discrete time for Hawkes processes.

The main contributions of this work are as follows:

- C1:** we prove that the expected *counts* of the Hawkes process satisfy a nearly identical self-consistent equation to the intensity, and we introduce a new method to solve the equation which first computes the impulse response of the system, and afterwards the solution using summations of infinite convolutions.
- C2:** we show how to construct a non-homogeneous Mean Behavior Poisson (MBP) process that approximates the mean behavior of the underlying Hawkes process (Section 3); the likelihood of this process allows the use of a broader class of Bregman divergence based loss functions.
- C3:** we introduce a set of tools (exogenous functions, loss functions) that allow MBP to fit the parameters of a Hawkes process that generated synthetic data, when either the exogenous or the endogenous events (or both) are presented as interval-censored.

Table 1: Notation used in this paper. Throughout this paper, we denote observed quantities using sans-serif font face.

Symbol	Meaning	Defined/Introduced
$\lambda(t)$	Hawkes Process Intensity	Eq. (3)
$\xi(t)$	Mean Behaviour Poisson Intensity	Eqs. (6) and (9)
$\Lambda(t)$	Hawkes Process Compensator	Eq. (2)
$\Xi(t)$	Mean Behaviour Poisson Compensator	Eq. (10)
$N(t)$	Hawkes Counting Process	Eq. (1)
$M(t)$	Mean Behavior Poisson Counting Process	Eq. (17)
$C(x, y]$	Observed counts in interval $(x, y]$	Eqs. (8) and (16)
$S(x, y]$	Observed immigrant counts in interval $(x, y]$	Eq. (42)
$F(x, y]$	Observed offspring counts in interval $(x, y]$	Eq. (52)
$B_\varphi(x)$	Bregman Divergence	Eq. (27)
$s_{m\delta}(t)$	Multi-impulse exogenous function	Eq. (40)
$s_\bullet(t)$	Latent Homogenous Poisson process exog. func.	Eq. (44)
Ψ_T	Set of immigrant events up to time T	Eq. (51)
Υ_T	Set of offspring events up to time T	Eq. (51)

C4: on a real-world dataset containing information about tweets and Youtube views associated with Youtube videos, we show our approach to outperform HIP (RizoIU et al., 2017b), the current state-of-the art in popularity prediction.

C5: we propose a new approximation to the integral equation, and prove it is strictly tighter than the original HIP approximation; this approximation can also exploit information about interval lengths and be utilised for predicting future event volumes

2. Background and notations

In this section, we provide an overview of the different mathematical objects used in this paper. First, in Section 2.1, we introduce point processes using random measures. Second, in Section 2.2, we introduce the Hawkes self-exciting point process and its parameter estimation. Last, in Section 2.4, we present the Hawkes intensity process — a Hawkes-based interval-censored process and the previous work closest to the present paper.

In this paper, we use the following elementary notations — for more specialized notations concerning point processes please refer to Table 1. We denote $\llbracket p \rrbracket = 1$ if p is true and $\llbracket p \rrbracket = 0$ if p is false. The Laplace transform and inverse Laplace transform are defined as $\mathcal{L}\{\cdot\}$ and $\mathcal{L}^{-1}\{\cdot\}$ respectively. The Dirac delta function $\delta(x)$ is defined by $\int_a^b \delta(x)f(x)dx = f(0)$ if f is continuous and $a < 0 < b$. The convolution of functions f and g is defined as $(f * g)(t) = \int_{-\infty}^{\infty} f(\tau)g(t - \tau) d\tau$.

2.1 Random measures, Point processes and Poisson processes

In this section, we briefly introduce point processes and Poisson processes using the notion of random measures. For a more complete (yet accessible) introduction of point processes

using random measures, we refer to (Grandell, 1977). We opted for this rigorous definition of point processes for completeness reasons. For a more intuitive and streamlined introduction using counting processes and intensity functions, we refer the reader to (Rizoiu et al., 2017a; Laub et al., 2015).

Point processes as random measures. Let (X, \mathcal{B}) be a measurable state space and let $(\Omega, \mathcal{F}, \mathbb{P})$ be a probability space. Let $M = M(X)$ be the space of all σ -finite measures on the sigma algebra \mathcal{B} . Let \mathcal{M} denote the smallest σ -algebra on M with respect to which the function $\mu \mapsto \mu(B)$ is measurable for all $B \in \mathcal{B}$. Let N be the space of all σ -finite counting measures on \mathcal{B} . A *random measure* (Kallenberg, 2017) on X is a random element η in M that is uniformly σ -finite. This means that there are measurable sets $B_n \in X$ $n \in \mathbb{N}$ such that $\eta(B_n) < \infty$ almost surely. A point process is a particular instance of a random measure which takes only integer values. That is, $\mathbb{P}(\eta \notin \mathbb{N}) = 0$. A temporal point process is a random measure on the real line taking value in the non-negative integer or infinity (Brillinger et al., 2002).

More intuitively, the temporal point processes are a family of stochastic processes $(t_n)_{n \in \mathbb{N}_+}$, in which each random variable t_n represents the occurrence time for an event (Klebaner, 2012). Such processes can also be specified as a *counting process* $(N(t))_{t \geq 0}$, where the random variable $N(t)$ represents the number of events that have occurred up to and including time t (Ross, 1995, pg. 59).

The Poisson process. Let Λ be a positive measure such that $\Lambda(A) < \infty$ for every bounded set A . In the literature of martingale treatments of point processes (Jacobsen, 2006), Λ is often denoted as the *compensator* – we also use this term throughout this paper. We assume that, for every collection of disjoint, bounded Borel measurable sets A_1, \dots, A_k , the $N(A_i)$ are independent Poisson random variables with rate $\Lambda(A_i)$. That is,

$$\mathbb{P}(N(A_i) = n_i, i = 1, \dots, k) = \prod_{i=1}^k \frac{\Lambda(A_i)^{n_i}}{n_i!} e^{-\Lambda(A_i)} \quad (1)$$

Next, we use the notion of random measures to define the Poisson process. Suppose that $\Lambda(A) = \lambda l(A)$, where $l(A)$ is the Lebesgue measure of A and $\lambda > 0$ a positive constant. We define *homogeneous Poisson process* $(N(t))_{t \geq 0}$ as

1. $N(0) = 0$ almost surely
2. for any $s < t$, $N(t) - N(s) \sim \text{Poisson}(\lambda(t - s))$
3. for any $s < t \leq s' < t'$, $N(t) - N(s) \perp\!\!\!\perp N(t') - N(s')$.

We say a Poisson process is non-homogeneous when λ is no longer a constant, but a non-negative function. Here, the compensator is redefined as $\Lambda(A) = \int_A \lambda(x) dx$, and the *non-homogeneous Poisson process* (NHPP) is

- (a) $N(0) = 0$ almost surely
- (b) for any $s < t$, $N(t) - N(s) \sim \text{Poisson}(\Lambda(s, t))$
- (c) for any $s < t \leq s' < t'$, $N(t) - N(s) \perp\!\!\!\perp N(t') - N(s')$.

Associated with the counting process are two additional sequences of interest. The first is the sequence of *event histories* $(\mathcal{H}(t))_{t \geq 0}$, where each random variable $\mathcal{H}(t)$ records the times of all events that have occurred up to and including time t . Strictly speaking $\mathcal{H}(t)$ is a filtration, that is, an increasing sequence of σ -algebras (Laub et al., 2015). The second is the sequence of *conditional intensities* $(\lambda(t | \mathcal{H}(t^-)))_{t \geq 0}$ — denoted for simplicity as $\lambda(t)$ —, where each random variable $\lambda(t)$ measures the expected rate of events occurring in an infinitesimal window around the time t . Formally, (Cox and Lewis, 1972, Equation 3.1),

$$\begin{aligned} \lambda(t) &\doteq \lim_{h \rightarrow 0^+} \frac{1}{h} \cdot \mathbb{E} [N(t^- + h) - N(t^-) | \mathcal{H}(t^-)] \\ &= \lim_{h \rightarrow 0} \frac{1}{h} \cdot \mathbb{P} (N(t^- + h) - N(t^-) = 1 | \mathcal{H}(t^-)), \end{aligned}$$

where the second equality holds for *simple* processes wherein multiple events cannot occur at the same time, that is the jump size $N(t) - N(t^-)$ at each time t can be either 0 or 1. Finally, we can generalize the definition of the *compensator* $\Lambda(s, t)$ as the integral of the intensity between two moments of time:

$$\Lambda(s, t) \doteq \int_s^t \lambda(\tau) d\tau, \quad (2)$$

where $0 \leq s < t$. We further shorthand $\Lambda(t) \doteq \Lambda(0, t)$.

Processes with independent increments and Markov processes. The process $\{N_t, t \in \mathbb{R}^+\}$ is said to have the *independent increments* property when, for any $u \leq s \leq t$, the random variables $N_t - N_s$ and N_u are independent. The process $N = (N_t)_{t \geq 0}$ is said to be a *Markov process* with respect to $\mathcal{H}(t)$ if $\mathbb{E}[X_s | \mathcal{H}(t)] = \mathbb{E}[X_s | X_t]$ whenever $s \geq t$. In simple terms, this means that the future of a Markov process is independent of its past. Moreover, if N is a Markov process and conditional stationary, it results that it is a homogeneous Markov process. That is, the transition probability function $\mathbb{P}(N(t+s) \leq y | N(t) = x)$ is independent to t . Processes with independent increments are Markov processes. However, the converse is not true — not every Markov process obeys the property of independent increments. One such example is the Ornstein-Uhlenbeck process (Uhlenbeck and Ornstein, 1930), a Markov process with the “return to mean” property – intuitively, the process is dragged towards zero when it is far away from zero. As a result, the increments are not independent and even negatively correlated. Given the definition in Eq. (1), the Poisson process has the independent increments property and, therefore, is a Markov process.

2.2 Hawkes process

The *Hawkes process* is a temporal point process with the property of *self-excitation*. Intuitively, self-excitation means that the occurrence of one event increases the likelihood of further events in the near future. The process was widely applied in analyzing social media (Kobayashi and Lambiotte, 2016; Cao et al., 2017; Zhang et al., 2019), earthquake aftershocks (Ogata, 1988; Helmstetter and Sornette, 2002a), nuclear physics (Snyder and Miller, 1991), neuronal activity (Apostolopoulou et al., 2019), online advertising (Parmar et al., 2017) and finance (Bacry et al., 2015).

The Hawkes process is a doubly stochastic point process – i.e., the event intensity function is also stochastic and depends upon the previous values of the process itself –

(Hawkes, 1971):

$$\begin{aligned} \lambda(t) &= s(t) + \int_0^{t^-} \phi(t-s) dN(s) \\ &= \underbrace{s(t)}_{\text{exogenous}} + \underbrace{\sum_{t_i < t} \phi(t-t_i)}_{\text{endogenous}}, \end{aligned} \quad (3)$$

where $s(\cdot)$ is the (deterministic) *background intensity* function which controls the arrival of external events into the system — dubbed as *immigrants*; $s(\cdot)$ is also known as the exogenous intensity. $\phi(\cdot)$ is the *kernel* function which controls the arrival of *offspring* — events spawned through self-excitement — by any one given event. The arrival of offspring generated by any previous event is controlled by the second term of Eq. (3), also known as the endogenous intensity. The immigrants and the offspring are collectively denoted as events.

The Hawkes process is said to have an exponential kernel when $\phi(\tau) = \kappa\theta e^{-\theta\tau}$, with κ the *excitation level* and $\theta > 0$ the *decay rate*; similarly, the Hawkes process has a power-law kernel when $\phi(\tau) = \kappa(\tau + c)^{-(1+\theta)}$, with c a time-warping parameter to keep the kernel bounded when τ approaches zero, and κ and θ have similar meanings as for the exponential kernel. Note that λ depends on the history of events that have occurred up to time t , and thus it is conditional on $\mathcal{H}(t)$ when studied prior to the current time t and it is a random variable for times larger than t .

Relation to the Poisson process and processes with independent increments.

The Hawkes process is not a Poisson process but rather a non-Markovian extension of the Poisson process. A Hawkes process can also be viewed as a cluster of Poisson processes, in which each event spawns offspring following a non-homogeneous Poisson process of intensity $\phi(t)$. The link between events and their offspring induces the *branching structure* (see (Rizoïu et al., 2017a) for more details). Because the Hawkes process's intensity function depends on the previous events, it follows that the Hawkes process is not a Markov process and, as a result, does not have the independent increments property (that the Poisson point process has). The number of jumps in a given interval is a function of the number of jumps that happened earlier. We will leverage this result in Section 4 for fitting Hawkes processes in the interval-censored setting.

2.3 Parameter estimation

Given a sequence $\Omega_T \doteq \{t_n \mid t_n \leq T\}$ of observed event times, we try to find the set of parameters θ of a given point process which represent best the sequence. As shown by Daley and Vere-Jones (2003), this amounts to minimizing the negative log-likelihood with respect to θ , which in turn maximizes the probability of events occurrence at the observed times Ω_T :

$$\mathcal{L}(\theta; T) \doteq - \sum_{t_n \in \Omega_T} \log \lambda(t_n; \theta) + \int_0^T \lambda(u; \theta) du. \quad (4)$$

Here T is the maximum time that the sequence is observed, usually $T \doteq \max_n t_n$. As we can see, the log-likelihood requires observing the timing of events, which may not be the case in

real application scenarios in which only volumes of events are observed (see Section 4). We denote the standard negative log-likelihood loss in Eq. (4) as the *point process log-likelihood* (PP-LL) loss function for the remainder of the paper.

2.4 Hawkes intensity process

RizoIU et al. (2017b) proposed the Hawkes intensity process (HIP), a Hawkes-derived process that operates in the interval-censored setting – i.e., the set of observation times $O = \{o_i \mid i = 0, \dots, m, o_i \leq T\}$ partitions the time line into non-overlapping segments and only the number of events in each segment is observed (see Section 4.1 for more details). The HIP fitting objective is

$$\min_{\theta} \sum_{i=1}^m (\mathbf{C}(o_{i-1}, o_i] - \xi(o_i; \theta))^2, \quad (5)$$

where $\mathbf{C}(o_{i-1}, o_i]$ are the observed number of events having occurred in the i^{th} interval $(o_{i-1}, o_i]$ and $\xi(t) \doteq \mathbb{E}[\lambda(t)]$ is the *expected intensity* of the Hawkes process.

The key ingredient of HIP is being able to efficiently compute ξ : Theorem 2.1 of (RizoIU et al., 2017b) provides an integral equation for $\xi(t)$, namely

$$\begin{aligned} \xi(t) &= s(t) + \int_0^t \phi(s) \cdot \xi(t-s) \, ds \\ &= s(t) + \int_0^t \phi(t-s) \cdot \xi(s) \, ds. \end{aligned} \quad (6)$$

For completeness, we include a derivation of this result in Appendix A. To optimize Eq. (5), one must (approximately) solve this integral equation to compute each $\xi(t; \theta)$. When $s(t) = \mu_0 + (\mu_1 - \mu_0) \cdot e^{-\gamma t}$, and ϕ corresponds to the exponential kernel, Dassios and Zhao (2013) showed that

$$\xi(t) = \mu_1 \cdot e^{-(\gamma-\alpha)t} + \frac{\mu_0 \cdot \gamma}{\gamma - \alpha} \cdot (1 - e^{-(\gamma-\alpha)t}).$$

For more general kernels, such as the power-law kernel, a closed-form for ξ is elusive. RizoIU et al. (2017b) proposed to approximately solve Eq. (6) by discretising time using the pre-defined observation endpoints $\{o_i\}_{i=0}^m$, yielding

$$\hat{\xi}[o_i; \theta] = \mu[o_i] + \sum_{s=0}^{i-1} \phi(o_i - o_s) \cdot \hat{\xi}[o_s; \theta], \quad (7)$$

where the bracket notation $\hat{\xi}[\cdot]$ is used to explicate the discretization. One can now use Eq. (7) to compute each $\hat{\xi}[\cdot; \theta]$, beginning with the base case $\hat{\xi}[0; \theta] = a$. Equipped with this, one solves the approximation to the HIP objective:

$$\min_{\theta} \sum_{i=1}^m (\mathbf{C}(o_{i-1}, o_i] - \hat{\xi}[o_i; \theta])^2. \quad (8)$$

RizoIU et al. (2017b) showed that the solution to Eq. (8) has good empirical performance. Conceptually, however, the approach has a few limitations:

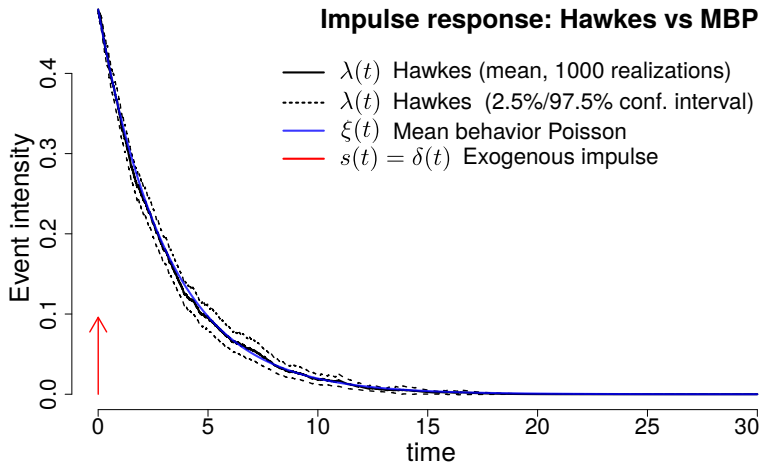


Figure 2: **Event intensity in Hawkes and MBP** as a result of a single exogenous event (shown in red). We generate 1000 Hawkes realizations using an exponential kernel (Eq. (13)) and the parameters $\kappa = 0.9, \theta = 1.15$. We show the mean and the 2.5% and 97.5% percentile of the Hawkes intensity $\lambda(t)$ (in black), and the (deterministic) MBP intensity $\xi(t)$ (in blue).

- L1:** There is a mismatch between the objective and the observed data; the observations are of event *counts*, while the objective measures closeness to the event *rates*. Intuitively, one should work with $\mathbb{E}[N(t)]$ rather than $\mathbb{E}[\lambda(t)]$.
- L2:** The HIP objective is not derived as the likelihood of a particular process, raising uncertainty as to precisely what sense it approximates the Hawkes likelihood. In the limiting case where each observation interval is made infinitesimally small, for example, it is unclear whether the solution to Eq. (5) approaches that of the standard Hawkes likelihood.
- L3:** It relies on $\hat{\xi}$, which is derived from an approximation to the underlying integral equation. This approximation is of unclear quality, and cannot handle intervals of unequal length.

For the remainder of the paper, when convenient, we suppress the functional dependence on parameters θ for intensity functions $\lambda(t), \xi(t)$ and compensators $\Lambda(t), \Xi(t)$.

3. The Mean Behavior Poisson (MBP) model

In this section, we first introduce the Mean Behavior Poisson (MBP) model – a Poisson process whose intensity function is the expected event intensity of a Hawkes process of the same parameters (Section 3.1). Next, we show that its compensator $\Xi(t)$ follows the same self-consistent equation as its intensity $\xi(t)$ (Section 3.2). Finally, we develop two methods to solve the self-consistent equation of MBP for arbitrary exogenous functions (Section 3.3).

3.1 Mean Behavior Poisson: model definition

The intensity of a Hawkes process (defined in Eq. (3)) is a stochastic function – i.e. at same time t the conditional intensity of two Hawkes realizations with the same parameters can

take very different values. Here we introduce a new process — dubbed the *Mean Behavior Poisson* (MBP) — which captures the expected behavior of all the Hawkes realizations defined by the same set of parameters. Formally, given a Hawkes process we define MBP as the non-homogeneous Poisson process with a deterministic intensity $\xi(t)$ — the expected Hawkes intensity over all possible realizations:

$$\begin{aligned}\xi(t) &\doteq \mathbb{E}_{\mathcal{H}_t}[\lambda(t)] = s(t) + \int_0^t \xi(\tau)\phi(t-\tau) d\tau \\ &= s(t) + (\xi * \phi)(t)\end{aligned}\tag{9}$$

where $\lambda(t)$ denotes the event intensity in the Hawkes process (Eq. (3)); $s(t)$ denotes exogenous intensity function; $\phi(t)$ denotes the kernel function of the Hawkes process and $*$ is the convolution operator.

We observe that the MBP intensity $\xi(t)$ is fully defined by the same objects as the Hawkes intensity $\lambda(t)$, that is the exogenous intensity $s(t)$ and the kernel function $\phi(t)$. We therefore say that Hawkes processes have a one-to-one correspondence to MBP processes. In Fig. 2 we visually denote the relation between the two processes by plotting the event intensity in Hawkes and in MBP. We sample 10,000 realizations of Hawkes, and we plot its mean event intensity and its 2.5% and 97.5% confidence intervals. We also plot the intensity of the mean behavior Poisson, which visually overlaps closely with the mean Hawkes intensity.

MBP and HIP. Visibly, MBP shares the same equation with HIP (Rizoiu et al., 2017b) (see Eq. (6)), however their usages are different: HIP discretizes Eq. (6) and aims to fit volumes of events, while Eq. (9) defines the intensity of a novel point process that, as far as we are aware, has not been studied in literature. In the next section, we study an important quantity of MBP – its *compensator* – and we show that it satisfies a nearly identical integral equation to the intensity equation.

3.2 The compensator of MBP

We define $\Xi(t)$ as the expectation of the Hawkes compensator (see Eq. (2)) over all possible realizations:

$$\Xi(t) = \mathbb{E}_{\mathcal{H}_t}[\Lambda(t)]$$

We show that the $\Xi(t)$ is the compensator of the MBP process using the Fubini theorem and passing the expectation inside the integral since $\lambda(t)$ is bounded (see Klebaner (2012, Theorem 8.4)):

$$\begin{aligned}\Xi(t) &= \int_0^t \mathbb{E}_{\mathcal{H}_t}[\lambda(z)] dz \stackrel{cf.(9)}{=} \int_0^t \xi(z) dz \\ &= \int_0^t \left[s(z) + \int_0^z \xi(z-y)\phi(y) dy \right] dz \\ &= \int_0^t s(z) dz + \int_{z=0}^t \int_{y=0}^z \xi(z-y)\phi(y) dy dz \\ &\stackrel{(a)}{=} \int_0^t s(z) dz + \int_{y=0}^t \int_{z=y}^t \xi(z-y)\phi(y) dz dy\end{aligned}$$

$$\begin{aligned}
 &= \int_0^t s(z) dz + \int_0^t \phi(y) \int_y^t \xi(z - y) dz dy \\
 &\stackrel{(b)}{=} \int_0^t s(z) dz + \int_0^t \phi(y) \int_0^{t-y} \xi(x) dx dy \\
 &\stackrel{(c)}{=} S(t) + \int_0^t \Xi(t - y) \phi(y) dy \\
 &= S(t) + (\Xi * \phi)(t)
 \end{aligned} \tag{10}$$

where (a) is obtained by reversing the order of the integrals and computing the new integration boundaries; (b) is obtained by performing the change of variable $x = z - y$; in (c) we apply $\Xi(t - y) \doteq \int_0^{t-y} \xi(x) dx$; and $S(t) \doteq \int_0^t s(z) dz$ is the cumulative immigrant intensity up to time t .

A cursory observation of Eq. (10) shows a distinct resemblance with Eq. (9): MBP's compensator $\Xi(t)$ follows a very similar self-consistent equation as its intensity $\xi(t)$, with the compensator's value at time t being a function of its values at every previous time $\tau < t$, decayed by the corresponding kernel function value. The similarity in the functional form of the two equations implies that similar methods can be applied to deduce their analytical solutions, detailed in the next section.

3.3 Solving the Mean Behavior Poisson equation

In this section, we propose two methods to solve Eq. (9), for arbitrary $s(t)$ and $\phi(t)$ functions. This type of equation is known as a Volterra integral equation of the second kind, which admits a solution only in particular cases. The first method is based on the Laplace transform, and has the downside of being applicable only to functions for which the transform and its inverse exist. The second method is a novel solution to the Volterra equation of the second kind, which employs notions of distribution theory to first compute the impulse response of the system, and afterwards the solution (Dong and van der Hoek, 2019).

Laplace transform. One natural approach to solving the MBP equation is using the Laplace transform.

Theorem 1 *Given the functions $s(t)$ and $\phi(t)$, a closed-form solution for Eq. (9) is*

$$\xi(t) = \mathcal{L}^{-1} \left\{ \frac{\mathcal{L}\{s(t)\}(\omega)}{1 - \mathcal{L}\{\phi(t)\}(\omega)} \right\} (t) \tag{11}$$

where $\mathcal{L}\{\cdot\}$ and $\mathcal{L}^{-1}\{\cdot\}$ denote the Laplace and the inverse of the Laplace transform respectively, and ω is defined in the frequency domain.

The derivation of Eq. (11) is shown in Appendix A.

This Laplace transform-based method has several drawbacks. First, it requires that the Laplace transform exists for both $s(t)$ and $\phi(t)$. This requirement is not always fulfilled by the exogenous intensity functions $s(t)$ that we construct in Definition 13, which involve Dirac delta functions, and for which the Laplace transform does not exist in the classical sense. Note that, while there are extensions for the Laplace transform to generalized functions (we refer the curious reader to van Dijk (2013, Ch. 8)), their direct application to solving Eq. (9) is not obvious, and they are outside the scope of this work.

Second, the method requires that the inverse Laplace function exists, which does not hold when ϕ involves a power-law or a Rayleigh time decay function. This is particularly limiting since the power-law kernel ($\phi(t) = \kappa(t + c)^{-(1+\theta)}$) has been shown to be the best performing in applications involving social media data (Rizoiu et al., 2017b; Mishra et al., 2016); the Rayleigh function ($\phi(t) = \kappa \frac{t}{\theta^2} e^{-\frac{t^2}{2\theta^2}}$) is widely used in epidemics modeling as it allows for a period of increasing intensity corresponding to disease incubation (Unwin et al., 2020).

Lastly, this method involves re-computing Eq. (11) every time that $s(t)$ changes – with all the difficulties stated above occurring at each recomputation – rendering the method difficult to apply when the $s(t)$ changes often, or when it is not known before-hand.

The impulse response solution. We propose a novel method to solve the MBP equation in Eq. (9) (and more generally Volterra equations of the second type), which deals with the shortcomings of the Laplace transform-based method. We first show that the Eq. (9) defines a linear, continuous-time, time-invariant system, and we discuss a method to derive its impulse response solution (Theorem 2). Next, we show how to use the impulse response to easily compute the solution for any arbitrary $s(t)$ (Corollary 3).

Theorem 2 *Let H be Hawkes process whose behavior is defined by the kernel function $\phi(t)$, and let M be the mean behavior Poisson (MBP) process associated with H , with the event intensity denoted by $\xi(t)$, and defined in Eq. (9). Then the intensity of M defines a causal, linear, continuous-time, time-invariant system of input $s(t)$ and output $\xi(t)$. The system is completely characterized by its impulse response defined by*

$$E(t) = \delta(t) + h(t), \text{ where } h(t) = \sum_{n=1}^{\infty} \phi^{\otimes n}(t)$$

where $\otimes n$ signifies n times convolution.

Proof We structure the proof into two parts. In the first part, we show that MBP is an LTI system, and in the second part we derive its impulse response.

For the first part of the proof, Rizoiu et al. (2017b, Corollary 2.2) have shown that Eq. (9) defines a causal, linear, continuous-time, time-invariant system of input $s(t)$ and output $\xi(t)$. For completeness reasons, we outline this proof here. It is easy to see that linearity holds by multiplying both sides of Eq. (9) by the same constant. The time-invariance property states that the response to a time-delayed input is identical and similarly time-delayed: if $s(t) \rightarrow \xi(t)$ then $s(t - t_0) \rightarrow \xi(t - t_0)$. Using Eq. (9) we compute the response for $s(t - t_0)$ as follows:

$$\begin{aligned} \xi(t - t_0) &= s(t - t_0) + \int_0^t \xi(\tau) \phi(t - t_0 - \tau) d\tau \\ &\stackrel{(a)}{=} s(t') + \int_0^{t'+t_0} \xi(\tau) \phi(t' - \tau) d\tau \\ &\stackrel{(b)}{=} s(t') + \int_0^{t'} \xi(\tau) \phi(t' - \tau) d\tau + \underbrace{\int_{t'}^{t'+t_0} \xi(\tau) \phi(t' - \tau) d\tau}_{=0} \end{aligned}$$

$$\stackrel{(c)}{=} s(t') + \int_0^{t'} \xi(\tau)\phi(t' - \tau) d\tau$$

where at (a) we make a change of variable $t' = t - t_0$; at line (b) we write the integral into two parts, i.e., $(0, t)$ and $(t', t' + t_0)$; at line (c) we observe that $\phi(t)$ is a causal function, i.e., $\phi(t) = 0$ for $t < 0$, or $\phi(t' - \tau) = 0$ for $\tau > t'$, and the integral term from t' to $t' + t_0$ disappears. $\xi(t)$ is also a causal function, which together with the linearity and time-invariance properties renders the MBP intensity system a causal, linear time-invariant (LTI) system.

In the second part of this proof, we concentrate on the impulse response function corresponding to the MBP system. The impulse response of a dynamic system is its output when presented with a brief input signal — dubbed impulse. The impulse response completely characterizes the system, as the response to linear combination of time-delayed impulses is a linear combination of time-delayed impulse responses. For continuous time dynamic systems, the impulse is denoted by the Dirac delta function $\delta(t)$. We denote as $E(t)$ the impulse response of MBP, with $E(t) = \delta(t) + h(t)$. From Eq. (9), it follows that

$$\begin{aligned} E(t) &= \delta(t) + \int_0^t E(\tau)\phi(t - \tau) d\tau \\ &= \delta(t) + (E * \phi)(t) \\ &\stackrel{(a)}{=} \delta(t) + ((\delta + h) * \phi)(t) \\ &= \delta(t) + (\delta * \phi)(t) + (h * \phi)(t) \\ &\stackrel{(b)}{=} \delta(t) + \underbrace{\phi(t) + (h * \phi)(t)}_{h(t)} \end{aligned}$$

where (a) is obtained by substituting $E(t)$ with $\delta(t) + h(t)$; (b) is obtained by noticing that the Dirac δ function is the neutral element for the convolution operation. Consequently and by dropping the time notation, we obtain

$$\begin{aligned} h &= \phi + h * \phi \\ &= \phi + (\phi + h * \phi) * \phi \\ &= \phi + \phi^{\otimes 2} + h * \phi \\ &= \phi + \phi^{\otimes 2} + \phi^{\otimes 3} + h * \phi \\ &= \dots \\ &= \sum_{n=1}^{\infty} \phi^{\otimes n}. \end{aligned}$$

■

Corollary 3 (to Theorem 2) *Let M be a mean behavior Poisson process associated with a Hawkes process of kernel $\phi(t)$, and let $E(t) = \delta(t) + h(t)$ be its impulse response function. Let $s(t)$ be an arbitrary generalized function denoting an external stimuli. Then $\xi(t) = (E * s)(t)$ is a solution to the MBP equation (Eq. (9)).*

Proof

$$\begin{aligned}
 \xi &= E * s = (\delta + h) * s = \delta * s + h * s \\
 &\stackrel{(a)}{=} s + E * \phi * s = s + (E * s) * \phi \\
 &= s + \xi * \phi
 \end{aligned}$$

where (a) is obtained by replacing $h = E * \phi$, knowing that $E = \delta + h$ and that E is the impulse response, i.e. a solution to $E = \delta + E * \phi$. \blacksquare

For example. Suppose

$$s(t) = \kappa\theta + (u_0 - \kappa\theta)e^{-\theta t} \quad (12)$$

and $\phi(t)$ is exponentially time-decaying. These particular forms for the $s(t)$ and $\phi(t)$ were proposed by Dassios and Zhao (2013), for which they also find a closed-form solution. We define the exponential kernel as

$$\phi(t) = \kappa\theta e^{-\theta t} \cdot \llbracket t \geq 0 \rrbracket. \quad (13)$$

Following Theorem 2 we first compute the impulse response as $E(t) = \delta(t) + h(t)$, with $h \in L^1(\mathbb{R})$ given by $h = \sum_{n=1}^{\infty} \phi^{\otimes n}$. For $t \geq 0$ and ϕ defined in Eq. (13) we have

$$\begin{aligned}
 \phi^{\otimes 2} &= (\phi * \phi)(t) \\
 &= \int_0^t \kappa\theta e^{-\theta\tau} \kappa\theta e^{-\theta(t-\tau)} d\tau \\
 &= \kappa^2\theta^2 e^{-\theta t} t
 \end{aligned}$$

and one can easily show that

$$\phi^{\otimes n}(t) = \kappa^n \theta^n e^{-\theta t} \frac{t^{n-1}}{(n-1)!}$$

By summing up, we compute $h(t)$ as

$$\begin{aligned}
 h(t) &= \sum_{n=0}^{\infty} \phi^{\otimes n}(t) = e^{-\theta t} \kappa\theta \sum_{n=0}^{\infty} \frac{(k\theta t)^n}{n!} \\
 &= e^{-\theta t} \kappa\theta e^{k\theta t} \\
 &= \kappa\theta e^{(k-1)\theta t}, \text{ for } t \geq 0
 \end{aligned}$$

Since $\phi(t < 0) = 0$, we have $h(t < 0) = 0$. It follows that the impulse response for MBP with the exponential kernel defined in Eq. (13) is

$$E(t) = \delta(t) + \kappa\theta e^{(\kappa-1)\theta t} \cdot \llbracket t \geq 0 \rrbracket \quad (14)$$

Note that the infinite convolutions sum has a closed form solution only for particular kernel functions. For all the other kernels, one can apply a semi-analytical approximation, as described by Dong and van der Hoek (2019).

From Corollary 3 it immediately follows that the solution for Eq. (9) with $s(t) = \kappa\theta + (u_0 - \kappa\theta)e^{-\theta t}$ is

$$\begin{aligned}\xi(t) &= (E * s)(t) = s(t) + (h * s)(t) \\ &= \frac{\kappa\theta}{1 - \kappa} \left(1 - e^{-(1-\kappa)\theta t}\right) + u_0 e^{-(1-\kappa)\theta t}\end{aligned}\quad (15)$$

The full details of the derivation (and derivations of other exogenous functions) are shown in Appendix B.1.

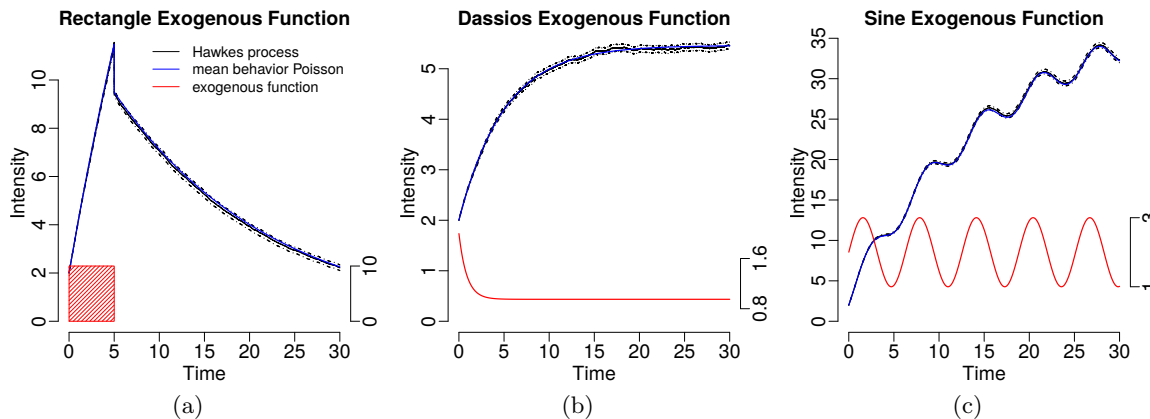


Figure 3: The intensity of 10,000 simulated realizations of a Hawkes process with exogenous function as a rectangle response, Dassios response (Dassios and Zhao, 2013), and sine response. Here the red part is the exogenous function both in the Hawkes process and MBP. The blue line is the MBP intensity, the solid black line is the mean intensity of the corresponding Hawkes process, and the black dashed lines are its 2.5% and 97.5% confidence intervals.

4. Interval-censored point processes

In this section, we consider how to fit MBP processes in the interval-censored setting; also known in some areas of the literature as panel count data (Sun and Zhao, 2013; Ding et al., 2018; Moreno et al., 2020). The Hawkes process generally cannot be fit in the interval-censored setting as it typically does not have the *independent increment* property. Given the correspondence in parameters between MBP processes and Hawkes processes, we can instead fit an MBP process using the interval-censored log-likelihood (IC-LL) as the MBP process does have the independent increment property. Finally, we present a method for numerically calculating the MBP compensator function, which is needed to calculate the IC-LL loss function.

4.1 Interval-censored Hawkes processes

Suppose that we have the set of observation times $O = \{o_i \mid i = 0, \dots, m, o_i \leq T\}$ which partitions into non-overlapping segments the time extent that the point process is observed

$t \in (0, T]$. Without loss of generality, we assume that the time points in O are ordered by index, $o_0 = 0$, and $o_m = T$. Further, for each segment defined by the half-open interval of consecutive points $(o_{i-1}, o_i]$ we observe the number of events which occurs in the interval, denoted by $C(o_{i-1}, o_i]$. We define this setting as the *interval-censored setting*. Fig. 4 illustrates the interval-censored setting for a simulated Hawkes process realization: panel B shows the event times, while panels B, E and F show the observed counts of events in each observation interval.

If we want to estimate the parameters of a Hawkes process in this setting, we cannot use the standard point process log-likelihood in Eq. (4) as it is defined for event times. Instead we aim to maximize the joint probability of the observed event volumes in each interval:

$$\max_{\theta} \mathbb{P}(N(o_{i-1}, o_i] = C(o_{i-1}, o_i], i \in \{1, \dots, m\}), \quad (16)$$

where $N(o_{i-1}, o_i] = N(o_i) - N(o_{i-1})$ is defined as the number of events in a realization on the half-open interval and θ are the Hawkes process's parameters.

However, there are a number of complications for computing Eq. (16) for Hawkes processes. Primarily, unlike the homogenous and inhomogenous Poisson processes, the Hawkes process does not have the independent increments property. As a result, we cannot evaluate Eq. (16) as we did in Eq. (1), i.e., the product of disjoint Poisson distributions with the expected number events set to the point process compensator. An alternative method for breaking down the Hawkes process is to decompose the process into the event count of each generation of offspring, formally known as a Galton-Watson branching process (Hawkes and Oakes, 1974). This provides a decompositions of Borel distributions (Borel, 1942). Kong et al. (2020b) derive the closed form solution for the case where the offspring distribution is evaluated at $t \rightarrow \infty$. However, there is no known analytical solution for computing the Borel distributions at finite time. A Monte-Carlo solution is available, but the computation cost does not scale well (O'Brien et al., 2020). Further, there is no known analytic or numeric solution for computing the conditional factorisation of the joint probability of all offspring generation Borel distributions. Thus in the general case, there is no closed form solution for a Hawkes process likelihood function in the interval-censored setting.

As a result of the aforementioned complications for finding a suitable loss function for Hawkes processes in the interval-censored setting, we propose a loss function which fits a MBP process instead.

Although we provide a loss function to fit MBP processes, we are not guaranteed in recovering the original Hawkes process' parameters which corresponds to the data before interval-censorship. Necessarily, the information contained in the interval-censored version of the data – when the observation periods are not infinitesimal in size – will contain less information than the original event time data. Furthermore, in the context of simulation we are restricted in the sense that MBP process is not a self-exciting process. Instead, by the parameter correspondence between Hawkes processes and MBP processes, the fitted parameters of the MBP can be used in a Hawkes process as an approximation of the underlying process.

4.2 Negative Poisson log-likelihood: Interval-censored loss

Unlike the Hawkes process, the MBP process introduced in Section 3 is a non-homogeneous Poisson process. Thus the MBP process has the independent increment property, allowing Eq. (16) to be evaluated as the likelihood of disjoint Poisson distributions (Daley and Vere-Jones, 2003, Chapter 2.4). The corresponding negative log-likelihood function of the MBP process is dubbed as the *interval-censored log-likelihood (IC-LL)*. The IC-LL was used with non-homogeneous Poisson processes by prior literature (Ding et al., 2018). In this work, we use IC-LL as a building block to estimate the parameters of Hawkes models (via MBP) and to build new loss functions via the Bregman divergence interpretation (see Section 5.1).

The Poisson distributions which compose the negative Poisson log-likelihood are defined with respect to the MBP compensator function $M(t)$, as per Eq. (1). Using this joint distribution, we can calculate the negative log-likelihood for a MBP by decomposing over each observation interval.

$$\begin{aligned}
 \mathcal{L}(\theta) &= -\log \mathbb{P}(M(o_{i-1}, o_i] = \mathbf{C}(o_{i-1}, o_i], i = 1, \dots, m) \\
 &= -\log \prod_{i=1}^m \mathbb{P}(M(o_{i-1}, o_i] = \mathbf{C}(o_{i-1}, o_i]) \\
 &= -\log \prod_{i=1}^m \left(\frac{\Xi(o_{i-1}, o_i]^{\mathbf{C}(o_{i-1}, o_i]}}{\mathbf{C}(o_{i-1}, o_i]!} \exp(-\Xi(o_{i-1}, o_i]) \right) \\
 &= -\sum_{i=1}^m (\mathbf{C}(o_{i-1}, o_i] \cdot \log \Xi(o_{i-1}, o_i] - \log(\mathbf{C}(o_{i-1}, o_i]!) - \Xi(o_{i-1}, o_i]) \\
 &= \sum_{i=1}^m \Xi(o_{i-1}, o_i] - \sum_{i=1}^m \mathbf{C}(o_{i-1}, o_i] \log \Xi(o_{i-1}, o_i] - \sum_{i=1}^m \log(\mathbf{C}(o_{i-1}, o_i]!) \\
 &= \sum_{i=1}^m \Xi(o_{i-1}, o_i] - \sum_{i=1}^m \mathbf{C}(o_{i-1}, o_i] \log \Xi(o_{i-1}, o_i] - \sum_{i=1}^m \log \mathbf{C}(o_{i-1}, o_i]. \quad (17)
 \end{aligned}$$

Notably, as we are aiming to optimise a parameter set θ of MBP, the constant which only depends on the event counts $-\sum_{i=1}^m \log \mathbf{C}(o_{i-1}, o_i]$ can be ignored. As such, we further rewrite the above loss function to the following equivalent loss function when minimised.

Proposition 4 *The interval-censored log-likelihood (IC-LL) for a MBP process with corresponding compensator Ξ under interval-censored data is*

$$\mathcal{L}_{\text{IC-LL}}(\theta) = \sum_{i=1}^m \Xi(o_{i-1}, o_i; \theta] - \sum_{i=1}^m \mathbf{C}(o_{i-1}, o_i] \log \Xi(o_{i-1}, o_i; \theta]. \quad (18)$$

In addition to the standard negative log-likelihood approach to derive the negative Poisson log-likelihood loss, we can justify this loss function by considering the sum of Bregman divergences.

4.3 Calculating the negative Poisson log-likelihood

The loss functions proposed above both require the computation of the compensator $\Xi(o_{i-1}, o_i]$, as defined in Eq. (10). From the definition of the compensator over an interval, we have

$$\begin{aligned}\Xi(o_{i-1}, o_i] &\doteq \int_{o_{i-1}}^{o_i} \xi(s) ds \\ &= \int_0^{o_i} \xi(s) ds - \int_0^{o_{i-1}} \xi(s) ds \\ &= \Xi(o_i) - \Xi(o_{i-1}).\end{aligned}\tag{19}$$

We explore the two cases where we either have an analytical solution for the MBP compensator or when we have to use numeric approximation to evaluate it.

Analytical solution. As we have foreshadowed in Section 3.2, the compensator of MBP follows the same functional form as the MBP intensity function ξ . Thus, we are able to use the same analytical methods for solving the compensator evaluated at a point. Specifically, we can apply Corollary 3 to derive an analytical solution:

Corollary 5 (to Theorem 2) *Let $\phi(t)$ be the kernel of a Hawkes process and $E(t) = \delta(t) + h(t)$ be its impulse response function, then for $S(t)$ a closed-form solution for the MBP compensator over a half-open interval $(x, y]$ is*

$$\Xi(x, y] = (E * S)(y) - (E * S)(x).\tag{20}$$

Proof Follows immediately from application of Eq. (19) and Corollary 3. ■

Numerical approximation. The cases in which the compensator $\Xi(o_{i-1}, o_i]$ cannot be solved analytically are generally due to the lack of a closed-form solution for the h term in Theorem 2. While the infinite sum of convolutions theoretically leads to an approximation algorithm outlined in (Dong and van der Hoek, 2019), the authors do not provide a stable implementation. Alternatively, we consider a numeric lower bound approximation of the MBP compensator. Specifically, we approximate the MBP counting process with a set of approximation points $\{d_j\}_{j=0}^D$, where $d_0 = 0$, $d_{j-1} < d_j$, and $0 < d_j < T$ for $j \in \{1, \dots, D\}$. Consider the following lower-bound on the MBP counting process using D approximation points:

$$M(t) \geq M_D^-(t) \doteq \sum_{j=1}^D M(d_{j-1}, d_j] \cdot \mathbb{I}[d_j < t \leq d_D].\tag{21}$$

Considering that the event count $M(t)$ is a monotonically increasing function, the lower bound $M_D^-(t)$ is intuitively a piecewise constant function, which gets updated at each d_j , and is constant in between approximation points. For equidistant approximation points

$$d_j = \frac{T}{D}i,$$

it can be shown that we can become arbitrarily accurate to $N(t)$ as the number of approximation points increases.

Proposition 6 *As $D \rightarrow \infty$, then $M_D^-(t) \rightarrow N(t)$.*

Using this lower bound counting process, we can approximate the compensator of MBP, which follows a self-consistent equation (as per Eq. (10)). We consider the following formulation of the compensator which uses the equivalence between compensator and expected counts $\Xi(t) = \mathbb{E}[M(t)]$ for non-homogeneous Poisson processes.

$$\begin{aligned}\Xi(t) &= S(t) + \int_0^t \Xi(t-y)\phi(y)dy \\ &= S(t) + \int_0^t \Xi(y)\phi(t-y)dy \\ &= S(t) + \int_0^t \mathbb{E}[M(y)]\phi(t-y)dy.\end{aligned}\tag{22}$$

We now define the following lower-bound compensator using the counting process approximation $M_D^-(t)$:

$$\begin{aligned}\Xi^-(t) &\doteq S(t) + \int_0^t \mathbb{E}[M_D^-(y)]\phi(t-y)dy \\ &= S(t) + \int_0^t \mathbb{E} \left[\sum_{j=1}^D M(d_{j-1}, d_j) \cdot \mathbb{I}[d_j < y \leq d_D] \right] \phi(t-y)dy \\ &= S(t) + \sum_{j=1}^D \mathbb{E} [M(d_{j-1}, d_j)] \int_0^t \mathbb{I}[d_j < y \leq d_D] \phi(t-y)dy \\ &\stackrel{(a)}{=} S(t) + \sum_{j=1}^{\bar{D}(t)} \mathbb{E} [M(d_{j-1}, d_j)] \int_{d_j}^{\min(t, d_D)} \phi(t-y)dy,\end{aligned}\tag{23}$$

where $\bar{D}(t) = \max\{i \in \{1, \dots, D\} : d_i < t\}$. Step (a) follows from simultaneously changing the integral upper-bound and the summation bound with respect to the Iverson brackets.

An upper-bound approximation equivalent is given by

$$\Xi^+(t) = S(t) + \sum_{j=1}^{\bar{D}(t)+1} \mathbb{E} [M(d_{j-1}, d_j)] \int_{d_{j-1}}^{\min(t, d_D)} \phi(t-y)dy.\tag{24}$$

The negative Poisson log-likelihood loss function requires to compute the compensator over intervals $\Xi(o_{i-1}, o_i]$, which we approximate using the compensator lower-bound Ξ_D^- :

$$\Xi(o_{i-1}, o_i] \approx \Xi_D^-(o_{i-1}, o_i] = \Xi_D^-(o_i) - \Xi_D^-(o_{i-1}).\tag{25}$$

By using Eq. (23), we can compute this approximation as follows,

Proposition 7 *The numeric approximation of the compensator over an interval $\Xi(o_{i-1}, o_i] \approx \Xi_{\bar{D}}(o_{i-1}, o_i]$ can be computed as*

$$\begin{aligned} \Xi_{\bar{D}}(o_{i-1}, o_i] &= S(o_i) - S(o_{i-1}) + \sum_{j=1}^{\bar{D}(o_i)} \mathbb{E}[M(d_{j-1}, d_j)] \int_{o_{i-1}-d_j}^{o_i-d_j} \phi(y) dy \\ &+ \sum_{j=\bar{D}(o_{i-1})+1}^{\bar{D}(o_i)} \mathbb{E}[M(d_{j-1}, d_j)] \int_0^{o_{i-1}-d_j} \phi(y) dy. \end{aligned} \quad (26)$$

The proof of Proposition 7 can be found in Appendix A.

The significance of Proposition 7 is that it allows us to utilize compensators which do not have closed form solutions, but also allows us to predict the compensator values of future time intervals using previous values. We utilize this prediction in Section 8.

5. Bregman generalisation of IC-LL

Previously in Section 4, we introduced the NPLL loss function for fitting in interval-censored data settings. In this section, we notice that the IC-LL loss function can be interpreted as a Bregman divergences — a generalized notion of distances. In doing so, we consider alternative loss functions which arise when changing the convex generator function of the Bregman divergence. This leads to a generalisation and correction of the HIP loss function (Rizoiu et al., 2017b).

5.1 Bregman divergence

We first begin with a brief introduction of Bregman divergences. Bregman divergences are a widespread tool for designing and analyzing algorithms within machine learning. Bregman divergences have been used to construct generalizations of algorithms to use different definitions of distances, i.e., clustering (Banerjee et al., 2005), boosting (Collins et al., 2002), and computational geometry (Nielsen et al., 2007). We will similarly use Bregman divergences to generalize IC-LL by interpreting the loss function as the generalized Kullback-Leibler divergence (KL-divergence) between compensator values and interval-censored event counts.

A Bregman divergence is a generalized notion of distances between points. Suppose we are given a strictly convex generator $\varphi : S \rightarrow \mathbb{R}$, where $\text{dom}(\varphi) = S$ is a convex set $S \subseteq \mathbb{R}^d$ and $\varphi(\cdot)$ is differentiable on the relative interior $\text{ri}(S)$. Then the Bregman divergence $B_\varphi : S \times \text{ri}(S) \rightarrow [0, \infty)$ is defined as (Banerjee et al., 2005):

$$B_\varphi(\mathbf{x}, \mathbf{y}) \doteq \varphi(\mathbf{x}) - \varphi(\mathbf{y}) - (\mathbf{x} - \mathbf{y})^t \nabla \varphi(\mathbf{y}). \quad (27)$$

A wide selection of popular divergences can be obtained by picking the appropriate generator function. In particular, we consider two specific convex generators for Bregman divergences.

KL-divergence. The KL-divergence can be obtained by considering the generator function

$$\varphi(\mathbf{x}) \doteq \sum_{i=1}^d x_i \log x_i, \quad (28)$$

yielding

$$\text{KL}(\mathbf{x}, \mathbf{y}) \doteq B_\varphi(\mathbf{x}, \mathbf{y}) = \sum_{i=1}^d x_i \log \frac{x_i}{y_i} - \mathbf{1}^t(\mathbf{x} - \mathbf{y}). \quad (29)$$

Squared loss. The squared loss function is obtained if we consider a squared Euclidean norm generator function

$$\hat{\varphi}(\mathbf{x}) \doteq \|\mathbf{x}\|^2, \quad (30)$$

yielding

$$\text{SSE}(\mathbf{x}, \mathbf{y}) \doteq B_{\hat{\varphi}}(\mathbf{x}, \mathbf{y}) = \|\mathbf{x} - \mathbf{y}\|^2. \quad (31)$$

Remark 8 *Notably, the unconstrained minimisation of a Bregman divergence (with respect to the second parameter) is unique and independent of choice of convex generator function. That is $\mathbb{E}[X]$ is the unique minimizer of $\min_{\mathbf{s} \in \text{ri}(S)} \mathbb{E}[B_\varphi(X, \mathbf{s})]$ for any generator φ , (Banerjee et al., 2005, Proposition 1).*

Another related quantity is the *Bregman information*, which is given by the unique minimised of the expectation:

$$I_\varphi(X) \doteq \min_{\mathbf{s} \in \text{ri}(S)} \mathbb{E}[B_\varphi(X, \mathbf{s})]. \quad (32)$$

In practice, this can be calculated by using the empirical expectation given a dataset $\mathcal{X} = \{\mathbf{x}_i\}_{i=1}^n$:

$$\hat{I}_\varphi(\mathcal{X}) \doteq \sum_{i=1}^n B_\varphi(\mathbf{x}_i, \mathbf{s}). \quad (33)$$

5.2 Connections to IC-LL

Given a single observation sequence, the IC-LL loss function is equivalent to the generalised KL-divergence with an additional constant factor. That is, IC-LL is equivalent to the KL-divergence loss under minimisation. First, let us define $\mathbf{C} \doteq (\mathbf{C}(o_0, o_1], \dots, \mathbf{C}(o_{m-1}, o_m])$ and $\Xi(\theta) \doteq (\Xi(o_0, o_1], \dots, \Xi(o_{m-1}, o_m])$ as an observed volume of interval-censored events and corresponding interval compensator values using parameters θ , respectively.

From a simple observation, we can see the KL-divergence equivalence with IC-LL.

Proposition 9 *The IC-LL loss function is the given by*

$$\mathcal{L}_{\text{IC-LL}}(\theta) = \text{KL}(\mathbf{C}, \Xi(\theta)) + \Gamma(\mathbf{C}), \quad (34)$$

where $\Gamma(\mathbf{C})$ is a constant only dependent on the observed events. Furthermore,

$$\arg \min_{\theta} \mathcal{L}_{\text{IC-LL}}(\theta) = \arg \min_{\theta} \text{KL}(\mathbf{C}, \Xi(\theta)). \quad (35)$$

The KL-divergence term in Eq. (34) can be rewritten as a Bregman divergence as follows:

$$B_\varphi(\mathbf{C}, \Xi(\theta)) + \Gamma(\mathbf{C}), \quad (36)$$

where φ is given by Eq. (28). Thus the natural question of what happens when we switch the choice of Bregman divergence arises. In particular, we consider the minimization of Eq. (36) parameterized by the convex generator φ .

We now consider switching the KL-divergence generator function to that of the squared loss function given by Eq. (30). This gives a sum of squared error loss function:

$$\begin{aligned} \mathcal{L}_{\text{SSE}} &= \text{SSE}(\mathbf{c}, \Xi) + \Gamma(\mathbf{C}) \\ &= \sum_{i=1}^m (\mathbf{C}(o_{i-1}, o_i] - \Xi(o_{i-1}, o_i; \theta))^2 + \Gamma(\mathbf{C}). \end{aligned} \quad (37)$$

This SSE loss function is actually a generalized version of the HIP loss function (RizoIU et al., 2017b); differing in only that the intensity function ξ is used instead of Ξ and the additional constant $\Gamma(\mathbf{C})$. However, in the later, we are incorrectly matching point process intensities to volumes of events. Eq. (37) fixes this by matching point process compensator values instead. In Section 5.3, we show under what assumptions Eq. (37) becomes equivalent to the original HIP loss function.

A notable connection to be noted is the bijection between (regular) Bregman divergences and (regular) exponential families (Banerjee et al., 2005, Theorem 6). In particular, the choice of Bregman divergence dictates what distribution the data is assumed to be sampled from for each observational interval. For example, by choosing the KL-divergence (Eq. (34)) each observational interval is assumed to be Poisson distributed, giving the IC-LL loss function. By considering SSE divergence (Eq. (37)), we are assuming that the event volume is Gaussian distributed; with constant standard deviation.

One way of establishing a connection between the two loss functions is by considering the SSE loss function as an approximation of the KL-divergence, where each interval is Poisson distributed. Concretely, let us define a Poisson distribution with true rate $\Xi(o_{i-1}, o_i]$ for an arbitrary event interval. Then suppose we have N many i.i.d. volume observations over this interval $\mathbf{C}_1(o_{i-1}, o_i], \dots, \mathbf{C}_N(o_{i-1}, o_i]$. It follows that given the empirical mean of these observations $\hat{\mathbf{C}}(o_{i-1}, o_i]$, by the central limit theorem, in the limit we have that

$$\hat{\mathbf{C}}(o_{i-1}, o_i] \sim \mathbf{N}(\Xi(o_{i-1}, o_i], \Xi(o_{i-1}, o_i]/N)$$

as a Poisson distribution has variance equal to its rate. Thus, the averaging of event sequence provides an SSE loss function by the bijection between Bregman divergences and exponential families (Banerjee et al., 2005, Theorem 6). With this, we can expect the KL loss function and SSE loss function to perform similarly for large numbers of samples.

Alternatively, we can consider IC-LL as the sum of single dimensional generalized KL-divergences (Bregman divergences), where the summation is over each observational interval. However, for this section we only consider the multi-dimensional Bregman divergences for conciseness.

One convenient property of the Bregman divergence is that the expected minimisation, with respect to the second argument, yields a unique solution (Banerjee et al., 2005, Proposition 1). Thus, with respect to the interval-censored volumes and MBP compensator, we would likewise calculate the risk of a loss function, for example IC-LL, with respect to the probability distribution of sequences.

Notably, the unique minimizer given by Banerjee et al. (2005, Proposition 1) does not depend on the specific Bregman divergence chosen. Thus intuitively, disregarding the Bregman divergence used, we are trying to match the expected volumes on each observation interval. Of course in our own setting, we are also constrained matching volumes with a particular parametrisation of a MBP compensator function. As such, the solutions we obtain from the corresponding Bregman divergence used will be effected by how the functional form of the MBP compensator interacts with geometry of the chosen divergence.

5.3 HIP as approximation

The HIP loss function used in (Rizoïu et al., 2017b) is incorrect in the general case. It incorrectly attempts to match the point process intensity with interval-censored volumes. However, by using the framework of Bregman divergence losses presented in Section 5.1, we prove that the HIP loss function is a SSE loss function, with the additional assumption that we have unit sized observation intervals where the MBP intensity function is constant over the interval and a discrete convolution approximation.

By assuming that we have unit time observation intervals and that the MBP intensity function is constant over the interval, we can show that the compensator function over that interval is equivalent to the intensity function of the MBP process.

Lemma 10 *Suppose that the MBP intensity function is constant over unit interval $(i-1, i]$, where $i \in \mathbb{Z}$. Then $\Xi(i-1, i] = \xi(i)$.*

Proof As the MBP intensity function is constant over the interval, let c the value it obtains. Thus,

$$\Xi(i-1, i] = \int_{i-1}^i \xi(s) ds = \int_{i-1}^i c ds = c = \xi(i). \quad \blacksquare$$

Lemma 10 shows that under the specific conditions we have specified, the MBP intensity function can be consider instead of the MBP compensator — which can be cumbersome to calculate/approximate for certain kernel functions chosen (as shown in Section 4.3).

In addition to this assumption, by using the SSE loss function we recover exact HIP loss function.

Theorem 11 *Suppose that the assumption that observation intervals are unit length with constant MBP intensity. Then the SSE loss function in Eq. (37) with the MBP intensity approximated with discrete convolution recovers the HIP loss function (Rizoïu et al., 2017b, Eq. (6))*

$$\frac{1}{2} \sum_{i=1}^t (\xi(i) - C(i-1, i])^2. \quad (38)$$

Proof Given the observation interval are unit length, the SSE loss function in Eq. (37) can be written as

$$\text{SSE}(\mathbf{c}, \Xi) = \sum_{i=1}^t (C(i-1, i] - \Xi(i-1, i]).$$

Additionally, by using Lemma 10 we have

$$\begin{aligned} \text{SSE}(\mathbf{c}, \Xi) &= \sum_{i=1}^t (\mathbf{C}(i-1, i] - \Xi(i-1, i]) \\ &= \sum_{i=1}^t (\mathbf{C}(i-1, i] - \xi(i)), \end{aligned}$$

which when optimised for, is equivalent with a 1/2 multiple. ■

With the HIP loss function recovered, to recover the HIP model we consider a MBP process with power-law kernel function. Additionally, we also approximate the intensity function by discrete convolution. This approximation step changes the integral in Eq. (9) to a summation

$$s(i) + \int_0^i \xi(i)\phi(t-\tau) d\tau \approx s[i] + \sum_{\tau=1}^i \xi[i-\tau]\phi[\tau], \quad (39)$$

where the square brackets indicate that the function is constant over the interval $(i-1, i]$.

Leaving the choice of kernel aside, the approximation via discrete convolution provides an MBP intensity function which adheres to the assumption in Theorem 11. Thus the entire HIP model can be realised using the loss function framework proposed in this section, generalising Eq. (7).

Theorem 12 *Suppose that we have unit length interval-censored event volumes. Suppose that we have an MBP process with power-law kernel and that the MBP intensity is approximated with a discrete convolution, Eq. (39). Then by using the SSE loss function, Eq. (37), we have the HIP model from Rizoïu et al. (2017b).*

Proof A MBP process with power-law kernel and discrete convolution approximation is equivalent to the MBP process introduced in (Rizoïu et al., 2017b, Eq. (4)).

By definition of the discrete convolution in Eq. (39), the intensity function is constant over each interval $(i-1, i]$. Thus by Theorem 11, the SSE loss function (which uses the MBP compensator) is equivalent to the HIP loss function (Rizoïu et al., 2017b, Eq. (6)). ■

Theorem 12 shows that our framework can generalise the method proposed by Rizoïu et al. (2017b). In particular, we can consider different kernel functions or use the compensator approximation method in Section 4.3 when observation intervals are not uniformly unit length. Importantly, using this framework, we can provide a closed-form solution of HIP when the power-law kernel is replaced with the exponential kernel — as the discrete convolution and uniform unit length observations are no longer required to approximate the MBP compensator.

6. Processes with observed exogenous stimuli

Our work in Sections 3 and 4 systematically assumes that the exogenous events arrive in the point process following a determined intensity function $s(t)$. However, in many real-world scenarios (including our real-world experiments in Section 8) the exogenous events

Table 2: Tabulation of possible data scenarios. ET = “event times” and IC = “interval-censored”. The last column specifies if an endogenous loss function can be used.

Scenario	Setting		Point Process				
	Immigrant	Offspring	Exog. Func.	HP	MBP	Loss Func.	Endo.?
A	-	ET	Any	✓	✓	PP-LL	×
B	ET	ET	Multi-Impulse	✓	✓	PP-LL	✓
C	IC	ET	LHPP	✓	✓	PP-LL	✓
D	-	IC	Any	×	✓	IC-LL/SSE	×
E	ET	IC	Multi-Impulse	×	✓	IC-LL/SSE	✓
F	IC	IC	LHPP	×	✓	IC-LL/SSE	✓

are directly observed, and $s(t)$ is unknown. We denote the setting in which the exogenous event can be differentiated from endogenous events as a *separable scenario*. Furthermore, when exogenous and endogenous events are separable, they may be observed at different granularity levels (event time vs. interval censored). For example, consider the case study of how tweets on Twitter affect YouTube views. The tweets are observed as event times, while YouTube views are only observable as aggregated volumes (due to platform affordability constraints).

Table 2 lists the six possible scenarios in which a point process can be observed. Scenarios A and D are not separable, and events are observed as event times (ET) or interval-censored (IC), respectively. Scenarios B, C, E, and F are separable and define all the possible combinations of ET and IC for exogenous and endogenous events. For these separable scenarios, Fig. 4 exemplifies how the same realization with separable exogenous events (upper red events) and endogenous events (lower blue events) can be observed with either one or both types of events as interval-censored.

In this section, we introduce two exogenous functions to approximate $s(t)$ which allow us to characterize the exogenous contribution of a Hawkes process, or MBP process, in separable scenarios. We introduce the *multi-impulse exogenous function* and the *latent homogeneous Poisson process exogenous function* which can be used when the exogenous data is observed as event times or interval-censored, respectively. We also build endogenous loss functions which account only for endogenous events, and allow us to fit model parameters in all possible regimes of observed data. Table 2 summarises, for each scenario, the corresponding exogenous function, loss function, whether it is applicable for Hawkes, MBP or both, and whether an endogenous loss function should be used.

6.1 Exogenous Event Times – Multi-Impulse

Consider a separable scenario in which we observe exogenous events as event times (scenarios B and E in Table 2). That is, we have a set of immigrant event times $\mathfrak{s}_z \in \Psi_T$. We define the corresponding exogenous intensity as the sum of Dirac delta functions, one for each observed exogenous event.

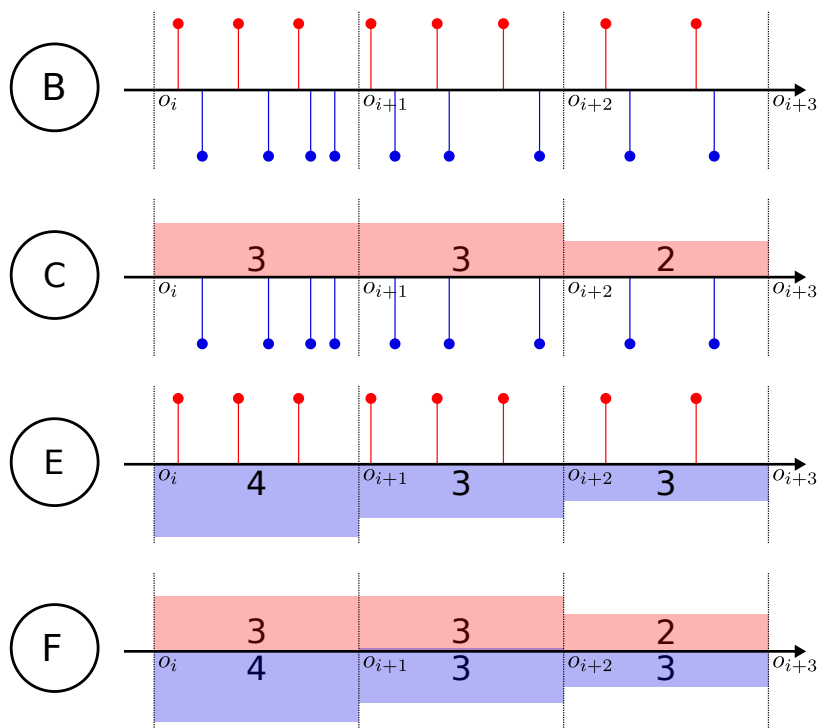


Figure 4: **From separable event times to different separable interval censored settings.** Each row corresponds to a separable setting in Table 2. Red components correspond to exogenous events; and blue components correspond to endogenous events. o_i denote the observation times based on which the data is interval-censored. The lollipop markers represent event times, while the area shaded area represent counts.

Definition 13 *The multi-impulse exogenous function for a set of immigrant event times $\mathfrak{s}_z \in \Psi_T$ is defined as*

$$s_{m\delta}(t) = \sum_{\mathfrak{s}_z \in \Psi_T} \delta(t - \mathfrak{s}_z). \quad (40)$$

Notably, the multi-impulse exogenous function is entirely deterministic with respect to a set of immigrant event times, and hence does not have any parameters to fit. Another point of interest is that $s_{m\delta}(t)$ is not a proper function, as Dirac delta functions are generalized functions and not computable in practice. Thus, the loss functions that leverage the multi-impulse exogenous function are incomputable. For these cases, we introduce in Section 6.3 the endogenous loss functions.

6.2 Exogenous Interval-Censored – Latent Homogeneous Poisson Process

Here we consider the separable scenarios in which the immigrant events are observed as interval-censored, with no assumption on the data of the endogenous response (scenarios C and F in Table 2). We assume given a set of pre-specified immigrant observation times $\{q_0, \dots, q_m\} \in Q$. For each interval $(q_{i-1}, q_i]$ we only observe the total immigrant counts $S(q_{i-1}, q_i]$, similarly to Section 4. Note that for scenario F, the immigrant observation times $q_i \in Q$ can be distinct from the endogenous observation time $o_i \in O$, although they are often identical in practice and in our experiments in Sections 7 and 8. The rest of this section assumes the more general case when $Q \neq O$.

For the scenarios in which immigrants are observed interval-censored, we assume that in each observation interval $(q_{i-1}, q_i]$ immigrants are generated by a *latent homogeneous Poisson process (LHPP)* of constant intensity $s(t) = \lambda_i$. Together, the LHPPs corresponding to observation intervals define a piece-wise constant non-homogeneous Poisson process with intensity

$$\sum_{i=1}^m \lambda_i \cdot \mathbb{I}[q_{i-1} < t \leq q_i]. \quad (41)$$

We consider the parameters λ_i which are most likely.

Proposition 14 *Given a latent homogeneous Poisson process defined over observation intervals $(q_{i-1}, q_i]$ and corresponding immigrant event counts $S(q_{i-1}, q_i]$, the most likely intensity values are*

$$\lambda_i = \frac{S(q_{i-1}, q_i]}{q_i - q_{i-1}}. \quad (42)$$

Proof Suppose we have a homogeneous Poisson point process $N(t)$ defined over arbitrary half-open interval $(x, y]$, $x \leq y$ with a realization of C many events occurring on that interval. The number of events over a given interval in a homogeneous Poisson process follows a Poisson distribution of parameter $\lambda(y - x)$. Thus, the most likely intensity value is given by

$$\begin{aligned} \lambda^* &= \underset{\lambda}{\operatorname{Argmax}} \mathbb{P}(N(x, y] = C; \lambda) \\ &= \underset{\lambda}{\operatorname{Argmax}} \frac{(\lambda(y - x))^C}{C!} \exp(-\lambda(y - x)) \end{aligned}$$

$$\begin{aligned}
&= \underset{\lambda}{\text{Argmax}} C \log(\lambda(y-x)) - \log(C!) - \lambda(y-x) \\
&= \underset{\lambda}{\text{Argmax}} C \log(\lambda(y-x)) - \lambda(y-x).
\end{aligned}$$

The function we are maximizing is concave, thus by setting the derivative to zero we have,

$$\lambda^* = \frac{C}{y-x}. \quad (43)$$

Thus for each of the intervals $(q_{i-1}, q_i]$ and corresponding immigrant event counts $S(q_{i-1}, q_i]$ we have Eq. (42). \blacksquare

Thus using the optimal parameters for the latent homogeneous Poisson process, we have the LHPP exogenous function.

Definition 15 *Given the interval-censored exogenous volumes $S(q_{i-1}, q_i]$ over observation times $\{q_0, \dots, q_m\} \in Q$, then the latent homogeneous Poisson process (LHPP) exogenous function is*

$$s_{\bullet}(t) = \sum_{i=1}^m \frac{S(q_{i-1}, q_i]}{q_i - q_{i-1}} \cdot \llbracket q_{i-1} < t \leq q_i \rrbracket. \quad (44)$$

If more information is available about the process generating the immigrant events, it can be integrated this into the shape of the exogenous intensity functions (for example, by considering a non-homogeneous Poisson process in each interval). Furthermore, Eq. (44) can also be derived starting from the distribution of exogenous events within each interval $(q_j, q_{j+1}]$ (see ??). This can come in handy when it is known how the exogenous events are distributed in each interval. Note that the uniform distribution assumed in ?? equates the latent homogeneous Poisson process defined in this section.

6.3 Endogenous Loss Functions

When the exogenous events are observed – i.e. they are deterministic – they do not contribute to the loss function. We propose the *endogenous loss function*, which is defined as only the contribution of endogenous events of the point process to the loss function. This circumvents the incomputability issues when using the multi-impulse exogenous function, as per Section 6.1. As a result, we only need to fit our model with respect to the offspring events, whether they appear in point or interval-censored form.

Suppose that we have a valid point process intensity function $\lambda(t)$ with a corresponding loss function $\mathcal{L}(\theta)$ to fit for the parameter θ of $\lambda(t)$. More precisely, we can consider the loss function as a function of both the intensity function and parameter space $\mathcal{L}(\theta, \lambda)$. Further, we assume that we have a point process intensity function we can be decomposed into the sum of an exogenous function and endogenous function. That is,

$$\lambda(t) = \lambda^{\text{exo}}(t) + \lambda^{\text{endo}}(t), \quad (45)$$

where $\lambda^{\text{exo}}(t)$ solely characterizes the immigrant events and $\lambda^{\text{endo}}(t)$ solely characterizes the offspring events. An example of a valid decomposition can be found in Eq. (3), in which we

can see that the Hawkes process intensity can be explicitly defined as the sum of exogenous function $s(t)$ and endogenous intensity contribution $\sum_{t_i < t} \phi(t - t_i)$.

For MBP, we can define the exogenous-endogenous function decomposition as

$$\xi(t) = \xi^{\text{exo}}(t) + \xi^{\text{endo}}(t) \quad (46)$$

$$\xi^{\text{exo}}(t) = s(t) \quad (47)$$

$$\xi^{\text{endo}}(t) = \int_0^t \xi(y) \phi(t - y) dy. \quad (48)$$

Additionally, if a closed-form solution of the intensity function $\xi(t)$ exists, as per Section 3.3, we are able to find a closed-form solution of the endogenous function component

$$\xi^{\text{endo}}(t) = \xi(t) - \xi^{\text{exo}}(t). \quad (49)$$

Using the endogenous function from our decomposition, we are able to define a new corresponding endogenous process, which has intensity function equal to the endogenous function $\lambda^{\text{endo}}(t)$. Thus, we define the *endogenous loss function* of the original point process as

$$\mathcal{L}^{\text{endo}}(\theta^{\text{endo}}) \doteq \mathcal{L}(\theta^{\text{endo}}, \lambda^{\text{endo}}), \quad (50)$$

where θ^{endo} are the fitting parameters of $\lambda(t)$ which only occur in $\lambda^{\text{endo}}(t)$.

When the exogenous events are observed and we use either the multi-impulse exogenous function in Eq. (40) or the interval-censored immigrant exogenous function in Eq. (44), the parameter space of the endogenous point process is equivalent original parameter space $\theta^{\text{endo}} = \theta$ (i.e. scenarios B, C, E and F).

For example, the endogenous loss function of MBP using the PP-LL loss function, as per Eq. (4), is defined as

$$\mathcal{L}^{\text{endo}}(\theta^{\text{endo}}) = - \sum_{f_i \in \Upsilon_T} \log \xi^{\text{endo}}(f_i) + \int_0^T \xi^{\text{endo}}(s) ds, \quad (51)$$

where Υ_T is the set of offspring events. Notably, this endogenous loss function is appropriate when the offspring data is in point format (i.e. scenarios B and C).

In the scenarios when the offspring data is in an interval-censored format (i.e. scenarios E and F), we can no longer use Eq. (51). Instead we can consider the endogenous version of an interval-censored loss function introduced in Section 4. Consider the Bregman divergence interpretation of a loss function, with convex generator $\varphi(z)$. The endogenous version of the loss function is defined as,

$$\mathcal{L}^{\text{endo}}(\theta^{\text{endo}}) = \sum_{i=1}^m B_{\varphi}(\hat{f}_i, \Xi^{\text{endo}}(o_{i-1}, o_i]), \quad (52)$$

$$\text{where } \Xi^{\text{endo}}(t) = \int_0^t \xi^{\text{endo}}(s) ds$$

$$\text{and } \hat{f}_i = F(o_{i-1}, o_i].$$

Here $F(o_{i-1}, o_i]$ denotes offspring volumes on the interval $(o_{i-1}, o_i]$.

Table 2 outlines when using an endogenous loss function is suitable. In addition, experiments in Section 7 show that even across the different settings where the endogenous loss function is not required, the performance to the non-endogenous standard loss functions are similar.

7. Synthetic Experiments

In this section, we empirically validate our proposals by refitting a synthetically generated dataset with each of the six scenarios described in Table 2. In Section 7.1, we generate datasets of separable Hawkes realizations starting from two parameter combinations – one clearly subcritical (branching factor $n^* \ll 1$) and another approaching criticality ($n^* \simeq 1$) – and two exogenous functions. Next, in Section 7.2, we selectively interval-censor types of events in the datasets to render them compatible with the different scenarios in Table 2. Last, we present our results in Section 7.3.

7.1 Synthetic Datasets

We generate synthetic datasets usable in all scenarios (A-F in Table 2). We start from two exogenous functions and two sets of Hawkes parameters. For each of the four combinations, we generate separable Hawkes realizations – i.e. immigrants are distinguishable from the offspring. This allows to test all defined scenarios (for example, to fit in scenario C we hide the generating exogenous function and we interval-censor the immigrants, more details in Section 7.2).

Exogenous functions. We select two functions for $s(t)$ the exogenous events intensity. The first function is a piece-wise constant function, inspired from the latent homogeneous Poisson process defined in Section 6.2. We select this function to allow control over the number of exogenous events in each observation interval. We denote the synthetic datasets generated with this exogenous function as **HP-pc**, and the resulted sampling event intensity is defined as:

$$\lambda(t) = \sum_{j=1}^n \frac{S(q_{j-1}, q_j]}{q_j - q_{j-1}} \mathbb{I}[q_{j-1} < t \leq q_j] + \sum_{t_i \in \Omega_t} \kappa \theta e^{-\theta(t-t_i)}, \quad (53)$$

where $q_j \in Q_T = \{0, 5, 10, 15\}$, $n = 2$; and $S(q_0, q_1] = 7$, $S(q_1, q_2] = 6$, and $S(q_2, q_3] = 8$.

The second immigrant function is a sinusoidal function, which emulates the seasonality often observed in real-world processes. We denote this dataset as **HP-sin**, and realizations are sampled from the event intensity:

$$\lambda(t) = \sin(t) + 2 + \sum_{t_i \in \Omega_t} \kappa \theta e^{-\theta(t-t_i)} \quad (54)$$

Hawkes kernel parametrization. For each of the above-defined exogenous function, we consider a Hawkes process with exponential memory kernel $\phi(t) = \kappa \theta e^{-\theta t}$. We consider two parameter combinations. The first combination defines a Hawkes process in a clearly

subcritical regime (i.e. each event spawn significantly less than one offspring): $\kappa = 0.6$, $\theta = 0.8$, resulting in a branching factor $n^* = 0.6$. The second combination is in a nearly-critical regime, where each event spawns in average close to one offspring. This results in realizations with larger numbers of events and pronounced clustering effects. We use the parameter set: $\kappa = 0.95$, $\theta = 1.15$, resulting in a branching factor $n^* = 0.95$.

Simulation algorithm. To be usable with all scenarios in Table 2, we generate sequences in which the exogenous and endogenous event times are distinguishable. We use a simulation algorithm that leverages the cluster structure of Hawkes process (Hawkes and Oakes, 1974; Reinhart, 2018), by first sampling the exogenous events and then all their direct and indirect offspring. The steps for generating the synthetic event sequences are:

1. First, we sample immigrants from the fixed exogenous function.
2. Second, we obtain offspring by sampling a Hawkes process with no background intensity and with the immigrant as the first event. We use rejection sampling (Dassios and Zhao, 2013). We denote the collection of an immigrant together with its offspring as a cascade (Rizoiu et al., 2017b).
3. Finally, we combine all cascades to obtain a sequence, which is a realization of a Hawkes process with the benchmark parameters.

For scenarios where we do not require the separation between immigrants and offspring (i.e., A and D), we combine the exogenous and endogenous time points. For scenarios that require one or both dimensions interval-censored, we compute the corresponding volumes by counting the number of events over pre-specified observation intervals.

7.2 Experimental Setup

Pre-process synthetic realizations. In our experiments in Section 7.3, the aim is to recover the parameters κ and θ of the *true* model used to generate the synthetic datasets. We test over all scenarios in Table 2, and for each scenario we use the exact same set of realizations constructed in Section 7.1. Prior to fitting, for each scenario we perform the following pre-processing on the realizations:

- A. We remove the distinction between immigrants and offspring, and we provide the immigrant intensity $s(t)$;
- B. We hide the immigrant intensity $s(t)$, and we observe immigrants and offspring separately;
- C. We interval-censor the immigrants, and we observe offspring as event times;
- D. We remove the distinction between immigrants and offspring, we interval-censor the resulting event stream, and we provide the immigrant intensity $s(t)$;
- E. We hide the immigrant intensity $s(t)$, we interval-censor the offsprings, and we observe immigrants (event times) and offspring (interval-censored) separately;
- F. We hide the immigrant intensity $s(t)$ and we individually interval-censor the immigrant stream and the offspring stream

Models and loss functions. For the scenarios where the offspring events are observed as event times (scenarios A-C), we fit both Hawkes and MBP processes using the PP-LL loss (Eq. (4)). This allows estimating the performances of MBP to estimate Hawkes parameters. For scenarios in which the offspring are interval-censored (D-F), we only fit MBP using both IC-LL (Eq. (18)) and SSE (Eq. (37)) loss functions. This allows comparing the performances of the two loss functions. For the separable settings (B, C, E, F) we prefer fitting using the endogenous version of the loss function. However, for scenario C, we compare the standard point process and the endogenous version of the loss function. Finally, for the non-separable scenarios (A and D), we use the non-endogenous loss functions as there is no distinction between immigrants and offspring.

Closed-form vs. approximate loss functions. We test the fitting performance gap between the closed-form and approximate versions of our models, using the approximation method specified in Section 4.3. Scenario E is used to test our numerically approximated models when a high number of discretization points are given, additionally presenting both endogenous and non-endogenous versions of the IC-LL and SSE loss function. Additionally, discretization tests which do not involve parameter estimation can be found in Appendix E.1 and further non-endogenous loss functions experiments can be found in Appendix E.2.

Additional setup. For Scenarios A-C, we consider 1,000 event sequences, which are further split into 50 groups to estimate parameters. For Scenarios D-F, we consider 10,000 sequences, also split into 50 groups to be jointly fit. The additional volume of sequences is to account for the loss of information from interval-censoring. For the scenarios where endogenous events are observed as event time (scenarios A - C), we consider both `HP-pc` and `HP-sin` datasets. For interval-censored endogenous events (scenarios D-F), only the more challenging `HP-sin` datasets are considered to limit computation time. In both cases, the sequences we generate are sampled until time-step $T = 30$. When we are testing interval-censored settings, we use uniform observation intervals with 5, 10, 15, 30, 60, and 100 observation periods — for example, with 10 observation intervals we calculate volumes over intervals $(0, 3], (3, 6], \dots, (27, 30]$.

In each scenario and model tested we fit 50 of that model corresponding to the 50 groups of synthetic sequences. We then calculate the average of the estimated parameters and compare the aggregated statistic against the true parameters.

7.3 Results

Our investigations in this section have four goals. First, we test the performance of MBP for retrieving the Hawkes parameters used to generate the datasets for scenarios A-C (Hawkes cannot be used for scenarios D-F). Second, we seek to quantify the performance loss due to increasingly larger data granularity when moving from scenario A to F. Third, we investigate the effects of using the endogenous loss introduced in Section 6.3 for the separable scenarios B, C, E, and F. Forth, we study the effects of using the lower bound approximation in Section 4.3 for scenarios D, E, F, and the impact of the number of discretization points.

7.3.1 FITTING FOR SCENARIOS A TO F

Scenario A. Table 3 shows the results of fitting the Hawkes realizations with both the Hawkes process and MBP for non-separable data and with knowledge of the parametrization

of the exogenous function. Visibly, the parameters fitted with Hawkes are closest to the true parameters, which is expected as the data is generated from a Hawkes model—i.e., this is the upper bound of how well parameters can be retrieved on each dataset. Perhaps surprisingly, MBP has very similar fitting performances, and we only observe a degradation on the `HP-sin` dataset. This suggests that MBP can be used as a drop-in alternative for fitting the parameters of Hawkes processes.

Table 3: Synthetic experiments for Scenario A: non-separable data, event times.

True model	True Params.	Model Fit	
HP-pc	$\kappa = 0.6$ $\theta = 0.8$	HP	κ 0.58 ± 0.043 θ 0.80 ± 0.087
		MBP	κ 0.58 ± 0.043 θ 0.78 ± 0.145
	$\kappa = 0.95$ $\theta = 1.15$	HP	κ 0.95 ± 0.015 θ 1.17 ± 0.073
		MBP	κ 0.95 ± 0.016 θ 1.21 ± 0.246
HP-sin	$\kappa = 0.6$ $\theta = 0.8$	HP	κ 0.60 ± 0.019 θ 0.80 ± 0.098
		MBP	κ 0.60 ± 0.018 θ 0.75 ± 0.192
	$\kappa = 0.95$ $\theta = 1.15$	HP	κ 0.95 ± 0.008 θ 1.14 ± 0.062
		MBP	κ 0.95 ± 0.010 θ 1.22 ± 0.227

Table 4: Synthetic experiments for Scenario B: separable data, exogenous and endogenous event times.

True model	True Params.	Model	
HP-pc	$\kappa = 0.6$ $\theta = 0.8$	HP-Endo	κ 0.59 ± 0.056 θ 0.81 ± 0.135
		MBP-Endo	κ 0.59 ± 0.056 θ 0.8 ± 0.093
	$\kappa = 0.95$ $\theta = 1.15$	HP-Endo	κ 0.94 ± 0.025 θ 1.17 ± 0.067
		MBP-Endo	κ 0.94 ± 0.025 θ 1.37 ± 0.228
HP-sin	$\kappa = 0.6$ $\theta = 0.8$	HP-Endo	κ 0.59 ± 0.024 θ 0.74 ± 0.11
		MBP-Endo	κ 0.59 ± 0.024 θ 0.75 ± 0.098
	$\kappa = 0.95$ $\theta = 1.15$	HP-Endo	κ 0.95 ± 0.021 θ 1.07 ± 0.28
		MBP-Endo	κ 0.95 ± 0.027 θ 1.1 ± 0.124

Scenario B. We distinguish between immigrants and offspring in this scenario, but we do not know the immigrant intensity. We fit the two synthetic datasets using the endogenous versions of MBP and Hawkes process with the multi-impulse exogenous function. Table 4 shows the obtained fitted parameters indicating very similar performances for both the Hawkes and MBP process. MBP even shows a slight advantage for all combinations of parameter and data sets, except for `HP-pc` dataset and parameters $\kappa = 0.95$ and $\theta = 1.15$. Furthermore, MBP even shows a lower standard deviation indicating that it is more stable when predicting parameters. These results also show the effectiveness of using the multi-impulse exogenous function in the presence of separable data, together with the endogenous loss function.

Scenario C. Table 5 shows the results of fitting in Scenario C, in which immigrants and offspring are separable, immigrants are interval-censored, and offspring are event times. Again, we can conclude that MBP and the Hawkes process have very similar performances. Similar to Scenario B, the only degradation in approximation quality is for `HP-pc` with the parameters $\kappa = 0.95$ and $\theta = 1.15$. Note that Table 5 also presents results for the non-endogenous version of the loss function, which we discuss in Section 7.3.2.

Scenario D. In this scenario, we do not distinguish between immigrants and offspring, and we observe the process as interval-censored. We use for the first time the novel loss functions introduced in Section 4. I.e., we fit the synthetic data using the IC-LL and SSE loss functions together with the MBP process. Note that we cannot use the standard Hawkes

Table 5: Synthetic experiments for Scenario C: separable data, interval-censored exogenous events and endogenous event times.

True model	True Params.	Model		True model	True Params.	Model	
HP-pc	$\kappa = 0.6$ $\theta = 0.8$	HP	κ 0.57 ± 0.064 θ 0.74 ± 0.097	HP-sin	$\kappa = 0.6$ $\theta = 0.8$	HP	κ 0.59 ± 0.025 θ 0.52 ± 0.08
		HP-Endo	κ 0.59 ± 0.056 θ 0.8 ± 0.093			HP-Endo	κ 0.59 ± 0.024 θ 0.75 ± 0.098
		MBP	κ 0.59 ± 0.059 θ 0.83 ± 0.138			MBP	κ 0.59 ± 0.024 θ 0.72 ± 0.138
		MBP-Endo	κ 0.59 ± 0.056 θ 0.81 ± 0.139			MBP-Endo	κ 0.59 ± 0.023 θ 0.73 ± 0.107
	$\kappa = 0.95$ $\theta = 1.15$	HP	κ 0.94 ± 0.025 θ 1.12 ± 0.065		$\kappa = 0.95$ $\theta = 1.15$	HP	κ 0.95 ± 0.021 θ 0.99 ± 0.117
		HP-Endo	κ 0.94 ± 0.025 θ 1.17 ± 0.067			HP-Endo	κ 0.95 ± 0.021 θ 1.1 ± 0.124
		MBP	κ 0.94 ± 0.025 θ 1.37 ± 0.237			MBP	κ 0.95 ± 0.03 θ 1.07 ± 0.296
		MBP-Endo	κ 0.94 ± 0.025 θ 1.37 ± 0.229			MBP-Endo	κ 0.95 ± 0.028 θ 1.07 ± 0.282

process when the events are observed as interval-censored (see Section 4). Table 6 shows the obtained fitting results for an increasing number of observation intervals. We fit using both the closed-form solution and the approximation introduced in Section 4.3. For the approximation, we use as many approximation points as the number of intervals.

We observe that the closed-form MBP processes perform exceptionally well, with no noticeable differences between IC-LL and SSE loss. In particular, for closed-form models, we obtain highly accurate parameter fittings even for small numbers of observations. However, when we use the numeric approximation of compensators, we observe a decrease in the accuracy of the recovered parameters. The degradation is prevalent only for θ , which is consistently overestimated. Interestingly, an increase in observation intervals does not yield sizable improvements for the approximate models. Thus, for this scenario, knowing the functional form of the underlying interval-censored Hawkes process (the exogenous function and kernel function) appears more important than having finer-grained observation periods.

Scenario E. Here, we separately observe immigrants (as event times) and offspring (interval-censored). We fit using the multi-impulse exogenous function and the SSE and IC-LL loss functions, with both the closed-form solution and the numerical approximation. Table 7 shows that both loss functions achieve highly accurate parameter fittings for the closed-form models, even for low numbers of observation intervals. However, the approximate models require higher numbers of observation intervals to recover the parameters. For $\kappa = 0.6$ and $\theta = 0.8$, we require at least 30 observation intervals to converge close to the correct θ value. For the other parameter setting, we need at least 60 intervals. Notably, the κ parameter is easier to fit and can be approximated using fewer intervals. We further explore the dependence of parameter estimation for the numerically approximated models in Section 7.3.2.

Scenario F. This is a separable scenario, in which both immigrants and offspring are interval-censored. Table 8 shows the fitting results, and we observe that the quality of parameter estimation improves as we increase the number of observation intervals. Inter-

Table 6: Synthetic experiments for Scenario D: non-separable data, interval-censored events. Note that only MBP can fit this kind of data.

True Params.	Loss Func.	Model	Number of Observation Intervals						
			5	10	15	30	60	100	
$\kappa = 0.6$ $\theta = 0.8$	SSE	Closed	κ	0.6 ± 0.007	0.6 ± 0.007	0.6 ± 0.007	0.6 ± 0.007	0.6 ± 0.006	0.6 ± 0.006
			θ	0.81 ± 0.092	0.81 ± 0.087	0.8 ± 0.07	0.8 ± 0.076	0.8 ± 0.072	0.8 ± 0.075
		Approx	κ	0.6 ± 0.007	0.6 ± 0.007	0.6 ± 0.007	0.6 ± 0.007	0.6 ± 0.006	0.6 ± 0.006
			θ	0.85 ± 0.099	0.85 ± 0.096	0.84 ± 0.077	0.84 ± 0.082	0.84 ± 0.079	0.84 ± 0.081
	IC-LL	Closed	κ	0.6 ± 0.007	0.6 ± 0.007	0.6 ± 0.007	0.6 ± 0.007	0.6 ± 0.006	0.6 ± 0.006
			θ	0.82 ± 0.091	0.81 ± 0.086	0.81 ± 0.072	0.8 ± 0.076	0.8 ± 0.073	0.8 ± 0.076
		Approx	κ	0.6 ± 0.007	0.6 ± 0.007	0.6 ± 0.007	0.6 ± 0.007	0.6 ± 0.006	0.6 ± 0.006
			θ	0.85 ± 0.098	0.85 ± 0.095	0.84 ± 0.08	0.84 ± 0.083	0.84 ± 0.08	0.84 ± 0.083
$\kappa = 0.95$ $\theta = 1.15$	SSE	Closed	κ	0.95 ± 0.004	0.95 ± 0.005				
			θ	1.16 ± 0.082	1.16 ± 0.091	1.16 ± 0.065	1.16 ± 0.1	1.16 ± 0.079	1.16 ± 0.088
		Approx	κ	0.95 ± 0.004	0.95 ± 0.005				
			θ	1.24 ± 0.093	1.24 ± 0.103	1.24 ± 0.074	1.24 ± 0.114	1.24 ± 0.09	1.24 ± 0.1
	IC-LL	Closed	κ	0.95 ± 0.004	0.95 ± 0.005				
			θ	1.16 ± 0.074	1.16 ± 0.078	1.16 ± 0.06	1.16 ± 0.09	1.16 ± 0.07	1.16 ± 0.082
		Approx	κ	0.95 ± 0.004	0.95 ± 0.005				
			θ	1.24 ± 0.083	1.24 ± 0.089	1.24 ± 0.068	1.24 ± 0.103	1.24 ± 0.079	1.24 ± 0.093

Table 7: Synthetic experiments for Scenario E: separable data, event time exogenous events and interval-censored endogenous events.

True Params.	Loss Func.	Model	Number of Observation Intervals						
			5	10	15	30	60	100	
$\kappa = 0.6$ $\theta = 0.8$	SSE	Closed	κ	0.60 ± 0.006	0.60 ± 0.006	0.60 ± 0.005	0.60 ± 0.006	0.60 ± 0.005	0.60 ± 0.005
			θ	0.79 ± 0.055	0.79 ± 0.047	0.79 ± 0.042	0.79 ± 0.039	0.79 ± 0.036	0.79 ± 0.036
		Approx	κ	10 ± 0	0.62 ± 0.006	0.61 ± 0.006	0.60 ± 0.006	0.60 ± 0.006	0.60 ± 0.006
			θ	0.01 ± 0	8.82 ± 0.866	9.55 ± 1.589	1.09 ± 0.091	0.91 ± 0.052	0.86 ± 0.043
	IC-LL	Closed	κ	0.60 ± 0.006	0.60 ± 0.005				
			θ	0.80 ± 0.053	0.80 ± 0.042	0.79 ± 0.037	0.79 ± 0.035	0.79 ± 0.032	0.79 ± 0.032
		Approx	κ	10 ± 0	0.63 ± 0.006	0.61 ± 0.006	0.60 ± 0.005	0.60 ± 0.005	0.60 ± 0.005
			θ	0.01 ± 0	8.22 ± 1.192	9.98 ± 0.103	1.17 ± 0.089	0.94 ± 0.045	0.87 ± 0.038
$\kappa = 0.95$ $\theta = 1.15$	SSE	Closed	κ	0.95 ± 0.004					
			θ	1.15 ± 0.076	1.15 ± 0.075	1.15 ± 0.073	1.15 ± 0.073	1.15 ± 0.072	1.15 ± 0.072
		Approx	κ	10 ± 0	1.14 ± 0.007	1.03 ± 0.005	0.96 ± 0.003	0.95 ± 0.004	0.95 ± 0.004
			θ	0.01 ± 0	9.41 ± 0.764	10 ± 0	10 ± 0	1.77 ± 0.177	1.43 ± 0.111
	IC-LL	Closed	κ	0.95 ± 0.004					
			θ	1.16 ± 0.068	1.16 ± 0.067	1.16 ± 0.065	1.16 ± 0.065	1.16 ± 0.065	1.16 ± 0.065
		Approx	κ	10 ± 0	1.17 ± 0.007	1.04 ± 0.005	0.96 ± 0.003	0.95 ± 0.004	0.95 ± 0.004
			θ	0.02 ± 0	9.95 ± 0.032	10 ± 0	10 ± 0	1.82 ± 0.164	1.46 ± 0.101

Table 8: Synthetic experiments for Scenario F: separable data, interval-censored exogenous and endogenous events.

True Params.	Loss Func.	Model	Number of Observation Intervals						
			5	10	15	30	60	100	
$\kappa = 0.6$ $\theta = 0.8$	SSE	Closed	κ	0.726 ± 0.004	0.682 ± 0.005	0.668 ± 0.005	0.642 ± 0.005	0.62 ± 0.005	0.612 ± 0.005
			θ	0.647 ± 0.021	0.641 ± 0.024	0.801 ± 0.031	0.995 ± 0.052	0.915 ± 0.052	0.865 ± 0.045
		Approx	κ	10 ± 0	0.621 ± 0.006	0.605 ± 0.006	0.601 ± 0.006	0.601 ± 0.006	0.601 ± 0.006
			θ	0.005 ± 0	8.823 ± 0.866	9.546 ± 1.589	1.09 ± 0.091	0.909 ± 0.052	0.856 ± 0.043
	IC-LL	Closed	κ	0.729 ± 0.004	0.69 ± 0.005	0.672 ± 0.005	0.642 ± 0.005	0.621 ± 0.005	0.613 ± 0.005
			θ	0.642 ± 0.019	0.675 ± 0.023	0.828 ± 0.029	0.997 ± 0.045	0.929 ± 0.044	0.878 ± 0.039
$\kappa = 0.95$ $\theta = 1.15$	SSE	Closed	κ	0.958 ± 0.002	1.496 ± 2.17	1.494 ± 2.171	0.95 ± 0.004	0.95 ± 0.004	0.95 ± 0.004
			θ	1.765 ± 0.098	1.362 ± 0.358	1.301 ± 0.344	1.283 ± 0.089	1.216 ± 0.08	1.19 ± 0.076
		Approx	κ	10 ± 0	1.139 ± 0.007	1.033 ± 0.005	0.958 ± 0.003	0.95 ± 0.004	0.95 ± 0.004
			θ	0.014 ± 0	9.409 ± 0.764	10 ± 0	10 ± 0	1.765 ± 0.177	1.433 ± 0.111
	IC-LL	Closed	κ	0.959 ± 0.002	0.953 ± 0.003	0.95 ± 0.003	0.949 ± 0.003	0.95 ± 0.004	0.95 ± 0.004
			θ	1.687 ± 0.085	1.501 ± 0.087	1.448 ± 0.092	1.323 ± 0.081	1.239 ± 0.073	1.205 ± 0.069
Approx	κ	10 ± 0	1.165 ± 0.007	1.043 ± 0.005	0.959 ± 0.003	0.949 ± 0.004	0.95 ± 0.004		
	θ	0.019 ± 0	9.953 ± 0.032	10 ± 0	10 ± 0	1.823 ± 0.164	1.456 ± 0.101		

estingly, the performance improvement is more constant for the IC-LL than SSE, as the number of intervals grows. When using the SSE, the parameters are estimated particularly poorly for 10 and 15 intervals. We also note that the numerical approximation requires between 60 and 100 intervals to approach the true parameters for this scenario. Knowing that these results are directly comparable with those for Scenario E (Table 7), we conclude that fitting in Scenario F is the most challenging as most information gets lost when interval-censoring.

7.3.2 ENDOGENOUS LOSS AND NUMBER OF APPROXIMATION POINTS

Endogenous vs. non-endogenous loss. Table 5 includes results for both the endogenous and non-endogenous loss function for Scenario C. We see that the endogenous versions consistently outperform the non-endogenous version. This is most prominent in the **HP-sin** dataset with parameters $\kappa = 0.6$ and $\theta = 0.8$, where the two Hawkes process models have drastic differences in the fitted θ parameter. Table 9 further shows comparisons between endogenous and non-endogenous numeric approximation models for Scenario E, with many approximation points. Here we see little or no improvement between endogenous and non-endogenous when using the SSE loss function. For the IC-LL loss function, we see that the endogenous version is more stable. Together with Scenario F’s conclusions (that IC-LL is more stable than SSE), we conjecture that the use of the endogenous IC-LL is preferable.

Number of approximation points. All results previously reported in this section use for the numerical approximation the same number of approximation points as the number of observation intervals. In Table 9, we report on the numeric approximation for Scenario E when 300 approximation points are used irrespective of the number of observation intervals. Intuitively, a larger number of approximation points should yield better estimates of the compensator and better parameter fits, with the cost of higher computation time. We see that only slight improvement for the normal IC-LL loss function as the number of observation intervals increases. For all other settings, endogenous or not, the estimated parameters

Table 9: Large number of discretization points experiment. Scenario E: separable data, interval-censored exogenous and endogenous events.

Loss Func.	Model		Number of Observation Intervals					
			5	10	15	30	60	100
SSE	Normal	κ	0.95 ± 0.003	0.95 ± 0.003	0.95 ± 0.003	0.95 ± 0.003	0.95 ± 0.003	0.95 ± 0.003
		θ	1.23 ± 0.072	1.23 ± 0.071	1.23 ± 0.071	1.23 ± 0.07	1.23 ± 0.069	1.23 ± 0.069
	Endogenous	κ	0.95 ± 0.003	0.95 ± 0.003	0.95 ± 0.003	0.95 ± 0.003	0.95 ± 0.003	0.95 ± 0.003
		θ	1.23 ± 0.072	1.23 ± 0.071	1.23 ± 0.071	1.23 ± 0.07	1.23 ± 0.069	1.23 ± 0.069
IC-LL	Normal	κ	0.95 ± 0.003	0.95 ± 0.003	0.95 ± 0.003	0.95 ± 0.003	0.95 ± 0.003	0.95 ± 0.003
		θ	0.95 ± 0.054	0.96 ± 0.071	0.97 ± 0.071	0.98 ± 0.06	1 ± 0.055	1.03 ± 0.055
	Endogenous	κ	0.95 ± 0.003	0.95 ± 0.003	0.95 ± 0.003	0.95 ± 0.003	0.95 ± 0.003	0.95 ± 0.003
		θ	1.24 ± 0.065	1.24 ± 0.064	1.24 ± 0.064	1.24 ± 0.063	1.24 ± 0.063	1.24 ± 0.063

are surprisingly stable. This suggests that the performances of the approximation method are dependent on the number of approximation points rather than intervals.

8. Real World Experiments

We evaluate our proposed MBP process and its variants on **ACTIVE** (Rizoiu et al., 2017b), a real-world social media dataset containing views to Youtube videos and the tweets that mention them. The task is to predict the future popularity of Youtube videos (their future views) by accounting for the exogenous influence of tweets and the endogenous amplification within Youtube (for example, due to word-of-mouth processes). Both the exogenous (immigrants) and the endogenous (offspring) are in interval-censored format – counts per day. Therefore, we fit using Scenario F (also denoted here below as IC-IC) on a subset of days, and we forecast the future. We compare our MBP process to the HIP process presented in Rizoiu et al. (2017b), the current state of the art in predicting popularity under exogenous influence. The predicted number of views produced by each model is evaluated using average percentile error (APE) and symmetric mean absolute percentage error (sMAPE).

8.1 Dataset and prediction setting

Dataset. We use the **ACTIVE** dataset introduced by Rizoiu et al. (2017b). The dataset contains information about more than 14,000 YouTube videos published between 2014-05-29 and 2014-12-26, and the corresponding Tweets in the time range share the video. For each video, we consider the first 120 days of views and Tweets. We fit model parameters on the first 90 days and we use the later 30 days for evaluation. We denote the number of Tweets at day i for a video as $[\#Tweets \text{ on day } i]$ and the number of YouTube views for a video at day i as $[\#Views \text{ on day } i]$.

Prediction setting. We replicate the evaluation setup introduced in (Rizoiu et al., 2017b). To evaluate our models, we predict the number of times a YouTube video is viewed from day 91 to 120. We consider that the number of tweets (the exogenous influence) is known in the prediction period.

Compared approaches. We evaluate the approximate compensator MBP processes, closed-form MBP processes, and HIP processes, which can be considered an approximation of the MBP process, as per Section 5.3. We also fit and evaluate these models for

both the IC-LL and SSE loss functions; and the exponential and power-law trigger kernel when applicable (the closed-form MBP process only exists for the exponential kernel). Furthermore, we use the LHPP exogenous function as the ACTIVE dataset is in the IC-IC setting. It follows that the LHPP exogenous function simplifies to the number of Tweets per day as the ACTIVE dataset presents unit-sized observation intervals (in days). Notably, in (Rizoiu et al., 2017b), the HIP process uses only the power-law triggering kernel with the SSE loss function. Thus, the HIP process with exponential kernel and IC-LL loss function combinations are new to our MBP process framework.

Three fitting procedure augmentations. Following Rizoiu et al. (2017b), we introduce three augmentations to improve fitting and forecasting performances. The first two augmentations enhance the exogenous intensity function, while the third is a workaround for the local optima in the loss function.

The first two augmentations are required because the models we discuss in this work make the implicit assumption that the exogenous intensity $s(t)$ completely describes all the immigrants that enter the process. For scenarios B, C, E, F, this implies that the observed exogenous events are the only possible parents for the offspring. However, this assumption is unrealistic for real data. For example, the views of YouTube videos can also be driven by other sources of influences outside Tweets, such as Facebook or the radio. We account for unobserved exogenous influence by augmenting the exogenous intensity $s(t)$. First, we scale $s(t)$ with a fitted constant μ . Second, we add two learnable parameters (γ and ν) to account for unobserved external intensity. The augmented exogenous intensity for each day i is:

$$\hat{s}[i] = \gamma \cdot \llbracket t = 0 \rrbracket + \nu \cdot \llbracket t > 0 \rrbracket + \mu \cdot [\text{\#Tweets on day } i], \quad (55)$$

where μ corresponds to the scaling constant of the observed exogenous influence; and γ and ν correspond to parameters accounting for unobserved external influence.

The third augmentation deals with the non-convexity of the loss surface (see Appendix D for more details), which can cause the gradient descent minimizer to get stuck into local optima. We address this by refitting each video 10 times, starting with randomly selected initial parameters. We chose as the final parameters the combination with the lowest loss.

Forecasting future views using MBP. We forecast the expected views in the days 91 to 120 using the numeric approximation scheme for the compensators, found in Proposition 7, and leveraging the observed views in days 1 to 90. Specifically, the forecasted number of views on day i is:

$$\begin{aligned} \text{Predicted}[i] &= \hat{s}[90 + i] + \sum_{j=1}^{90} [\text{\#Views on day } j] \int_{i-j-1}^{i-j} \phi(y + 90) dy \\ &+ \sum_{k=91}^{90+i-1} \Xi[k - 1, k] \int_{i-k-1}^{i-k} \phi(y + 90) dy, \quad \text{for } i \geq 91 \end{aligned} \quad (56)$$

where $\hat{s}[j]$ is defined as per Eq. (55).

We obtain this prediction scheme by replacing the compensator values evaluated between days 1 and 90 with the observed views — as the expectation of the compensator is equivalent to the expected number of events for a non-homogeneous point process. Thus, the fitted compensator only needs to be used when extrapolating past days 90.

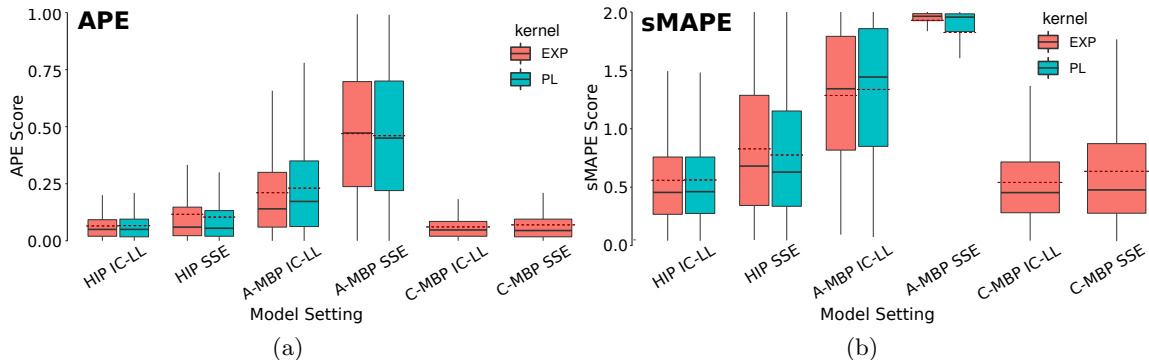


Figure 5: **Evaluation of future popularity prediction using APE (a) and sMAPE (b).** For each model, the boxplots aggregate the APE for all videos in the dataset. A-MBP denotes the approximate compensator MBP process variant, and C-MBP denotes the closed-form compensator MBP process variant. For each boxplot, the solid line denotes the median, and the dashed line denotes the mean. The combination HIP SSE PL is the baseline reported in (Rizoiu et al., 2017b)

Evaluation measures. We evaluate the prediction for days 91 to 120 using two evaluation metrics: (1) average percentile error (APE) and (2) symmetric mean absolute percentage error (sMAPE). APE was introduced in Rizoiu et al. (2017b) and is defined as the absolute difference between the recorded YouTube views percentiles and the predicted YouTube views percentile. The measure accounts for the long-tail distribution of online popularity. Intuitively, the impact of errors of the same size should be more significant for unpopular videos than for popular videos. sMAPE is defined as a normalized error of the true YouTube views and the predicted YouTube views over the entire sequence. Noteworthy, sMAPE is a local error measure (only depends on one video). In contrast, APE is a global measure that depends on both the error on the current video and the errors made on all other videos.

8.2 Results

We measure the APE (Fig. 5a) and sMAPE (Fig. 5b) for all HIP and MBP configurations, summarized as boxplots. We measure the impact of the choices of three components: the kernel (power-law vs. exponential), the loss functions (IC-LL vs. SSE), and the model (closed-form MBP, approximate MBP, and HIP). Note that the combination HIP, SSE, and PL kernel is the baseline reported in (Rizoiu et al., 2017b), for which we match the performances claimed by its authors.

We can see that the choice of the kernel does not change the APE value by much, with power-law slightly over-performing exponential (as previously reported in literature (Mishra et al., 2016)). Visibly, the choice of loss function has a more significant impact on performances, with IC-LL constantly outperforming SSE. This is particularly visible for the approximate MBP processes (A-MBP) and also present for both HIP and the closed-form MBP to a lesser extent. The result is not surprising as the IC-LL loss function comes from the minimization of the corresponding Poisson distribution defined by the MBP com-

pensator, whereas the SSE loss function comes from changing the convex generator of a Bregman divergence to obtain an alternative loss function.

The choice of model is also significant, with the closed-form MBP performing best for each of the loss function choices. This was expected, as HIP and the approximate MBP are both approximations to the closed-form MBP process (for power-law, MBP processes not having a closed-form solution). Perhaps surprisingly, the HIP has lower APE values than approximate MBP process with the same loss function and triggering kernel. This is because the HIP approximation is designed explicitly for unit time intervals — as presented in Section 5.3 — and would perform better than the more general approximate MBP.

We draw very similar conclusions from studying sMAPE performance measure (Fig. 5b). The only main difference is that the choice of kernel engenders a larger performance difference; for example, the 75% quantile for HIP SSE is much lower for power-law than exponential; similarly, the approximate MBP (A-MBP) SSE with power-law has a lower 25% quantile than the exponential kernel. A-MBP IC-LL performs slightly worse with a power-law triggering kernel than the exponential triggering kernel, similar to the APE boxplot.

Summary. Overall, we summarize the three main findings shown by both the local and global error metrics. First, the IC-LL loss function outperforms SSE. Second, the closed-form MBP outperforms numerical approximations (A-MBP and HIP). This follows naturally, given both of those processes are approximations of the closed-form MBP process. Third, the HIP approximation (Rizoiu et al., 2017b) — which is specialized for unit time intervals — outperforms the general approximation presented in the compensator approximation MBP process.

9. Related Work

We structure the related work into three main themes. First, we focus on prior work dedicated to estimating the parameters of Hawkes processes, in both event-time and interval-censored settings. Second, we consider alternative theoretic modeling paradigms and augmented Hawkes processes, and we investigate their link to the Hawkes processes. Finally, we consider the applications of Hawkes processes and other models in various domains.

9.1 Hawkes model parameter estimation

Several techniques have been proposed for estimating the parameters of a Hawkes model from data. Here, we concentrate on techniques using event-time data (other than the typical maximum likelihood estimates detailed in Section 2.3) and interval-censored data, both parametric and non-parametric.

Event time models. In the setting of online learning, Piggott and Solo (2018) propose an online estimator for the parameters of a Hawkes process by using a Laguerre basis expansion. The RedQueen algorithm (Zarezade et al., 2017) provides a framework for expressing a Hawkes process’s counting process and intensity function as a jump stochastic differential equation, providing an online algorithm with provable guarantees (Zarezade et al., 2018). Several studies have linked the Hawkes process to the infinite-server queues when the Hawkes process characterizes the arrivals into the queue. Koops et al. (2018) obtain a system of differential equations that characterize the joint distribution of arrival

intensity and the number of customers. Similarly, Daw and Pender (2018b) find differential equations to characterize the moments in several different settings. Finally, Gao and Zhu (2018) show that the queue length process is limited to a non-Markovian Gaussian process in the asymptotic regime of a stationary Hawkes process. More related to the current work, Xu et al. (2017) address the problem of fitting a Hawkes process observed during a finite interval of time – denoted as a double-censored event sequence. Note that their definition of *censored* is different than our interval-censoring in Section 4.1, i.e., they observe all event times during the given interval and nothing before and after. To avoid edge effects when the history is missing, Xu et al. (2017) simulate many possible prefixes for the given observed window.

Most of the approaches mentioned above estimate Hawkes processes using parametric models. In contrast, Dion and Lemler (2020) use trigonometric basis vectors to provide a non-parametric estimator of one-dimensional diffusion processes characterized by Hawkes processes. Similarly, Li et al. (2017) use a Fourier transform to provide a non-parametric estimator for the multidimensional Hawkes process. Zhang et al. (2019, 2020) propose Bayesian estimation procedures for the parameters of the Hawkes process kernel, which leverage the Hawkes process’s cluster structure.

The above approaches are typically limited to event time data and cannot estimate model parameters in the presence of interval-censored or mixed data. Our approach can estimate parameters seamlessly from both event time and interval-censored data and operate on mixtures of the two.

Interval-censored models. A series of studies show that the Hawkes process can be estimated in the interval-censored setup using an integer-valued auto-regressive (INAR) model. Kirchner (2016), and in their follow-up work in (Kirchner, 2017), show that the distribution of the resulting ‘bin-count sequences’ (i.e., number of events in each interval) can be approximated by the (multivariate) INAR(p) model. They establish a least-squares estimation of the INAR(p) model, which yields estimates for the underlying multivariate Hawkes process after appropriate scaling. The quality of the estimates is compared against maximum likelihood estimates (on event-times) in (Kirchner and Bercher, 2018). At first glance, these studies are similar to our work, as the link to the INAR model provides a discrete-time estimator of the Hawkes process. However, they do not expose the connection between the Hawkes process’s event-time and interval-censored formulations. Therefore, they do not establish a correspondence between the discrete and continuous regimes.

For other interval-censored settings, Lu (2019) presents several Taylor’s expansion approximation algorithms for several thinning-based count processes, including the previously mentioned INAR model. Similarly, Manolakis et al. (2019) provide a survey of signal processing approaches for interval-censored processes, detailing many different auto-regressive models. Like the INAR model, there is no theoretical correspondence between the various discrete models and the underlying true continuous-time process.

Closest to our work, the Hawkes intensity process (HIP) (Rizoïu et al., 2017b) defines an estimator as the Hawkes process intensity function’s expectation. It fits the new process in an interval-censored setting by using a sum of squared error loss function. This study has a series of shortcomings already outlined in Section 2.4. In comparison, this work introduces a new point process (the non-homogeneous Mean Behavior Poisson (MBP) process) whose intensity is the expected intensity of a Hawkes process of equivalent parameters. The MBP

allows fitting both event-time and interval-censored data. We further show the specific assumption needed to recover the HIP process.

Among the non-parametric approaches, Shlomovich et al. (2020) propose the estimation of aggregated Hawkes process using a Monte Carlo Expectation-Maximization algorithm. A spectral method of approximating stationary Hawkes process, based on Whittle’s approach, is established by considering a mixing condition with polynomial decay rates from their Poisson clustering structure (Cheysson and Lang, 2020). There are prior works that propose solutions using panel count data analysis – an inherently non-parametric approach. Ding et al. (2018) propose a Gaussian process-modulated Poisson process that permits panel data observations (i.e., interval-censored). Later, Moreno et al. (2020) wrap several popular panel count inference methods to deal with incomplete data and the Poisson process assumption’s mis-specification. Note that these approaches estimate Poisson processes, not Hawkes processes, and are not directly linked to the current work apart from the presentation of the data.

Our study differs from the above-mentioned by connecting the Hawkes process with a non-homogeneous Poisson process and providing a generalized treatment of the HIP models. Notably, our proposed mean behavior Poisson process relates to the Hawkes process by a direct parameter equivalence, which provides a bijection between the models which the previous literature did not have. Furthermore, we differentiate from prior studies by providing a singular model to fit both interval-censored and event-time data; only the log-likelihood function changes to accommodate the type of data. Finally, our proposed exogenous functions allow a mixed dataset of interval-censored and event-time data.

9.2 Other modeling paradigms and their links to the Hawkes model

The Hawkes processes are not the only option for modeling events in continuous time and various other models have also been used. Here we present some of these alternatives and how they related to Hawkes.

Linking Hawkes to other models. In their earlier work, Lewis and Shedler (1979) propose a foundational connection between homogeneous and non-homogeneous Poisson processes. They designed a thinning procedure – a simple and efficient algorithm for simulating non-homogeneous Poisson processes from homogeneous Poisson processes through thinning. This method was also adapted for Hawkes processes and is the de-facto method of simulating Hawkes process event sequences (Ogata, 1981). More recently, the Hawkes process has been linked to epidemic models (Rizoiu et al., 2018b). More specifically, the expectation of the intensity of the new infection in a stochastic Susceptible-Infectious-Recovery (SIR) epidemic model over all possible recovery processes is equal to the event intensity in a finite population Hawkes process (HawkesN). HawkesN is a Hawkes process in which the total number of events is limited and for which the remaining number of events modulates the intensity. Kong et al. (2020a) presented a generalized connection between Hawkes processes and epidemic models for arbitrary recovery time distributions and established relationships between the (latent and arbitrary) recovery time distribution, recovery hazard function, and the infection kernel of self-exciting processes.

Hawkes properties and augmented models. Other studies focus on analyzing other aspects of the Hawkes process that are not directly used to connect different models and

estimation procedures. Although these studies are only tangentially related to our work, we include some of these theoretical studies for completeness. Cordi et al. (2018) show that univariate symmetric Hawkes processes are only weakly causal. They find that reversed event sequences have similar point process log-likelihood scores and sometimes even yield better fits. Zino et al. (2018) investigate the epidemic threshold of Susceptible-Infected-Susceptible models in the presence and absence of self-excitation in time-varying networks. The paper additionally proposes a model where self-excitement govern the temporal evolution of an activity-driven network. Embrechts and Kirchner (2018) propose several graph-theoretic objects which summarize the branching structure of a multivariate Hawkes process. Daw and Pender (2018a) propose an ephemerally self-excited process which adds an additional stochastic component to the time in which excitement affects the process. Intuitively, this is motivated by how past events in epidemics only influence the future as long as the event stays active (say, as long as a person is infectious). Finally, Dion et al. (2019) introduce a new class of diffusion processes where jumps are driven by multivariate nonlinear Hawkes processes.

Other point process modeling paradigms. Other models have been used in event time modeling as an alternative to Hawkes processes. Before being used to estimate Hawkes processes (as described above), the integer auto-regressive (INAR) model was proposed as a discrete alternative to the continuous-valued auto-regressive process (Al-Osh and Alzaid, 1987). Renewal processes are also a common alternative to the Hawkes process. For example, Mishra et al. (2020) propose a generalized renewal process that arises from the expectation of an age-dependent branching process. The renewal process generalization accounts for exogenous events and the time varying-reproduction number for modeling epidemics; they tested their approach on COVID-19 case data in South Korea. Other point process modeling paradigms make use of Markov processes. For example, Soumaré and Tafolung (2017) propose a two-state Markov switching model to model risk-based pricing models. Stochastic differential equations are another method of characterizing the dynamics of event time processes, with links to the Hawkes process as per the prior mentioned RedQueen algorithm Zarezade et al. (2018). A stochastic differential equation framework has been proposed for modeling information diffusion over networks (Wang et al., 2016). Similarly, Zarezade et al. (2017) uses an optimal control problem for jump stochastic differential equations to predict when to post in a social network for visibility.

Our study presents a novel variant of the non-homogeneous Poisson process, the mean behavior Poisson. Although we mainly use MBP to approximate the Hawkes process in interval-censored settings, it can be used as an alternative to Hawkes self-excitation. MBP is a non-homogeneous Poisson process, which has nicer properties (see the independent increments discussion in Section 2). Furthermore, the exogenous functions that we introduce can be used for other point process intensity functions.

9.3 Applications of Hawkes processes

Earthquakes, finance, and epidemics. Hawkes processes have long been used for modeling events in various domains, from modeling the aftershocks of earthquakes to predicting social network interactions. One of the first domains to adapt Hawkes processes was earthquake modeling. The epidemic-type aftershock (ETAS) (Ogata, 1988) model assumes that

each earthquake generates aftershocks at a rate governed by a Hawkes model with a power-law decay rate. Later works show the connection to the Richter intensity scale and provide an analytical solution for Hawkes process variants (Ogata, 1999; Helmstetter and Sornette, 2002a,b). The Hawkes processes have also been used in financial markets. One such work uses a multivariate Hawkes process to account for dynamics of market prices by tailoring four Hawkes kernels for their domain (Bacry and Muzy, 2014). Similarly, Hawkes processes have also been used to study epidemic spread. Zino et al. (2020) use Hawkes processes to study the bursty activity patterns in social, temporal networks to help determine where targeted behavioral changes could accelerate the erratic of epidemics.

Information spread. With the rise of social media platforms, many studies use Hawkes processes to characterize how information develops and moves around social networks. These studies concentrate on either the users of the network or the individual pieces of content (like a post). Zhao et al. (2015) use self-exciting point processes to examine the Twitter social network and make predictions on a Tweet’s final number of reshares by looking at its current reshare history. Similarly, Kobayashi and Lambiotte (2016) predict the time evolution of retweet activity by taking into account the circadian nature of users and the aging of information. Hawkes has been effectively applied to social media platforms other than Twitter. The Hawkes process was found to outperform reinforced Poisson processes for individual micro-blogs on Sina Weibo, a Chinese micro-blogging network. Zarezade et al. (2016) propose a spatial-temporal Hawkes process with a periodic decaying kernel, which considers location-based data of users checking-in to leverage the observation that users are influenced by locations in which their close friends have recently visited. Wang and Resnick (2019) incorporate the periodic nature of users on social media by switching from a Hawkes process in the day into a non-homogeneous Poisson process at night.

Cascade size. Cha et al. (2009) analyze the Flickr social network, finding that popular photos do not necessarily spread widely and popular photos spread slowly. The study additionally found that information exchanged between friends likely accounted for over 50% of content sharing, with significant delays between any additional hops. Similarly, Goel et al. (2012) find that in a variety of social network domains, most of the cascade sizes in network diffusions are small, terminating within one degree of an initial “seed”. For large cascades, a study found that in addition to temporal and structural features being key predictors, breadth rather than depth is a better indicator of a large cascade. Finally, Yu et al. (2017) unify the task of predicting cascade sizes at a given time and the time when a cascade reaches a specific size. The authors propose an estimation of the cascading process, and the behavioral dynamics are aggregated.

User influence. In a Flickr dataset, Goyal et al. (2010) investigate the influence probabilities between users in a structured social network graph. The study presents three classes of models for the influence probabilities: the first which assumes that the influence does not change with time; the second assumes influence is a function of continuous time; the third proposes a discrete approximation of the continuous-time models. Matsubara et al. (2012) provide an economical alternative to the Hawkes process to model the rise and fall pattern of influence propagation used to investigate the fast propagation of news rumors in social networks. Kempe et al. (2003) propose a greedy strategy to find the most influential node in a network to determine which nodes can be targeted to trigger a large cascade of idea

adaptation. RizoIU et al. (2018a) propose a method to estimate user influence in retweet data sets when the direct retweeting relation (who retweets whom directly) is latent. They use a Hawkes-inspired retweeting probability and compute user influence as the expected number of retweets over all possible unfolding of retweet cascades.

Content popularity. Making predictions about the popularity of online content has been another focus of study in social networks. Szabo and Huberman (2010) present a method for accurately predicting the long-time popularity from early measurements of user access, with empirical results on YouTube and Digg datasets. Another study found that group-level popularity is a necessary and more practical measurement to predict the popularity of online content (Hoang et al., 2017). To predict online video popularity, Ding et al. (2015) propose a dual sentimental Hawkes process that incorporates sentimental features in addition to event counts. RizoIU et al. (2017b) propose the HIP model already discussed in Section 2.4 and apply it to characterize and predict the popularity online YouTube videos.

Fake users and news. There have also been studies on detecting differences in online content, such as differentiating between fake news and regular users. (Tschatschek et al., 2018) is one example of such a study, where a Bayesian inference algorithm is used for detecting fake news and jointly learning about the accuracy of users who flag such content over time. Kong et al. (2020b) propose a dual mixture model to jointly fit a group of cascades (large and small) relating to content from the same source. They use the resulted parameters to build diffusion embeddings for news sources – i.e., a vector that describes a news source based on how the retweet cascades concerning produced articles propagate through Twitter. The authors show that the diffusion embeddings induce a space in which controversial and reputable news sources are separable.

In this work, we address the application of popularity prediction — therefore, we classify the present work under the heading content popularity here above. In our experiments in Section 8.2, we show that we outperform HIP (the current state of the art in content popularity prediction).

10. Conclusion

This research establishes the Mean Behaviour Poisson (MBP) process, a novel Poisson process which has a direct parameter correspondence to the popular self-exciting Hawkes process. Unlike the original Hawkes process, the MBP process can be used in scenarios where the data is given by interval-censored volumes and not event times. This is accomplished by using our proposed interval-censored log-likelihood (IC-LL) to fit an MBP process. In addition to allowing the MBP process to be evaluated in this setting, we introduce the multi-impulse exogenous function and latent homogenous Poisson process exogenous function to account for scenarios when the exogenous events — which be either event times or interval-censored volumes — can be differentiated from the endogenous events. Furthermore, we provide a number of approximation methods such that the intensity and compensator function of the MBP process can be calculated when no analytical solution exists. The MBP framework further justifies the Hawkes Intensity Process (HIP) as an approximation of a MBP process (RizoIU et al., 2017b). Our models are further verified through empirical testing. We find that in real world datasets that our MBP process outperforms the previously proposed HIP model in the ACTIVE dataset.

Future work

Given the parameter correspondences between the univariate MBP process and Hawkes process, an important continuation of the work is finding a corresponding model to the multivariate and marked variants of the Hawkes process. The restriction of univariate Hawkes processes not being applicable interval-censored datasets holds true for the multivariate counterpart. Thus, having a multivariate MBP process would allow for parameter fitting for Hawkes processes in the absence of event times. Furthermore, finding theoretical bounds for our approximation methods for the MBP compensator is highly desirable as closed-form solutions for the MBP intensity and compensator functions are elusive for popular Hawkes process triggering kernels, i.e., the power-law kernel function.

References

- M. A. Al-Osh and A. A. Alzaid. First-order integer-valued autoregressive (INAR(1)) process. *Journal of Time Series Analysis*, 8(3):261–275, 1987. ISSN 14679892. doi: 10.1111/j.1467-9892.1987.tb00438.x.
- Ifigeneia Apostolopoulou, Scott Linderman, Kyle Miller, and Artur Dubrawski. Mutually regressive point processes. In *NeurIPS*, 2019.
- Emmanuel Bacry and Jean François Muzy. Hawkes model for price and trades high-frequency dynamics. *Quantitative Finance*, 14(7):1147–1166, 2014. ISSN 14697696. doi: 10.1080/14697688.2014.897000. URL <https://www.tandfonline.com/doi/abs/10.1080/14697688.2014.897000>.
- Emmanuel Bacry, Iacopo Mastromatteo, and Jean-François Muzy. Hawkes processes in finance. *Market Microstructure and Liquidity*, 01(01), 2015.
- Arindam Banerjee, Srujana Merugu, Inderjit S Dhillon, and Joydeep Ghosh. Clustering with bregman divergences. *Journal of machine learning research*, 6(Oct):1705–1749, 2005.
- E Borel. Sur l’emploi du théoreme de bernoulli pour faciliter le calcul d’une infinité de coefficients. application au probleme de l’attentea un guichet. *CR Acad. Sci. Paris*, 214: 452–456, 1942.
- Clive Bowsher. Modelling security market events in continuous time: Intensity based, multivariate point process models. *Journal of Econometrics*, 141(2):876 – 912, 2007.
- D.R. Brillinger, P.M. Guttorp, and F.P. Schoenberg. *Encyclopedia of environmetrics*, volume 3. Wiley, 2002.
- Qi Cao, Huawei Shen, Keting Cen, Wentao Ouyang, and Xueqi Cheng. DeepHawkes: Bridging the gap between prediction and understanding of information cascades. In *International Conference on Information and Knowledge Management, Proceedings*, volume Part F131841, pages 1149–1158, New York, NY, USA, nov 2017. Association for Computing Machinery. ISBN 9781450349185. doi: 10.1145/3132847.3132973. URL <https://dl.acm.org/doi/10.1145/3132847.3132973>.

- Meeyoung Cha, Alan Mislove, and Krishna P. Gummadi. A measurement-driven analysis of information propagation in the Flickr social network. In *WWW'09 - Proceedings of the 18th International World Wide Web Conference*, pages 721–730, 2009. ISBN 9781605584874. doi: 10.1145/1526709.1526806.
- Felix Cheysson and Gabriel Lang. Strong mixing condition for Hawkes processes and application to Whittle estimation from count data. mar 2020. URL <http://arxiv.org/abs/2003.04314>.
- Michael Collins, Robert E Schapire, and Yoram Singer. Logistic regression, adaboost and bregman distances. *Machine Learning*, 48(1-3):253–285, 2002.
- Marcus Cordi, Damien Challet, and Ioane Muni Toke. Testing the causality of Hawkes processes with time reversal. *Journal of Statistical Mechanics: Theory and Experiment*, 2018(3):033408, mar 2018. ISSN 17425468. doi: 10.1088/1742-5468/aaac3f.
- D. R. Cox and V. Isham. *Point Processes*. Chapman & Hall, 1980.
- D. R. Cox and P. A. W. Lewis. Multivariate point processes. In *Proceedings of the Sixth Berkeley Symposium on Mathematical Statistics and Probability, Volume 3: Probability Theory*, pages 401–448, Berkeley, Calif., 1972. University of California Press.
- Riley Crane and Didier Sornette. Robust dynamic classes revealed by measuring the response function of a social system. *Proceedings of the National Academy of Sciences*, 105(41):15649–15653, 2008.
- D.J. Daley and D. Vere-Jones. *An introduction to the theory of point processes. Vol. I. Probability and its Applications* (New York). Springer-Verlag, New York, second edition, 2003.
- Angelos Dassios and Hongbiao Zhao. Exact simulation of hawkes process with exponentially decaying intensity. *Electronic Communications in Probability*, 18:13 pp., 2013.
- Andrew Daw and Jamol Pender. An Ephemeral Self-Exciting Point Process. nov 2018a. URL <http://arxiv.org/abs/1811.04282>.
- Andrew Daw and Jamol Pender. Queues Driven by Hawkes Processes. *Stochastic Systems*, 8(3):192–229, sep 2018b. ISSN 1946-5238. doi: 10.1287/stsy.2018.0014.
- Hongyi Ding, Young Lee, Issei Sato, and Masashi Sugiyama. Variational inference for Gaussian processes with panel count data. In *34th Conference on Uncertainty in Artificial Intelligence 2018, UAI 2018*, volume 1, pages 290–299. Association For Uncertainty in Artificial Intelligence (AUAI), mar 2018. ISBN 9781510871601. URL <http://arxiv.org/abs/1803.04232>.
- Wanying Ding, Yue Shang, Lifan Guo, Xiaohua Hu, Rui Yan, and Tingting He. Video popularity prediction by sentiment propagation via implicit network. In *International Conference on Information and Knowledge Management, Proceedings*, volume 19-23-Oct-2015, pages 1621–1630. Association for Computing Machinery, oct 2015. ISBN 9781450337946. doi: 10.1145/2806416.2806505.

- Charlotte Dion and Sarah Lemler. Nonparametric drift estimation for diffusions with jumps driven by a Hawkes process. *Statistical Inference for Stochastic Processes*, 23(3):489–515, oct 2020. ISSN 15729311. doi: 10.1007/s11203-020-09213-5. URL <https://link.springer.com/article/10.1007/s11203-020-09213-5>.
- Charlotte Dion, Sarah Lemler, and Eva Löcherbach. Exponential ergodicity for diffusions with jumps driven by a Hawkes process. apr 2019. URL <http://arxiv.org/abs/1904.06051>.
- Leanne J Dong and John van der Hoek. An explicit numerical algorithms to the solution of volterra integral equation of the second kind. *ArXiv e-prints*, 2019.
- P. Embrechts and M. Kirchner. Hawkes graphs. *Theory of Probability and its Applications*, 62(1):132–155, may 2018. ISSN 10957219. doi: 10.1137/S0040585X97T988538.
- Xuefeng Gao and Lingjiong Zhu. Functional central limit theorems for stationary Hawkes processes and application to infinite-server queues. *Queueing Systems*, 90(1-2):161–206, oct 2018. ISSN 15729443. doi: 10.1007/s11134-018-9570-5.
- Sharad Goel, Duncan J. Watts, and Daniel G. Goldstein. The structure of online diffusion networks. In *Proceedings of the ACM Conference on Electronic Commerce*, pages 623–638, 2012. ISBN 9781450314152. doi: 10.1145/2229012.2229058.
- Amit Goyal, Francesco Bonchi, and Laks V.S. Lakshmanan. Learning influence probabilities in social networks. In *WSDM 2010 - Proceedings of the 3rd ACM International Conference on Web Search and Data Mining*, pages 241–250, 2010. ISBN 9781605588896. doi: 10.1145/1718487.1718518.
- Jan Grandell. Point processes and random measures. *Advances in Applied Probability*, pages 502–526, 1977.
- Stephen J. Hardiman, Nicolas Bercot, and Jean-Philippe Bouchaud. Critical reflexivity in financial markets: a Hawkes process analysis. *European Physics Journal B*, 86(10):442, 2013.
- Alan G. Hawkes. Spectra of some self-exciting and mutually exciting point processes. *Biometrika*, 58(1):83, 1971.
- Alan G Hawkes and David Oakes. A cluster process representation of a self-exciting process. *Journal of Applied Probability*, 11(3):493–503, 1974.
- Agnès Helmstetter and Didier Sornette. Subcritical and supercritical regimes in epidemic models of earthquake aftershocks. *Journal of Geophysical Research: Solid Earth*, 107(B10):ESE 10–1–ESE 10–21, oct 2002a. ISSN 2169-9356. doi: 10.1029/2001jb001580.
- Agnès Helmstetter and Didier Sornette. Diffusion of epicenters of earthquake aftershocks, Omori’s law, and generalized continuous-time random walk models. *Phys. Rev. E*, 66(6):061104.1–061104.24, 2002b. URL <http://link.aps.org/doi/10.1103/PhysRevE.66.061104>.

- Agnes Helmstetter and Didier Sornette. Subcritical and supercritical regimes in epidemic models of earthquake aftershocks. *Journal of Geophysical Research: Solid Earth*, 107 (B10), 2002c.
- Minh X. Hoang, Xuan Hong Dang, Xiang Wu, Zhenyu Yan, and Ambuj K. Singh. GPOP: Scalable group-level popularity prediction for online content in social networks. In *26th International World Wide Web Conference, WWW 2017*, pages 725–733. International World Wide Web Conferences Steering Committee, 2017. ISBN 9781450349130. doi: 10.1145/3038912.3052626.
- Martin Jacobsen. Compensators and Martingales. In *Point Process Theory and Applications*, pages 33–102. Birkhäuser-Verlag, Boston, 2006. doi: 10.1007/0-8176-4463-6_4. URL http://link.springer.com/10.1007/0-8176-4463-6_4.
- Olav Kallenberg. *Random measures, theory and applications*, volume 1. Springer, 2017.
- David Kempe, Jon Kleinberg, and Éva Tardos. Maximizing the spread of influence through a social network. In *Proceedings of the ACM SIGKDD International Conference on Knowledge Discovery and Data Mining*, pages 137–146, 2003. doi: 10.1145/956750.956769.
- M. Kirchner and A. Bercher. A nonparametric estimation procedure for the Hawkes process: comparison with maximum likelihood estimation. *Journal of Statistical Computation and Simulation*, 88(6):1106–1116, apr 2018. ISSN 15635163. doi: 10.1080/00949655.2017.1422126. URL <https://www.tandfonline.com/doi/abs/10.1080/00949655.2017.1422126>.
- Matthias Kirchner. Hawkes and INAR(∞) processes. *Stochastic Processes and their Applications*, 126(8):2494–2525, aug 2016. ISSN 03044149. doi: 10.1016/j.spa.2016.02.008. URL <https://linkinghub.elsevier.com/retrieve/pii/S0304414916000399>.
- Matthias Kirchner. An estimation procedure for the Hawkes process. *Quantitative Finance*, 17(4):571–595, apr 2017. ISSN 1469-7688. doi: 10.1080/14697688.2016.1211312. URL <https://www.tandfonline.com/doi/full/10.1080/14697688.2016.1211312>.
- Fima C. Klebaner. *Introduction to Stochastic Calculus with Applications*. Imperial College Press, 3 edition, 2012.
- Ryota Kobayashi and Renaud Lambiotte. TiDeH: Time-dependent Hawkes process for predicting retweet dynamics. In *Proceedings of the 10th International Conference on Web and Social Media, ICWSM 2016*, pages 191–200. AAAI Press, 2016. ISBN 9781577357582.
- Quyu Kong, Marian-Andrei Rizoïu, and Lexing Xie. Modeling Information Cascades with Self-exciting Processes via Generalized Epidemic Models. In *Proceedings of the 13th International Conference on Web Search and Data Mining*, pages 286–294, New York, NY, USA, jan 2020a. ACM. ISBN 9781450368223. doi: 10.1145/3336191.3371821.
- Quyu Kong, Marian-Andrei Rizoïu, and Lexing Xie. Describing and Predicting Online Items with Reshare Cascades via Dual Mixture Self-exciting Processes. In *Proceedings of the 29th ACM International Conference on Information & Knowledge Management*,

- pages 645–654, New York, NY, USA, oct 2020b. ACM. ISBN 9781450368599. doi: 10.1145/3340531.3411861.
- D. T. Koops, M. Saxena, O. J. Boxma, and M. Mandjes. Infinite-server queues with Hawkes input. *Journal of Applied Probability*, 55(3):920–943, sep 2018. ISSN 00219002. doi: 10.1017/jpr.2018.58. URL [/core/journals/journal-of-applied-probability/article/infinitieserver-queues-with-hawkes-input/29A985198A710AB1F7636DCEAEA9C0E6](https://doi.org/10.1017/jpr.2018.58).
- P. J. Laub, T. Taimre, and P. K. Pollett. Hawkes Processes. *ArXiv e-prints*, July 2015.
- P. A.W. Lewis and G. S. Shedler. SIMULATION OF NONHOMOGENEOUS POISSON PROCESSES BY THINNING. *Naval research logistics quarterly*, 26(3):403–413, 1979. ISSN 00281441. doi: 10.1002/nav.3800260304.
- Sha Li, Xiaofeng Gao, Weiming Bao, and Guihai Chen. FM-Hawkes: A Hawkes process based approach for modeling online activity correlations. In *International Conference on Information and Knowledge Management, Proceedings*, volume Part F131841, pages 1119–1128, New York, NY, USA, nov 2017. Association for Computing Machinery. ISBN 9781450349185. doi: 10.1145/3132847.3132883. URL <https://dl.acm.org/doi/10.1145/3132847.3132883>.
- Yang Lu. The predictive distributions of thinning-based count processes. *Scandinavian Journal of Statistics*, page sjos.12438, dec 2019. ISSN 0303-6898. doi: 10.1111/sjos.12438. URL <https://onlinelibrary.wiley.com/doi/abs/10.1111/sjos.12438>.
- Dimitris Manolakis, Nicholas Bosowski, and Vinay K. Ingle. Count Time-Series Analysis: A Signal Processing Perspective. *IEEE Signal Processing Magazine*, 36(3):64–81, may 2019. ISSN 15580792. doi: 10.1109/MSP.2018.2885853.
- Yasuko Matsubara, Yasushi Sakurai, B. Aditya Prakash, Lei Li, and Christos Faloutsos. Rise and fall patterns of information diffusion: Model and implications. In *Proceedings of the ACM SIGKDD International Conference on Knowledge Discovery and Data Mining*, pages 6–14, 2012. ISBN 9781450314626. doi: 10.1145/2339530.2339537.
- Swapnil Mishra, Marian-Andrei RizoIU, and Lexing Xie. Feature Driven and Point Process Approaches for Popularity Prediction. In *Proceedings of the 25th ACM International Conference on Information and Knowledge Management - CIKM '16*, pages 1069–1078, Indianapolis, IN, USA, 2016. ACM Press. ISBN 9781450340731. doi: 10.1145/2983323.2983812. URL <http://dl.acm.org/citation.cfm?doid=2983323.2983812><http://arxiv.org/pdf/1608.04862.pdf>.
- Swapnil Mishra, Tresnia Berah, Thomas A. Mellan, H. Juliette T. Unwin, Michaela A Vollmer, Kris V Parag, Axel Gandy, Seth Flaxman, and Samir Bhatt. On the derivation of the renewal equation from an age-dependent branching process: an epidemic modelling perspective. jun 2020. URL <http://arxiv.org/abs/2006.16487>.
- Alexander Moreno, Zhenke Wu, Jamie Yap, David Wetter, Cho Lam, Inbal Nahum-Shani, Walter Dempsey, and James M Rehg. A Robust Functional EM Algorithm for Incomplete Panel Count Data. mar 2020.

- Frank Nielsen, Jean-Daniel Boissonnat, and Richard Nock. Bregman voronoi diagrams: Properties, algorithms and applications. *arXiv preprint arXiv:0709.2196*, 2007.
- Joseph D. O’Brien, Alberto Aleta, Yamir Moreno, and James P. Gleeson. Quantifying Uncertainty in a Predictive Model for Popularity Dynamics. jan 2020. URL <https://arxiv.org/abs/2001.09490>.
- Yosihiko Ogata. On Lewis’ simulation method for point processes. *IEEE Transactions on Information Theory*, 27(1):23–31, 1981.
- Yosihiko Ogata. Statistical Models for Earthquake Occurrences and Residual Analysis for Point Processes. *Journal of the American Statistical Association*, 83(401):9–27, mar 1988. ISSN 0162-1459. doi: 10.1080/01621459.1988.10478560.
- Yosihiko Ogata. Seismicity Analysis through Point-process Modeling: A Review. In *Seismicity Patterns, their Statistical Significance and Physical Meaning*, volume 155, pages 471–507. Birkhäuser Basel, Basel, aug 1999. doi: 10.1007/978-3-0348-8677-2_14.
- T. Ozaki. Maximum likelihood estimation of Hawkes’ self-exciting point processes. *Annals of the Institute of Statistical Mathematics*, 31(1):145–155, 1979. ISSN 1572-9052.
- Krunal Parmar, Samuel Bushi, Sourangshu Bhattacharya, and Surender Kumar. Forecasting ad-impressions on online retail websites using non-homogeneous hawkes processes. In *CIKM*, 2017.
- Marc Piggott and Victor Solo. Non-Negative Online Estimation for Hawkes Process Networks. In *ICASSP, IEEE International Conference on Acoustics, Speech and Signal Processing - Proceedings*, volume 2018-April, pages 6333–6337. Institute of Electrical and Electronics Engineers Inc., sep 2018. ISBN 9781538646588. doi: 10.1109/ICASSP.2018.8462138.
- Alex Reinhart. A Review of Self-Exciting Spatio-Temporal Point Processes and Their Applications. *Statistical Science*, 33(3):299–318, aug 2018. ISSN 0883-4237. doi: 10.1214/17-STS629. URL <https://projecteuclid.org/euclid.ss/1534147221>.
- Marian-Andrei Rizoiu, Young Lee, and Swapnil Mishra. Hawkes processes for events in social media. *Frontiers of Multimedia Research*, pages 191–218, aug 2017a. doi: 10.1145/3122865.3122874. URL <http://arxiv.org/abs/1708.06401>.
- Marian-Andrei Rizoiu, Lexing Xie, Scott Sanner, Manuel Cebrian, Honglin Yu, and Pascal Van Hentenryck. Expecting to be hip: Hawkes intensity processes for social media popularity. In *Proceedings of the 26th International Conference on World Wide Web, WWW ’17*, pages 735–744, 2017b.
- Marian-Andrei Rizoiu, Timothy Graham, Rui Zhang, Yifei Zhang, Robert Ackland, and Lexing Xie. #DebateNight: The Role and Influence of Socialbots on Twitter During the 1st 2016 U.S. Presidential Debate. In *International AAAI Conference on Web and Social Media (ICWSM ’18)*, pages 1–10, Stanford, CA, USA, 2018a.

- Marian Andrei Rizoiu, Swapnil Mishra, Quyu Kong, Mark Carman, and Lexing Xie. SIR-hawkes: Linking epidemic models and hawkes processes to model diffusions in finite populations. In *The Web Conference 2018 - Proceedings of the World Wide Web Conference, WWW 2018*, pages 419–428, New York, New York, USA, apr 2018b. Association for Computing Machinery, Inc. ISBN 9781450356398. doi: 10.1145/3178876.3186108. URL <http://dl.acm.org/citation.cfm?doid=3178876.3186108>.
- Sheldon M. Ross. *Stochastic Processes*. Wiley, 2nd edition, 1995. ISBN 0471120626.
- Leigh Shlomovich, Edward Cohen, Niall Adams, and Lekha Patel. A Monte Carlo EM Algorithm for the Parameter Estimation of Aggregated Hawkes Processes. jan 2020. URL <http://arxiv.org/abs/2001.07160>.
- Donald L. Snyder and Michael I. Miller. *Random point processes in time and space*. Springer-Verlag, 2nd edition, 1991.
- Issouf Soumaré and Ernest Tafolog. Risk-based capital for credit insurers with business cycles and dynamic leverage. *Quantitative Finance*, 17(4):597–612, apr 2017. ISSN 14697696. doi: 10.1080/14697688.2016.1206960.
- Jianguo Sun and Xingqiu Zhao. *Statistical Analysis of Panel Count Data*, volume 80 of *Statistics for Biology and Health*. Springer New York, New York, NY, 2013. ISBN 978-1-4614-8714-2. doi: 10.1007/978-1-4614-8715-9.
- Gabor Szabo and Bernardo A. Huberman. Predicting the popularity of online content. *Communications of the ACM*, 53(8):80–88, aug 2010. ISSN 0001-0782. doi: 10.1145/1787234.1787254. URL <https://dl.acm.org/doi/10.1145/1787234.1787254>.
- Sebastian Tschiatschek, Adish Singla, Manuel Gomez Rodriguez, Arpit Merchant, and Andreas Krause. Fake News Detection in Social Networks via Crowd Signals. In *The Web Conference 2018 - Companion of the World Wide Web Conference, WWW 2018*, pages 517–524, New York, New York, USA, apr 2018. Association for Computing Machinery, Inc. ISBN 9781450356404. doi: 10.1145/3184558.3188722. URL <http://dl.acm.org/citation.cfm?doid=3184558.3188722>.
- George E Uhlenbeck and Leonard S Ornstein. On the theory of the brownian motion. *Physical review*, 36(5):823, 1930.
- H Juliette T Unwin, Isobel Routledge, Seth Flaxman, Marian-Andrei Rizoiu, Shengjie Lai, Justin Cohen, Daniel J Weiss, Swapnil Mishra, and Samir Bhatt. Using Hawkes Processes to model imported and local malaria cases in near-elimination settings. *medRxiv*, page 2020.07.17.20156174, jan 2020. doi: 10.1101/2020.07.17.20156174. URL <http://medrxiv.org/content/early/2020/07/17/2020.07.17.20156174.abstract>.
- Gerrit van Dijk. *Distribution Theory Convolution, Fourier Transform, and Laplace Transform*. De Gruyter Graduate Lectures, De Gruyter, Berlin, 2013.
- Tiandong Wang and Sidney I. Resnick. Common Growth Patterns for Regional Social Networks: a Point Process Approach. nov 2019. URL <http://arxiv.org/abs/1911.07902>.

- Yichen Wang, Evangelos Theodorou, Apurv Verma, and Le Song. A Stochastic Differential Equation Framework for Guiding Information Diffusion. *arXiv preprint*, pages 1–22, 2016. URL <http://arxiv.org/abs/1603.09021>.
- Hongteng Xu, Dixin Luo, and Hongyuan Zha. Learning Hawkes Processes from Short Doubly-Censored Event Sequences. In *Proceedings of the 34th International Conference on Machine Learning - Volume 70*, ICML’17, pages 3831–3840. JMLR.org, 2017.
- Linyun Yu, Peng Cui, Fei Wang, Chaoming Song, and Shiqiang Yang. Uncovering and predicting the dynamic process of information cascades with survival model. *Knowledge and Information Systems*, 50(2):633–659, feb 2017. ISSN 02193116. doi: 10.1007/s10115-016-0955-7.
- Ali Zarezade, Sina Jafarzadeh, and Hamid R. Rabiee. Spatio-Temporal Modeling of Users’ Check-ins in Location-Based Social Networks. nov 2016. URL <http://arxiv.org/abs/1611.07710>.
- Ali Zarezade, Utkarsh Upadhyay, Hamid R. Rabiee, and Manuel Gomez-Rodriguez. RedQueen: An online algorithm for smart broadcasting in social networks. In *WSDM 2017 - Proceedings of the 10th ACM International Conference on Web Search and Data Mining*, pages 51–60. Association for Computing Machinery, Inc, feb 2017. ISBN 9781450346757. doi: 10.1145/3018661.3018684.
- Ali Zarezade, Abir De, Utkarsh Upadhyay, Hamid R. Rabiee, and Manuel Gomez-Rodriguez. Steering Social Activity: A Stochastic Optimal Control Point of View. *Journal of Machine Learning Research*, 18(205):1–35, 2018. URL <http://jmlr.org/papers/v18/17-416.html>.
- Rui Zhang, Christian Walder, Marian-Andrei Rizoiu, and Lexing Xie. Efficient Non-parametric Bayesian Hawkes Processes. In *Proceedings of the Twenty-Eighth International Joint Conference on Artificial Intelligence*, pages 4299–4305, California, aug 2019. International Joint Conferences on Artificial Intelligence Organization. ISBN 978-0-9992411-4-1. doi: 10.24963/ijcai.2019/597.
- Rui Zhang, Christian Walder, and Marian-Andrei Rizoiu. Variational Inference for Sparse Gaussian Process Modulated Hawkes Process. *Proceedings of the AAAI Conference on Artificial Intelligence*, 34(04):6803–6810, apr 2020. ISSN 2374-3468. doi: 10.1609/aaai.v34i04.6160.
- Qingyuan Zhao, Murat A. Erdogdu, Hera Y. He, Anand Rajaraman, and Jure Leskovec. SEISMIC: A self-exciting point process model for predicting tweet popularity. In *Proceedings of the ACM SIGKDD International Conference on Knowledge Discovery and Data Mining*, volume 2015-August, pages 1513–1522. Association for Computing Machinery, aug 2015. ISBN 9781450336642. doi: 10.1145/2783258.2783401.
- Ke Zhou, Hongyuan Zha, and Le Song. Learning social infectivity in sparse low-rank networks using multi-dimensional Hawkes processes. In *Conference on Artificial Intelligence and Statistics (AISTATS)*, pages 641–649, 2013.

Lorenzo Zino, Alessandro Rizzo, and Maurizio Porfiri. Modeling memory effects in activity-driven networks. *SIAM Journal on Applied Dynamical Systems*, 17(4):2830–2854, 2018. ISSN 15360040. doi: 10.1137/18M1171485.

Lorenzo Zino, Alessandro Rizzo, and Maurizio Porfiri. Analysis and control of epidemics in temporal networks with self-excitement and behavioral changes. *European Journal of Control*, 54:1–11, jul 2020. ISSN 09473580. doi: 10.1016/j.ejcon.2019.12.007.

Contents (Appendix)

A Proofs and Derivations	55
B MBP Calculations	63
B.1 MBP Intensity Functions	63
B.2 MBP Compensator Functions	68
C Latent Homogeneous Poisson Process Exogenous Function - Probabilistic Approach	72
D Convexity analysis	73
D.1 Hawkes process	74
D.2 Mean Behaviour Poisson	74
E Experiments	77
E.1 Number of Approximation Points	77
E.2 Other Non-endogenous Experiments	77

A. Proofs and Derivations

We present proofs and derivations of all proofs not presented in the main text.

Proof [Derivation of Eq. (6)] We shall show that for a Hawkes process,

$$\xi(t) = \mu(t) + \int_0^t \phi(s) \cdot \xi(t - s) ds.$$

Similar identities also exist (Laub et al., 2015, pg. 8), (Helmstetter and Sornette, 2002c, Equation 9). Invoking an idea from stochastic calculus (see for instance, Lipster and Shiryayev or Klebaner), let us define the martingale

$$M(\cdot) \doteq N(\cdot) - \Lambda(\cdot),$$

where $\Lambda(\cdot) = \int_0^t \lambda(s) ds$ is a compensator. We have:

$$\begin{aligned} \xi(t) &= \mathbb{E} [\lambda(t)] \\ &= \mathbb{E} \left[\mu(t) + \int_0^{t^-} \phi(t - s) dN(s) \right] \\ &= \mathbb{E} \left[\mu(t) + \int_0^{t^-} \phi(t - s) [dN(s) - \lambda(s)ds] + \int_0^{t^-} \phi(t - s)\lambda(s) ds \right] \\ &= \mu(t) + \mathbb{E} \left[\int_0^{t^-} \phi(t - s) (dN(s) - \lambda(s)ds) + \int_0^{t^-} \phi(t - s)\lambda(s) ds \right] \\ &= \mu(t) + \mathbb{E} \left[\int_0^{t^-} \phi(t - s) (dN(s) - \lambda(s)ds) + \int_0^{t^-} \phi(t - s)\lambda(s) ds \right] \end{aligned}$$

$$= \mu(t) + \mathbb{E} \left[\int_0^{t-} \phi(t-s) \lambda(s) ds \right].$$

Since the term is $\int_s^t \phi(t-s)(dN(s) - \lambda(s))ds$ is a martingale and has expectation 0,

$$\begin{aligned} &= \mu(t) + \int_0^{t-} \phi(t-s) \mathbb{E}[\lambda(s)] ds \\ &= \mu(t) + \int_0^{t-} \phi(t-s) \xi(s) ds \\ &= \mu(t) + \int_0^{t-} \phi(s) \xi(t-s) ds. \end{aligned}$$

■

Proof [Proof of Theorem 1] The closed form MBP equation is given by

$$\xi(t) = s(t) + \int_0^t \phi(t-\tau) \cdot \xi(\tau) d\tau = s(t) + (\phi * \xi)(t).$$

Applying the Laplace transform to both sides, we have,

$$\begin{aligned} \mathcal{L}\{\xi(t)\}(\omega) &= \mathcal{L}\{s(t) + (\phi * \xi)(t)\}(\omega) \\ &= \mathcal{L}\{s(t)\}(\omega) + \mathcal{L}\{(\phi * \xi)(t)\}(\omega) \\ &= \mathcal{L}\{s(t)\}(\omega) + \mathcal{L}\{\phi(t)\}(\omega) \cdot \mathcal{L}\{\xi(t)\}(\omega). \end{aligned}$$

Solving for $\mathcal{L}\{\xi(t)\}(\omega)$, we have

$$\mathcal{L}\{\xi(t)\}(\omega) = \frac{\mathcal{L}\{s(t)\}(\omega)}{1 - \mathcal{L}\{\phi(t)\}(\omega)}.$$

Thus,

$$\xi(t) = \mathcal{L}^{-1} \left\{ \frac{\mathcal{L}\{s(t)\}(\omega)}{1 - \mathcal{L}\{\phi(t)\}(\omega)} \right\} (t).$$

■

Proof [Proof of Proposition 9] Let $\varphi(z) \doteq z \log z$ define a convex function. For clarity, further define $C_i \doteq C(o_{i-1}, o_i]$ and $\Xi_i \doteq \Xi(o_{i-1}, o_i]$. We may compute the loss composed of the sum of Bregman divergences with convex generator φ :

$$\begin{aligned} \mathcal{L}(\theta) &= \sum_{i=1}^m B_\varphi(C_i, \Xi_i) \\ &= \sum_{i=1}^m [\varphi(C_i) - \varphi(\Xi_i) - \varphi'(\Xi_i) \cdot (C_i - \Xi_i)] \\ &= \sum_{i=1}^m [C_i \log C_i - \Xi_i \log \Xi_i - (\log \Xi_i + 1) \cdot (C_i - \Xi_i)] \end{aligned}$$

$$\begin{aligned}
 &= \sum_{i=1}^m [\mathbf{C}_i \log \mathbf{C}_i - \mathbf{C}_i + \Xi_i - \mathbf{C}_i \log \Xi_i] \\
 &= \sum_{i=1}^m \Xi_i - \sum_{i=1}^m \mathbf{C}_i \log \Xi_i + \sum_{i=1}^m \mathbf{C}_i (\log \mathbf{C}_i - 1).
 \end{aligned}$$

As $\sum_{i=1}^m \mathbf{C}_i (\log \mathbf{C}_i - 1)$ is just a constant with respect to θ , the minimisation of $\mathcal{L}(\theta)$ with respect to θ , is equivalent to

$$\mathcal{L}_{IC-LL}(\theta) = \sum_{i=1}^m \Xi_i - \sum_{i=1}^m \mathbf{C}_i \log \Xi_i.$$

■

Proof [Proof of SSE equivalence in Section 5.1] Let $\hat{\varphi}(z) \doteq z^2$ define a convex function. For clarity, further define $\mathbf{C}_i \doteq \mathbf{C}(o_{i-1}, o_i]$ and $\Xi_i \doteq \Xi(o_{i-1}, o_i]$.

$$\mathcal{L}(\theta) = \sum_{i=1}^m B_{\hat{\varphi}}(\mathbf{C}_i, \Xi_i) = \sum_{i=1}^m [\mathbf{C}_i^2 - \Xi_i^2 - 2\Xi_i(\mathbf{C}_i - \Xi_i)] = \sum_{i=1}^m [\mathbf{C}_i - \Xi_i]^2$$

which is exactly the SSE between \mathbf{C}_i and Ξ_i . ■

Proof [Proof of Proposition 6] We aim to prove that both the lower-bound counting process and upper-bound counting process converge to the original counting process as the discretization points increase. To consider the convergence of our counting process approximation, we further assume that the approximation points are equidistant apart

$$d_j^D = \frac{T}{D}j.$$

We explicitly add the superscript D is to denote the number of approximation points in the discretization sequence. Further we let $\mathcal{D}^D = \left\{ d_j^D \right\}_{j=0}^D$ as the set of approximation points.

We consider the convergence of the counting functions in L^1 -space, as counting processes are simple functions by definition. In particular, for the lower-bound counting process we aim to show that

$$\lim_{D \rightarrow \infty} \int_0^T |M(t) - M_D^-(t)| dt = 0.$$

However, as $M_D^-(t)$ is a lower-bound to $M(t)$ and by linearity of integration we can instead consider

$$\int_0^T |M(t) - M_D^-(t)| dt = \int_0^T M(t) dt - \int_0^T M_D^-(t) dt.$$

For the original counting process $M(t)$ we assume that we have an arbitrary realisation $\mathcal{T} = \{t_i\}_{i=1}$ over a time period $t_i \in (0, T]$. Thus we consider the integral of the counting

process $M(t)$ as the following,

$$\begin{aligned}
 \int_0^T M(t)dt &= \int_0^T \left[\sum_{s \in [0, T]} M(\{s\}) \cdot \mathbb{I}[s \leq t] \right] dt \\
 &= \sum_{s \in [0, T]} M(\{s\}) \cdot \int_s^T dt \\
 &= \sum_{s \in [0, T]} M(\{s\}) \cdot (T - s) \\
 &= \sum_{t_i \in \mathcal{T}} \delta(t_i) \cdot (T - t_i).
 \end{aligned}$$

For the lower-bound counting process, we first introduce indexing sets $I_j^D = \{i : t_i \in (d_{j-1}^D, d_j^D]\}$ which are the indices of the event times which occur in the half-open interval $(d_{j-1}^D, d_j^D]$. Thus we have,

$$\begin{aligned}
 \int_0^T M_D^-(t)dt &= \int_0^T \left[\sum_{j=1}^{2^D} M(d_{j-1}^D, d_j^D] \cdot \mathbb{I}[d_j^D < t \leq d_D^D] \right] dt \\
 &= \int_0^T \left[\sum_{j=1}^{2^D} M(d_{j-1}^D, d_j^D] \cdot \mathbb{I}[d_j^D < t \leq T] \right] dt \\
 &= \sum_{j=1}^{2^D} M(d_{j-1}^D, d_j^D] \cdot \int_{d_j^D}^T dt \\
 &= \sum_{j=1}^{2^D} M(d_{j-1}^D, d_j^D] \cdot (T - d_j^D) \\
 &= \sum_{j=1}^{2^D} \left(\sum_{i \in I_j^D} \delta(t_i) \right) \cdot (T - d_j^D).
 \end{aligned}$$

However, we know that $(d_{j-1}^D, d_j^D]$ will become a singleton set as $D \rightarrow \infty$ from the uniformity of discretization points. Further we know that for any D , the union $\bigcup_{j=1}^{2^D} (d_{j-1}^D, d_j^D] = (0, T]$. Thus in the limit of $D \rightarrow \infty$, we have $\{(d_{j-1}^D, d_j^D] : i \in \{1, 2, \dots, 2^D\}\} \rightarrow \{\{t\} : t \in (0, T]\}$. Thus, we compute the limit as the following,

$$\begin{aligned}
 \lim_{D \rightarrow \infty} \int_0^T M_D^-(t)dt &= \lim_{D \rightarrow \infty} \left(\sum_{j=1}^{2^D} \sum_{i \in I_j^D} \delta(t_i) \cdot (T - d_j^D) \right) \\
 &= \sum_{t \in (0, T]} \delta(t) \cdot \mathbb{I}[t \in \mathcal{T}] \cdot (T - t)
 \end{aligned}$$

$$\begin{aligned}
 &= \sum_{t_i \in \mathcal{T}} \delta(t_i) \cdot (T - t_i) \\
 &= \int_0^T M(t) dt.
 \end{aligned}$$

Thus,

$$\begin{aligned}
 \lim_{D \rightarrow \infty} \int_0^T |M(t) - M_D^-(t)| dt &= \lim_{D \rightarrow \infty} \left(\int_0^T M(t) dt - \int_0^T M_D^-(t) dt \right) \\
 &= \lim_{D \rightarrow \infty} \int_0^T M(t) dt - \lim_{D \rightarrow \infty} \int_0^T M_D^-(t) dt \\
 &= \int_0^T M(t) dt - \lim_{D \rightarrow \infty} \int_0^T M_D^-(t) dt \\
 &= \int_0^T M(t) dt - \int_0^T M(t) dt \\
 &= 0.
 \end{aligned}$$

The proof is identical when the upper-bound approximation $M_D^+(t)$ is chosen instead. \blacksquare

Proof [Derivation of Eq. (24)] We consider the following compensator generated by the upper-bound counting process $M_D^+(t)$:

$$\begin{aligned}
 \Xi^+(t) &\doteq S(t) + \int_0^t \mathbb{E}[M_D^+(y)] \phi(t-y) dy \\
 &= S(t) + \int_0^t \mathbb{E} \left[\sum_{j=1}^D M(d_{j-1}, d_j) \cdot \mathbb{1}[d_{j-1} < y \leq d_D] \right] \phi(t-y) dy \\
 &= S(t) + \sum_{j=1}^D \mathbb{E} [M(d_{j-1}, d_j)] \int_0^t \mathbb{1}[d_{j-1} < y \leq d_D] \phi(t-y) dy \\
 &= S(t) + \sum_{j=1}^{\bar{D}(t)+1} \mathbb{E} [M(d_{j-1}, d_j)] \int_{d_{j-1}}^{\min(t, d_D)} \phi(t-y) dy,
 \end{aligned}$$

where $\bar{D}(t) = \max\{i \in \{1, \dots, D\} : d_i < t\}$. This is a similar equation to Eq. (23). \blacksquare

Proof [Proof of Proposition 7] We simplify the compensator interval approximation $\Xi_D^-(o_{i-1}, o_i]$. We further assume that we have the anti-derivative of the kernel function $\phi = \Phi'$. Thus we have,

$$\begin{aligned}
 \Xi_D^-(o_{i-1}, o_i] &= \Xi_D^-(o_i) - \Xi_D^-(o_{i-1}) \\
 &= S(o_i) - S(o_{i-1}) + \sum_{j=1}^{\bar{D}(o_i)} \mathbb{E} [M(d_{j-1}, d_j)] \int_{d_j}^{\min(o_i, d_D)} \phi(o_i - y) dy
 \end{aligned}$$

$$\begin{aligned}
& - \sum_{j=1}^{\bar{D}(o_{i-1})} \mathbb{E} [M(d_{j-1}, d_j)] \int_{d_j}^{\min(o_{i-1}, d_D)} \phi(o_{i-1} - y) dy \\
= & S(o_i) - S(o_{i-1}) + \sum_{j=1}^{\bar{D}(o_i)} \mathbb{E} [M(d_{j-1}, d_j)] \int_{d_j}^{o_i} \phi(o_i - y) dy \\
& - \sum_{j=1}^{\bar{D}(o_{i-1})} \mathbb{E} [M(d_{j-1}, d_j)] \int_{d_j}^{o_{i-1}} \phi(o_{i-1} - y) dy \\
= & S(o_i) - S(o_{i-1}) + \sum_{j=1}^{\bar{D}(o_{i-1})} \mathbb{E} [M(d_{j-1}, d_j)] \left[\int_{d_j}^{o_i} \phi(o_i - y) dy - \int_{d_j}^{o_{i-1}} \phi(o_{i-1} - y) dy \right] \\
& + \sum_{j=\bar{D}(o_{i-1})+1}^{\bar{D}(o_i)} \mathbb{E} [M(d_{j-1}, d_j)] \int_{d_j}^{o_i} \phi(o_i - y) dy \\
= & S(o_i) - S(o_{i-1}) + \sum_{j=1}^{\bar{D}(o_{i-1})} \mathbb{E} [M(d_{j-1}, d_j)] [-(\Phi(0) - \Phi(o_i - d_j)) + (\Phi(0) + \Phi(o_{i-1} - d_j))] \\
& + \sum_{j=\bar{D}(o_{i-1})+1}^{\bar{D}(o_i)} \mathbb{E} [M(d_{j-1}, d_j)] [-\Phi(0) + \Phi(o_i - d_j)] \\
= & S(o_i) - S(o_{i-1}) + \sum_{j=1}^{\bar{D}(o_{i-1})} \mathbb{E} [M(d_{j-1}, d_j)] [\Phi(o_i - d_j) - \Phi(o_{i-1} - d_j)] \\
& + \sum_{j=\bar{D}(o_{i-1})+1}^{\bar{D}(o_i)} \mathbb{E} [M(d_{j-1}, d_j)] [\Phi(o_i - d_j) - \Phi(0)] \\
= & S(o_i) - S(o_{i-1}) + \sum_{j=1}^{\bar{D}(o_{i-1})} \mathbb{E} [M(d_{j-1}, d_j)] \int_{o_{i-1}-d_j}^{o_i-d_j} \phi(y) dy \\
& + \sum_{j=\bar{D}(o_{i-1})+1}^{\bar{D}(o_i)} \mathbb{E} [M(d_{j-1}, d_j)] \int_0^{o_i-d_j} \phi(y) dy \\
= & S(o_i) - S(o_{i-1}) + \sum_{j=1}^{\bar{D}(o_{i-1})} \mathbb{E} [M(d_{j-1}, d_j)] \int_{o_{i-1}-d_j}^{o_i-d_j} \phi(y) dy \\
& + \sum_{j=\bar{D}(o_{i-1})+1}^{\bar{D}(o_i)} \mathbb{E} [M(d_{j-1}, d_j)] \int_{o_{i-1}-d_j}^{o_i-d_j} \phi(y) dy \\
& + \sum_{j=\bar{D}(o_{i-1})+1}^{\bar{D}(o_i)} \mathbb{E} [M(d_{j-1}, d_j)] \int_0^{o_{i-1}-d_j} \phi(y) dy
\end{aligned}$$

$$\begin{aligned}
&= S(o_i) - S(o_{i-1}) + \sum_{j=1}^{\bar{D}(o_i)} \mathbb{E}[M(d_{j-1}, d_j)] \int_{o_{i-1}-d_j}^{o_i-d_j} \phi(y) dy \\
&\quad + \sum_{j=\bar{D}(o_{i-1})+1}^{\bar{D}(o_i)} \mathbb{E}[M(d_{j-1}, d_j)] \int_0^{o_{i-1}-d_j} \phi(y) dy.
\end{aligned}$$

■

Table 10: Solutions for different immigrant intensities $s(t)$, and the exponentially time-decaying kernel in Eq. (13) of the main text. Ψ_T acts as a set of immigrant event times.

$s(t)$	MBP Intensity Function $\xi(t)$
I $\delta(t - a)$	$\delta(t - a) + \kappa\theta \exp((k - 1)\theta(t - a)) \cdot \llbracket t \geq a \rrbracket$
II $\sum_{s_z \in \Psi_T} \delta(t - s_z)$	$\sum_{s_z \in \Psi_T} \left[\delta(t - s_z) + \kappa\theta \exp((k - 1)\theta(t - s_z)) \cdot \llbracket t \geq s_z \rrbracket \right]$
III $\llbracket a \leq t < b \rrbracket$	$\frac{\kappa}{1-\kappa} \left[\frac{1}{k} - \exp((k - 1)\theta(t - a)) \right] \cdot \llbracket a < t \leq b \rrbracket + \frac{\kappa}{1-\kappa} \left[\exp((k - 1)\theta(t - b)) - \exp((k - 1)\theta(t - a)) \right] \cdot \llbracket t > b \rrbracket$
IV $\sum_{i=1}^m \frac{S(q_{i-1}, q_i)}{q_i - q_{i-1}} \cdot \llbracket q_{i-1} < t \leq q_i \rrbracket$	$\sum_{i=1}^m \frac{S(q_{i-1}, q_i)}{q_i - q_{i-1}} \left[\frac{\kappa}{1-\kappa} \left[\frac{1}{k} - \exp((k - 1)\theta(t - q_{i-1})) \right] \cdot \llbracket q_{i-1} < t \leq q_i \rrbracket + \frac{\kappa}{1-\kappa} \left[\exp((k - 1)\theta(t - q_i)) - \exp((k - 1)\theta(t - q_{i-1})) - \exp((k - 1)\theta(t - q_i)) \right] \cdot \llbracket t > q_i \rrbracket \right]$
V $\kappa\theta + (u_0 - \kappa\theta) \exp(-\theta t)$	$\frac{\kappa\theta}{1-\kappa} (1 - \exp(-(1 - \kappa)\theta t)) + u_0 \exp(-(1 - \kappa)\theta t)$
VI $\sin(t) + \alpha$	$-\frac{\alpha}{\kappa-1} + \frac{\kappa}{\kappa-1} \frac{\alpha + \alpha\theta^2 - 2\alpha\kappa\theta^2 + \alpha\kappa^2\theta^2 + \theta\kappa - \theta}{1 + \theta^2 - 2\kappa\theta^2 + \kappa^2\theta^2} \exp((k - 1)\theta t) + \frac{\sin(t) + \theta^2 \sin(t) - \kappa\theta^2 \cos(t)}{1 + \theta^2 - 2\kappa\theta^2 + \kappa^2\theta^2}$

B. MBP Calculations

B.1 MBP Intensity Functions

We consider the closed form solutions of an MBP intensity function $\xi(t)$ with exponential kernel for various immigrant intensity functions. We use Corollary 3 where we have

$$h(t) = k\theta \exp((k-1)\theta t) \cdot \llbracket t \geq 0 \rrbracket.$$

and

$$\begin{aligned} E(t) &= \delta(t) + h(t) \\ \xi(t) &= (E * s)(t) = s(t) + (h * s)(t). \end{aligned}$$

Specifically, we calculate each row of Table 10.

Row I. Consider $s(t) = \delta(t - a)$ for $a \geq 0$. Thus,

$$\begin{aligned} (h * s)(t) &= (h(t) * \delta(t - a)) \\ &= h(t - a) \cdot \llbracket t \geq a \rrbracket. \end{aligned}$$

Together we have,

$$\xi(t) = \delta(t - a) + \kappa\theta \exp((k-1)\theta(t - a)) \cdot \llbracket t \geq a \rrbracket.$$

Row II. Consider $s(t) = \sum_{\mathfrak{s}_z \in \Psi_T} \delta(t - \mathfrak{s}_z)$ for some set of events Ψ_T . As the MBP intensity is a LTI (Rizoiu et al. (2017b)[Corollary 2.2]), we can simply express the MBP intensity as the sum of Row I.

Together we have,

$$\xi(t) = \sum_{\mathfrak{s}_z \in \Psi_T} \left[\delta(t - \mathfrak{s}_z) + \kappa\theta \exp((k-1)\theta(t - \mathfrak{s}_z)) \cdot \llbracket t \geq \mathfrak{s}_z \rrbracket \right].$$

Row III. Consider $s(t) = \llbracket a < t \leq b \rrbracket$ an interval. Then,

$$(h * s)(t) = (h(t) * \llbracket a < t \leq b \rrbracket).$$

We break the calculation into three cases: (1) $t \leq a$; (2) $a < t \leq b$; and (3) $t > b$.

Case (1): Suppose that $t \leq a$, then simply $(h(t) * \llbracket a < t \leq b \rrbracket) = 0$.

Case (2): Suppose that $a < t \leq b$. Then we have,

$$\begin{aligned} (h(t) * \llbracket a < t \leq b \rrbracket) &= \int_0^\infty \llbracket a < \tau \leq b \rrbracket \cdot h(t - \tau) \, d\tau \\ &= \int_a^t h(t - \tau) \, d\tau \\ &= \frac{\kappa\theta}{(1 - \kappa)\theta} \exp((k-1)\theta(t - \tau)) \Big|_{\tau=a}^{\tau=t} \\ &= \frac{\kappa}{1 - \kappa} [1 - \exp((k-1)\theta(t - a))]. \end{aligned}$$

Case (3): Suppose that $t > b$. Then we have,

$$\begin{aligned}
 (h(t) * \llbracket a < t \leq b \rrbracket) &= \int_0^\infty \llbracket a < \tau \leq b \rrbracket \cdot h(t - \tau) \, d\tau \\
 &= \int_a^b h(t - \tau) \, d\tau \\
 &= \frac{\kappa\theta}{(1 - \kappa)\theta} \cdot \exp((k - 1)\theta(t - \tau)) \Big|_{\tau=a}^{\tau=b} \\
 &= \frac{\kappa}{1 - \kappa} [\exp((k - 1)\theta(t - b)) - \exp((k - 1)\theta(t - a))].
 \end{aligned}$$

Thus together we have that

$$(h(t) * \llbracket a < t \leq b \rrbracket) = \begin{cases} 0 & t \leq a \\ \frac{\kappa}{1 - \kappa} [1 - \exp((k - 1)\theta(t - a))] & a < t \leq b. \\ \frac{\kappa}{1 - \kappa} [\exp((k - 1)\theta(t - b)) - \exp((k - 1)\theta(t - a))] & t > b \end{cases}$$

Giving,

$$\begin{aligned}
 \xi(t) &= \llbracket a < t \leq b \rrbracket + \frac{\kappa}{1 - \kappa} [1 - \exp((k - 1)\theta(t - a))] \cdot \llbracket a < t \leq b \rrbracket \\
 &\quad + \frac{\kappa}{1 - \kappa} [\exp((k - 1)\theta(t - b)) - \exp((k - 1)\theta(t - a))] \cdot \llbracket t > b \rrbracket \\
 &= \frac{\kappa}{1 - \kappa} \left[\frac{1}{k} - \exp((k - 1)\theta(t - a)) \right] \cdot \llbracket a < t \leq b \rrbracket \\
 &\quad + \frac{\kappa}{1 - \kappa} [\exp((k - 1)\theta(t - b)) - \exp((k - 1)\theta(t - a))] \cdot \llbracket t > b \rrbracket.
 \end{aligned}$$

Row IV. Consider $s(t) = \sum_{i=1}^m \frac{S(q_{i-1}, q_i)}{q_i - q_{i-1}} \cdot \llbracket q_{i-1} < t \leq q_i \rrbracket$ for a set of intervals with non-negative immigrant volumes $S(q_{i-1}, q_i)$. As the MBP intensity is an LTI (Rizoiu et al. (2017b)[Corollary 2.2]), we can simply express the MBP intensity as the weighted sum of Row III.

$$\begin{aligned}
 \xi(t) &= \sum_{i=1}^m \frac{S(q_{i-1}, q_i)}{q_i - q_{i-1}} \left[\frac{\kappa}{1 - \kappa} \left[\frac{1}{k} - \exp((k - 1)\theta(t - q_{i-1})) \right] \cdot \llbracket q_{i-1} < t \leq q_i \rrbracket \right. \\
 &\quad \left. + \frac{\kappa}{1 - \kappa} [\exp((k - 1)\theta(t - q_i)) - \exp((k - 1)\theta(t - q_{i-1}))] \cdot \llbracket t > q_i \rrbracket \right].
 \end{aligned}$$

Row V. Proof shown in the main text.

Row VI. Consider $s(t) = \sin(t) + \alpha$. Then

$$(h * s)(t) = (h * \alpha)(t) + (h * \sin)(t).$$

For $(h * \alpha)(t)$ we have,

$$(h * \alpha)(t) = \alpha \int_0^t h(\tau) \, d\tau$$

$$\begin{aligned}
 &= \frac{\alpha\kappa}{\kappa-1} (\exp((k-1)\theta t) - 1) \\
 &= \frac{\alpha\kappa}{\kappa-1} \exp((k-1)\theta t) - \frac{\alpha\kappa}{\kappa-1}.
 \end{aligned}$$

For $(h * \sin)(t)$ first consider the indefinite integral

$$\Delta = \int \sin(\tau) \exp(a(t-\tau)) d\tau.$$

By integration by parts,

$$-\frac{1}{a} \sin(\tau) \exp(a(t-\tau)) + \frac{1}{a} \int \cos(\tau) \exp(a(t-\tau)) d\tau.$$

Then by integration by parts again,

$$\begin{aligned}
 &-\frac{1}{a} \sin(\tau) \exp(a(t-\tau)) + \frac{1}{a} \left[-\frac{1}{a} \cos(\tau) \exp(a(t-\tau)) - \frac{1}{a} \int \sin(\tau) \exp(a(t-\tau)) d\tau \right] \\
 &= -\frac{1}{a} \sin(\tau) \exp(a(t-\tau)) - \frac{1}{a^2} \cos(\tau) \exp(a(t-\tau)) - \frac{1}{a^2} \int \sin(\tau) \exp(a(t-\tau)) d\tau \\
 &= -\exp(a(t-\tau)) \left[\frac{1}{a} \sin(\tau) + \frac{1}{a^2} \cos(\tau) \right] - \frac{1}{a^2} \int \sin(\tau) \exp(a(t-\tau)) d\tau \\
 &= -\exp(a(t-\tau)) \left[\frac{1}{a} \sin(\tau) + \frac{1}{a^2} \cos(\tau) \right] - \frac{1}{a^2} \Delta.
 \end{aligned}$$

Thus,

$$\begin{aligned}
 \Delta &= -\exp(a(t-\tau)) \left[\frac{1}{a} \sin(\tau) + \frac{1}{a^2} \cos(\tau) \right] - \frac{1}{a^2} \Delta \\
 (\iff) \quad \Delta &= \frac{-\exp(a(t-\tau)) [a \sin(\tau) + \cos(\tau)]}{a^2 + 1}.
 \end{aligned}$$

Therefore for $(h * \sin)(t)$ we have

$$\begin{aligned}
 (h * \sin)(t) &= \kappa\theta \frac{-\exp((k-1)\theta(t-\tau)) [(k-1)\theta \sin(\tau) + \cos(\tau)]}{(k-1)^2\theta^2 + 1} \Bigg|_{\tau=0}^{\tau=t} \\
 &= \kappa\theta \frac{-\exp((k-1)\theta(t-\tau)) [(k-1)\theta \sin(\tau) + \cos(\tau)]}{1 + \theta^2 - 2\kappa\theta^2 + \kappa^2\theta^2} \Bigg|_{\tau=0}^{\tau=t} \\
 &= -\kappa\theta \frac{[(k-1)\theta \sin(t) + \cos(t)]}{1 + \theta^2 - 2\kappa\theta^2 + \kappa^2\theta^2} + \kappa\theta \frac{\exp((k-1)\theta t)}{1 + \theta^2 - 2\kappa\theta^2 + \kappa^2\theta^2}.
 \end{aligned}$$

Thus for the MBP intensity,

$$\begin{aligned}
 \xi(t) &= \sin(t) + \alpha + (h * \sin)(t) \\
 &= \sin(t) + \alpha + \frac{\alpha\kappa}{\kappa-1} \exp((k-1)\theta t) - \frac{\alpha\kappa}{\kappa-1} \\
 &\quad - \kappa\theta \frac{[(k-1)\theta \sin(t) + \cos(t)]}{1 + \theta^2 - 2\kappa\theta^2 + \kappa^2\theta^2} + \kappa\theta \frac{\exp((k-1)\theta t)}{1 + \theta^2 - 2\kappa\theta^2 + \kappa^2\theta^2}.
 \end{aligned}$$

Now we collect the trigonometric terms, the exponential terms, and the other constants.
The trigonometric terms:

$$\begin{aligned}
 & \sin(t) - \kappa\theta \frac{[(k-1)\theta \sin(t) + \cos(t)]}{1 + \theta^2 - 2\kappa\theta^2 + \kappa^2\theta^2} \\
 &= \sin(t) - \frac{\kappa^2\theta^2 \sin(t) - \kappa\theta^2 \sin(t) + \kappa\theta \cos(t)}{1 + \theta^2 - 2\kappa\theta^2 + \kappa^2\theta^2} \\
 &= \frac{\sin(t) + \theta^2 \sin(t) - 2\kappa\theta^2 \sin(t) + \kappa^2\theta^2 \sin(t) - \kappa^2\theta^2 \sin(t) + \kappa\theta^2 \sin(t) - \kappa\theta \cos(t)}{1 + \theta^2 - 2\kappa\theta^2 + \kappa^2\theta^2} \\
 &= \frac{\sin(t) + \theta^2 \sin(t) - \kappa\theta^2 \sin(t) - \kappa\theta \cos(t)}{1 + \theta^2 - 2\kappa\theta^2 + \kappa^2\theta^2}.
 \end{aligned}$$

The exponential terms:

$$\begin{aligned}
 & \frac{\alpha\kappa}{\kappa-1} \exp((k-1)\theta t) + \kappa\theta \frac{\exp((k-1)\theta t)}{1 + \theta^2 - 2\kappa\theta^2 + \kappa^2\theta^2} \\
 &= \frac{\kappa}{\kappa-1} \frac{\alpha + \alpha\theta^2 - 2\alpha\kappa\theta^2 + \alpha\kappa^2\theta^2 + \theta\kappa - \theta}{1 + \theta^2 - 2\kappa\theta^2 + \kappa^2\theta^2} \exp((k-1)\theta t).
 \end{aligned}$$

The constant terms:

$$\alpha - \frac{\alpha\kappa}{\kappa-1} = -\frac{\alpha}{\kappa-1}.$$

Thus together,

$$\begin{aligned}
 \xi(t) &= -\frac{\alpha}{\kappa-1} + \frac{\kappa}{\kappa-1} \frac{\alpha + \alpha\theta^2 - 2\alpha\kappa\theta^2 + \alpha\kappa^2\theta^2 + \theta\kappa - \theta}{1 + \theta^2 - 2\kappa\theta^2 + \kappa^2\theta^2} \exp((k-1)\theta t) \\
 &\quad + \frac{\sin(t) + \theta^2 \sin(t) - \kappa\theta^2 \sin(t) - \kappa\theta \cos(t)}{1 + \theta^2 - 2\kappa\theta^2 + \kappa^2\theta^2}.
 \end{aligned}$$

Table 11: Solutions for different immigrant intensities $s(t)$, and the exponentially time-decaying kernel in Eq. (13) of the main text. Ψ_T acts as a set of immigrant event times.

$s(t)$	MBP Compensator Function $\Xi(t)$
I $\delta(t - a)$	$\llbracket \tau \geq a \rrbracket + \frac{\kappa}{\kappa-1} (\exp((k-1)\theta(\tau-a)) - 1)$
II $\sum_{\mathfrak{s}_z \in \Psi_T} \delta(t - \mathfrak{s}_z)$	$\sum_{\mathfrak{s}_z \in \Psi_T} \llbracket t \geq \mathfrak{s}_z \rrbracket \cdot \frac{\kappa}{\kappa-1} (\exp((k-1)\theta(t - \mathfrak{s}_z)) + 1)$
III $\llbracket a \leq t < b \rrbracket$	$(t-a) \cdot \frac{\kappa}{1-\kappa} \left[\frac{1}{k} - \exp((k-1)\theta(t-a)) \right] \cdot \llbracket a < t \leq b \rrbracket + \frac{\kappa t}{1-\kappa} \left[\exp((k-1)\theta(t-b)) - \exp((k-1)\theta(t-a)) \right] \cdot \llbracket t > b \rrbracket + \frac{\kappa b}{1-\kappa} \left[\frac{1}{k} - \exp((k-1)\theta(t-b)) \right] \cdot \llbracket t > b \rrbracket + \frac{\kappa a}{1-\kappa} \left[\exp((k-1)\theta(t-a)) - \frac{1}{k} \right] \cdot \llbracket t > b \rrbracket$
IV $\sum_{i=1}^m \frac{S(q_{i-1}, q_i)}{q_i - q_{i-1}} \cdot \llbracket q_{i-1} < t \leq q_i \rrbracket$	$\frac{(t - q_{m^*(t)}) S(q_{m^*(t)+1} - q_{m^*(t)})}{q_{m^*(t)+1} - q_{m^*(t)}} + \sum_{i=1}^{m^*(t)} S(q_{i-1}, q_i) + \sum_{i=1}^{m^*(t)} \frac{S(q_{i-1}, q_i)}{q_i - q_{i-1}} \frac{\kappa}{1-\kappa} \left[\exp((\kappa-1)\theta(t - q_i)) - 1 - \exp((\kappa-1)\theta(t - q_{i-1})) + \exp((\kappa-1)\theta(q_i - q_{i-1})) \right] + \frac{\kappa}{1-\kappa} \left[t - q_{m^*(t)} + \frac{1}{\theta(\kappa-1)} - \frac{1}{\theta(\kappa-1)} \exp((k-1)\theta(t - q_{m^*(t)})) \right] d\tau$, where $m^*(t) = 1 + \max\{i \mid q_i > t\}$
V $\kappa\theta + (u_0 - \kappa\theta) \exp(-\theta t)$	$\frac{\kappa\theta t}{(1-\kappa)} + \frac{u_0-1}{(1-\kappa)\theta} (1 - \exp(-(1-\kappa)\theta t))$
VI $\sin(t) + \alpha$	$-\frac{\alpha t}{\kappa-1} + \frac{\kappa}{(\kappa-1)^2\theta} + \frac{\kappa}{1+\theta^2-2\kappa\theta^2+\kappa^2\theta^2} \frac{\alpha\kappa\theta^2+\theta\kappa-\theta}{1+\theta^2-2\kappa\theta^2+\kappa^2\theta^2} (\exp((k-1)\theta\tau) - 1) + \frac{-\cos(t)-\theta^2}{1+\theta^2-2\kappa\theta^2+\kappa^2\theta^2} \frac{\cos(t)-\kappa\theta \sin(t)+1+\theta^2-\kappa\theta^2}{1+\theta^2-2\kappa\theta^2+\kappa^2\theta^2}$

B.2 MBP Compensator Functions

We similarly calculate the corresponding MBP compensator function of the MBP intensity function we looked at above. In particular we similarly calculate each row of Table 11.

Row I. Consider $s(t) = \delta(t - a)$ for $a \geq 0$. We simply integrate the result of Row I in Table 10,

$$\begin{aligned}
 \Xi(t) &= \int_0^t \xi(\tau) d\tau \\
 &= \int_0^t \delta(\tau - a) + \kappa\theta \exp((k-1)\theta(\tau - a)) \cdot \llbracket \tau \geq a \rrbracket d\tau \\
 &= \int_0^t \delta(\tau - a) d\tau + \int_0^t \kappa\theta \exp((k-1)\theta(\tau - a)) \cdot \llbracket \tau \geq a \rrbracket d\tau \\
 &= \llbracket t \geq a \rrbracket + \llbracket t \geq a \rrbracket \cdot \int_a^t \kappa\theta \exp((k-1)\theta(\tau - a)) d\tau \\
 &= \llbracket t \geq a \rrbracket + \llbracket t \geq a \rrbracket \cdot \frac{\kappa}{\kappa-1} \exp((k-1)\theta(\tau - a)) \Bigg|_{\tau=a}^{\tau=t} \\
 &= \llbracket t \geq a \rrbracket + \llbracket t \geq a \rrbracket \cdot \frac{\kappa}{\kappa-1} (\exp((k-1)\theta(t-a)) - 1) \\
 &= \llbracket t \geq a \rrbracket \cdot \frac{\kappa}{\kappa-1} (\exp((k-1)\theta(t-a)) + 1).
 \end{aligned}$$

Row II. Consider $s(t) = \sum_{\mathfrak{s}_z \in \Psi_T} \delta(t - \mathfrak{s}_z)$ for some set of events Ψ_T . As MBP compensator is LTI, we compute the weighted sum of Row II.

$$\Xi(t) = \sum_{\mathfrak{s}_z \in \Psi_T} \llbracket t \geq \mathfrak{s}_z \rrbracket \cdot \frac{\kappa}{\kappa-1} (\exp((k-1)\theta(t - \mathfrak{s}_z)) + 1).$$

Row III. Consider $s(t) = \llbracket a < t \leq b \rrbracket$ an interval. First we consider the integral of $s(t)$.

$$S(t) = \int_0^t s(\tau) d\tau = (t-a) \cdot \llbracket a < t \leq b \rrbracket + (b-a) \cdot \llbracket t > b \rrbracket,$$

which can be simply computed by considering different values of t .

As the MBP compensator is a LTI, the result can be calculated as the weighted sum of of Row III in Table 10.

The first term,

$$\begin{aligned}
 &(t-a) \cdot \frac{\kappa}{1-\kappa} \left[\frac{1}{k} - \exp((k-1)\theta(t-a)) \right] \cdot \llbracket a < t \leq b \rrbracket \\
 &+ (t-a) \cdot \frac{\kappa}{1-\kappa} \left[\exp((k-1)\theta(t-b)) - \exp((k-1)\theta(t-a)) \right] \cdot \llbracket t > b \rrbracket.
 \end{aligned}$$

The second term,

$$(b-a) \cdot \frac{\kappa}{1-\kappa} \left[\frac{1}{k} - \exp((k-1)\theta(t-b)) \right] \cdot \llbracket t > b \rrbracket.$$

Together we have

$$\begin{aligned}
 \Xi(t) &= (t-a) \cdot \frac{\kappa}{1-\kappa} \left[\frac{1}{k} - \exp((k-1)\theta(t-a)) \right] \cdot \llbracket a < t \leq b \rrbracket \\
 &\quad + (t-a) \cdot \frac{\kappa}{1-\kappa} \left[\exp((k-1)\theta(t-b)) - \exp((k-1)\theta(t-a)) \right] \cdot \llbracket t > b \rrbracket \\
 &\quad + (b-a) \cdot \frac{\kappa}{1-\kappa} \left[\frac{1}{k} - \exp((k-1)\theta(t-b)) \right] \cdot \llbracket t > b \rrbracket \\
 &= (t-a) \cdot \frac{\kappa}{1-\kappa} \left[\frac{1}{k} - \exp((k-1)\theta(t-a)) \right] \cdot \llbracket a < t \leq b \rrbracket \\
 &\quad + \frac{\kappa t}{1-\kappa} \left[\exp((k-1)\theta(t-b)) - \exp((k-1)\theta(t-a)) \right] \cdot \llbracket t > b \rrbracket \\
 &\quad + \frac{\kappa b}{1-\kappa} \left[\frac{1}{k} - \exp((k-1)\theta(t-b)) \right] \cdot \llbracket t > b \rrbracket \\
 &\quad + \frac{\kappa a}{1-\kappa} \left[\exp((k-1)\theta(t-a)) - \frac{1}{k} \right] \cdot \llbracket t > b \rrbracket
 \end{aligned}$$

Row IV. To calculate this row, one could utilise the LTI with Row III. However, we derive this differently, which provides an equation which is easier to implement.

First, let us calculate the exogenous component.

$$\begin{aligned}
 S(t) &= \int_0^t s(\tau) \, d\tau \\
 &= \int_0^t \left(\sum_{i=1}^m \frac{S(q_{i-1}, q_i)}{q_i - q_{i-1}} \cdot \llbracket q_{i-1} < \tau \leq q_i \rrbracket \right) \, d\tau \\
 &= \sum_{i=1}^m \frac{S(q_{i-1}, q_i)}{q_i - q_{i-1}} \cdot \int_0^t \llbracket q_{i-1} < \tau \leq q_i \rrbracket \, d\tau
 \end{aligned}$$

The integral within the summation is what we need to calculate now $\int_0^t \llbracket q_{i-1} < \tau \leq q_i \rrbracket \, d\tau$. We split up the calculation into three cases: (1) $t \leq q_{i-1}$; (2) $q_{i-1} < t \leq q_i$; and (3) $t > q_i$.

Case (1): Suppose that $t \leq q_{i-1}$, then simply $\int_0^t \llbracket q_{i-1} < \tau \leq q_i \rrbracket \, d\tau = 0$.

Case (2): Suppose that $q_{i-1} < t \leq q_i$,

$$\int_0^t \llbracket q_{i-1} < \tau \leq q_i \rrbracket \, d\tau = \int_{q_{i-1}}^t 1 \, d\tau = t - q_{i-1}.$$

Case (3): Suppose that $t > q_i$,

$$\int_0^t \llbracket q_{i-1} < \tau \leq q_i \rrbracket \, d\tau = \int_{q_{i-1}}^{q_i} 1 \, d\tau = q_i - q_{i-1}.$$

For arbitrary fixed t , let $m^*(t) = 1 + \max\{i \mid q_i > t\}$. Then, by combining the three cases we have that,

$$S(t) = \frac{(t - q_{m^*(t)})S(q_{m^*(t)+1} - q_{m^*(t)})}{q_{m^*(t)+1} - q_{m^*(t)}} + \sum_{i=1}^{m^*(t)} S(q_{i-1}, q_i).$$

Similarly to the exogenous function, we consider the endogenous response in the same three cases. We directly use the piecewise derivations found in Row III of Table 10. Thus, we only need to compute $\int_0^t (h * s) d\tau$. First we consider $\int_0^t (h(\tau) * \llbracket q_{i-1} < \tau \leq q_i \rrbracket) d\tau$

Case (1): Suppose that $t \leq q_{i-1}$, then simply $\int_0^t (h(\tau) * \llbracket q_{i-1} < \tau \leq q_i \rrbracket) \llbracket t \leq q_{i-1} \rrbracket d\tau = 0$.

Case (2): Suppose that $q_{i-1} < t \leq q_i$,

$$\begin{aligned}
 & \int_0^t (h(\tau) * \llbracket q_{i-1} < \tau \leq q_i \rrbracket) \llbracket q_{i-1} < \tau \leq q_i \rrbracket d\tau \\
 &= \int_{q_{i-1}}^t (h * s)(\tau) d\tau \\
 &= \int_{q_{i-1}}^t \frac{\kappa}{1 - \kappa} [1 - \exp((k - 1)\theta(\tau - q_{i-1}))] d\tau \\
 &= \frac{\kappa}{1 - \kappa} \left[t - q_{i-1} - \int_{q_{i-1}}^t \exp((k - 1)\theta(\tau - q_{i-1})) d\tau \right] \\
 &= \frac{\kappa}{1 - \kappa} \left[t - q_{i-1} + \frac{1}{\theta(\kappa - 1)} - \frac{1}{\theta(\kappa - 1)} \exp((k - 1)\theta(t - q_{i-1})) \right].
 \end{aligned}$$

Case (3): Suppose that $t > q_i$,

$$\begin{aligned}
 & \int_0^t (h(\tau) * \llbracket q_{i-1} < \tau \leq q_i \rrbracket) \llbracket \tau > q_i \rrbracket d\tau \\
 &= \int_{q_i}^t (h * s)(\tau) d\tau \\
 &= \int_{q_i}^t \frac{\kappa}{1 - \kappa} [\exp((\kappa - 1)\theta(\tau - q_i)) - \exp((\kappa - 1)\theta(\tau - q_{i-1}))] d\tau \\
 &= \frac{\kappa}{1 - \kappa} [\exp((\kappa - 1)\theta(t - q_i)) - 1 - \exp((\kappa - 1)\theta(t - q_{i-1})) \\
 &\quad + \exp((\kappa - 1)\theta(q_i - q_{i-1}))].
 \end{aligned}$$

Thus, combining the three cases, we have that,

$$\begin{aligned}
 & \int_0^t (h * s)(\tau) d\tau \\
 &= \sum_{i=1}^m \frac{S(q_{i-1}, q_i)}{q_i - q_{i-1}} \int_0^t (h(t) * \llbracket q_{i-1} < t \leq q_i \rrbracket) d\tau \\
 &= \sum_{i=1}^{m^*(t)} \frac{S(q_{i-1}, q_i)}{q_i - q_{i-1}} \frac{\kappa}{1 - \kappa} [\exp((\kappa - 1)\theta(t - q_i)) - 1 - \exp((\kappa - 1)\theta(t - q_{i-1})) \\
 &\quad + \exp((\kappa - 1)\theta(q_i - q_{i-1}))] + \\
 &\quad \frac{\kappa}{1 - \kappa} \left[t - q_{m^*(t)} + \frac{1}{\theta(\kappa - 1)} - \frac{1}{\theta(\kappa - 1)} \exp((k - 1)\theta(t - q_{m^*(t)})) \right].
 \end{aligned}$$

Together, we can now compute the compensator function.

$$\begin{aligned}\Xi(t) &= \frac{(t - q_{m^*(t)})\mathcal{S}(q_{m^*(t)+1} - q_{m^*(t)})}{q_{m^*(t)+1} - q_{m^*(t)}} + \sum_{i=1}^{m^*(t)} \mathcal{S}(q_{i-1}, q_i] \\ &\quad + \sum_{i=1}^{m^*(t)} \frac{\mathcal{S}(q_{i-1}, q_i]}{q_i - q_{i-1}} \frac{\kappa}{1 - \kappa} [\exp((\kappa - 1)\theta(t - q_i)) - 1 - \exp((\kappa - 1)\theta(t - q_{i-1})) \\ &\quad + \exp((\kappa - 1)\theta(q_i - q_{i-1}))] \\ &\quad + \frac{\kappa}{1 - \kappa} \left[t - q_{m^*(t)} + \frac{1}{\theta(\kappa - 1)} - \frac{1}{\theta(\kappa - 1)} \exp((\kappa - 1)\theta(t - q_{m^*(t)})) \right] d\tau.\end{aligned}$$

Row V. To calculate the MBP compensator, we integrate Row V of Table 10.

$$\begin{aligned}\Xi(t) &= \int_0^t \xi(\tau) d\tau \\ &= \int_0^t \frac{\kappa\theta}{1 - \kappa} (1 - \exp(-(1 - \kappa)\theta\tau)) + u_0 \exp(-(1 - \kappa)\theta\tau) d\tau \\ &= \frac{\kappa\theta}{(1 - \kappa)} \left[\tau + \frac{1}{(1 - \kappa)\theta} \exp(-(1 - \kappa)\theta\tau) \right] - \frac{u_0}{(1 - \kappa)\theta} \exp(-(1 - \kappa)\theta\tau) \Bigg|_{\tau=0}^{\tau=t} \\ &= \frac{\kappa\theta t}{(1 - \kappa)} + \frac{u_0 - 1}{(1 - \kappa)\theta} (1 - \exp(-(1 - \kappa)\theta t)).\end{aligned}$$

Row VI. To calculate the MBP compensator, we integrate Row VI of Table 10.

$$\begin{aligned}\Xi(t) &= \int_0^t \xi(\tau) d\tau = \int_0^t \left[-\frac{\alpha}{\kappa - 1} + \frac{\kappa}{\kappa - 1} \frac{\alpha + \alpha\theta^2 - 2\alpha\kappa\theta^2 + \alpha\kappa^2\theta^2 + \theta\kappa - \theta}{1 + \theta^2 - 2\kappa\theta^2 + \kappa^2\theta^2} \exp((k - 1)\theta\tau) \right. \\ &\quad \left. + \frac{\sin(\tau) + \theta^2 \sin(\tau) - \kappa\theta^2 \sin(\tau) - \kappa\theta \cos(\tau)}{1 + \theta^2 - 2\kappa\theta^2 + \kappa^2\theta^2} \right] d\tau.\end{aligned}$$

We calculate the integral term by term. For the first term,

$$\int_0^t -\frac{\alpha}{\kappa - 1} d\tau = -\frac{\alpha t}{\kappa - 1}.$$

For the second term,

$$\begin{aligned}&\int_0^t \frac{\kappa}{\kappa - 1} \frac{\alpha + \alpha\theta^2 - 2\alpha\kappa\theta^2 + \alpha\kappa^2\theta^2 + \theta\kappa - \theta}{1 + \theta^2 - 2\kappa\theta^2 + \kappa^2\theta^2} \exp((k - 1)\theta\tau) d\tau \\ &= \frac{\kappa}{\kappa - 1} \frac{\alpha + \alpha\theta^2 - 2\alpha\kappa\theta^2 + \alpha\kappa^2\theta^2 + \theta\kappa - \theta}{1 + \theta^2 - 2\kappa\theta^2 + \kappa^2\theta^2} \int_0^t \exp((k - 1)\theta\tau) d\tau \\ &= \frac{\kappa}{(\kappa - 1)^2\theta} \frac{\alpha + \alpha\theta^2 - 2\alpha\kappa\theta^2 + \alpha\kappa^2\theta^2 + \theta\kappa - \theta}{1 + \theta^2 - 2\kappa\theta^2 + \kappa^2\theta^2} (\exp((k - 1)\theta\tau) - 1).\end{aligned}$$

For the third term,

$$\int_0^t \frac{\sin(\tau) + \theta^2 \sin(\tau) - \kappa\theta^2 \sin(\tau) - \kappa\theta \cos(\tau)}{1 + \theta^2 - 2\kappa\theta^2 + \kappa^2\theta^2} d\tau$$

$$\begin{aligned}
 &= \left. \frac{-\cos(\tau) - \theta^2 \cos(\tau) + \kappa\theta^2 \cos(\tau) - \kappa\theta \sin(\tau)}{1 + \theta^2 - 2\kappa\theta^2 + \kappa^2\theta^2} \right]_{\tau=0}^{\tau=t} \\
 &= \frac{-\cos(t) - \theta^2 \cos(t) + \kappa\theta^2 \cos(t) - \kappa\theta \sin(t) + 1 + \theta^2 - \kappa\theta^2}{1 + \theta^2 - 2\kappa\theta^2 + \kappa^2\theta^2}.
 \end{aligned}$$

Thus together,

$$\begin{aligned}
 \Xi(t) &= -\frac{\alpha t}{\kappa - 1} + \frac{\kappa}{(\kappa - 1)^2\theta} \frac{\alpha + \alpha\theta^2 - 2\alpha\kappa\theta^2 + \alpha\kappa^2\theta^2 + \theta\kappa - \theta}{1 + \theta^2 - 2\kappa\theta^2 + \kappa^2\theta^2} (\exp((k-1)\theta\tau) - 1) \\
 &\quad + \frac{-\cos(t) - \theta^2 \cos(t) + \kappa\theta^2 \cos(t) - \kappa\theta \sin(t) + 1 + \theta^2 - \kappa\theta^2}{1 + \theta^2 - 2\kappa\theta^2 + \kappa^2\theta^2}.
 \end{aligned}$$

C. Latent Homogeneous Poisson Process Exogenous Function - Probabilistic Approach

The Latent Homogenous Poisson Process (LHPP) exogenous function presented in Section 6.2 can be considered in a probabilistic approach. Instead of assigning a point process to dictate the interval-censored exogenous events, we consider a probability distribution $p(\mathfrak{s})$ corresponding to the probability an exogenous event occurs from $(0, T]$. Furthermore, we have the corresponding immigrant event times which are sampled from the probability distributions $\mathfrak{s} \in \Psi_T$.

We first consider the impulse response MBP process with the position of the impulse as a parameter,

$$\xi_\delta(t; \mathfrak{s}) \doteq \delta(t - \mathfrak{s}) + \int_0^t \phi(s) \cdot \xi_\delta(t - s; \mathfrak{s}) ds. \quad (57)$$

Then, we can consider the MBP process corresponding to the expectation of the intensity function with respect to the position of the impulse:

$$\begin{aligned}
 \mathbb{E}_{\mathfrak{s} \sim p(\mathfrak{s})} [\xi_\delta(t; \mathfrak{s})] &= \mathbb{E}_{\mathfrak{s} \sim p(\mathfrak{s})} \left[\delta(t - \mathfrak{s}) + \int_0^t \phi(s) \cdot \xi_\delta(t - s; \mathfrak{s}) ds \right] \\
 &= \mathbb{E}_{\mathfrak{s} \sim p(\mathfrak{s})} [\delta(t - \mathfrak{s})] + \mathbb{E}_{\mathfrak{s} \sim p(\mathfrak{s})} \left[\int_0^t \phi(s) \cdot \xi_\delta(t - s; \mathfrak{s}) ds \right] \\
 &= \mathbb{E}_{\mathfrak{s} \sim p(\mathfrak{s})} [\delta(t - \mathfrak{s})] + \int_0^t \phi(s) \cdot \mathbb{E}_{\mathfrak{s} \sim p(\mathfrak{s})} [\xi_\delta(t - s; \mathfrak{s})] ds \\
 &= \int_0^T \delta(t - \mathfrak{s}) \cdot p(\mathfrak{s}) d\mathfrak{s} + \int_0^t \phi(s) \cdot \mathbb{E}_{\mathfrak{s} \sim p(\mathfrak{s})} [\xi_\delta(t - s; \mathfrak{s})] ds \\
 &= p(t) + \int_0^t \phi(s) \cdot \mathbb{E}_{\mathfrak{s} \sim p(\mathfrak{s})} [\xi_\delta(t - s; \mathfrak{s})] ds.
 \end{aligned}$$

We now consider probability distributions $p_i(\mathfrak{s})$ defined as a uniform distribution over the exogenous event observation period $(q_{i-1}, q_i]$, for $i \in \{q_1, \dots, q_m\}$:

$$p_i(\mathfrak{s}) = \begin{cases} \frac{1}{q_i - q_{i-1}} & \mathfrak{s} \in (q_{i-1}, q_i] \\ 0 & \text{otherwise} \end{cases}$$

$$= \frac{1}{q_i - q_{i-1}} \cdot \llbracket q_{i-1} < \mathfrak{s} \leq q_i \rrbracket.$$

The probabilistic interpretation of the LHPP exogenous function can now be expressed as the weighted sum of MBP impulse expectations, where the weights are given by exogenous event volumes $S(q_{i-1}, q_i]$ and the summation is over the probability distribution $p_i(\mathfrak{s})$. That is, the intensity function is given by:

$$\begin{aligned} \xi_{\bullet}(t) &\doteq \sum_{i=1}^m S(q_{i-1}, q_i] \cdot \mathbb{E}_{\mathfrak{s} \sim p_i(\mathfrak{s})} [\xi_{\delta}(t; \mathfrak{s})] \\ &= \sum_{i=1}^m S(q_{i-1}, q_i] \cdot \left[p_i(t) + \int_0^t \phi(s) \cdot \mathbb{E}_{\mathfrak{s} \sim p_i(\mathfrak{s})} [\xi_{\delta}(t-s; \mathfrak{s})] ds \right] \\ &= \sum_{i=1}^m S(q_{i-1}, q_i] \cdot p_i(t) + \sum_{i=1}^m S(q_{i-1}, q_i] \cdot \left[\int_0^t \phi(s) \cdot \mathbb{E}_{\mathfrak{s} \sim p_i(\mathfrak{s})} [\xi_{\delta}(t-s; \mathfrak{s})] ds \right] \\ &= \sum_{i=1}^m S(q_{i-1}, q_i] \cdot p_i(t) + \int_0^t \phi(s) \cdot \left[\sum_{i=1}^m S(q_{i-1}, q_i] \cdot \mathbb{E}_{\mathfrak{s} \sim p_i(\mathfrak{s})} [\xi_{\delta}(t-s; \mathfrak{s})] \right] ds \\ &= \sum_{i=1}^m S(q_{i-1}, q_i] \cdot p_i(t) + \int_0^t \phi(s) \cdot \xi_{\bullet}(t-s) ds \\ &= \sum_{i=1}^m \frac{S(q_{i-1}, q_i]}{q_i - q_{i-1}} \cdot \llbracket q_{i-1} < t \leq q_i \rrbracket + \int_0^t \phi(s) \cdot \xi_{\bullet}(t-s) ds, \end{aligned}$$

where the exogenous term of the intensity function is the LHPP exogenous function $s_{\bullet}(t)$, Eq. (44).

D. Convexity analysis

In this section, we analyse the loss functions of the Hawkes process and MBP process using the standard point process log-likelihood. In particular, we consider process using the exponential triggering kernel and the following exogenous functions:

1. Multi-impulse response — Equation (40);
2. Step response:

$$s(t) = \llbracket t \geq 0 \rrbracket; \tag{58}$$

3. Dasio response — Equation (12).

To account for these exogenous functions, we consider the exogenous events Ψ_T and the endogenous events Ω_T are considered as separable.

The loss functions for both the Hawkes process and MBP process are now presented:

D.1 Hawkes process

- Multiple impulse response

$$\begin{aligned} \mathcal{L}(\theta; T) \doteq & - \sum_{t_n \in \{\Omega_T, \Psi_T\}} \log \left(\sum_{\mathfrak{s}_j \in \Psi_T} \delta(t_n - \mathfrak{s}_j) + \sum_{t_i \in \Omega_T} \kappa \theta e^{-\theta(t_n - t_i)} \right) \\ & + |\Psi_T| + \kappa \sum_{t_i \in \Omega_T} (1 - e^{-\theta(T - t_i)}). \end{aligned} \quad (59)$$

- Step response

$$\begin{aligned} \mathcal{L}(\theta; T) \doteq & - \sum_{t_n \in \{\Omega_T, \Psi_T\}} \log \left(\mathbb{[}t_n \geq 0\mathbb{]} + \sum_{t_i \in \Omega_T} \kappa \theta e^{-\theta(t_n - t_i)} \right) \\ & + T + \kappa \sum_{t_i \in \Omega_T} (1 - e^{-\theta(T - t_i)}). \end{aligned} \quad (60)$$

- Dassios response

$$\begin{aligned} \mathcal{L}(\theta; T) \doteq & - \sum_{t_n \in \{\Omega_T, \Psi_T\}} \log \left(\kappa \theta + (u_0 - \kappa \theta) e^{-\theta t_n} + \sum_{t_i \in \Omega_T} \kappa \theta e^{-\theta(t_n - t_i)} \right) \\ & + \kappa \theta T + \frac{u_0 - \kappa \theta}{\theta} (1 - e^{-\theta T}) + \kappa \sum_{t_i \in \Omega_T} (1 - e^{-\theta(T - t_i)}) \end{aligned} \quad (61)$$

It is trivial to verify that the objective function, which consist of a negative log-likelihood function and linear functions is a convex function with respect to κ but not θ .

D.2 Mean Behaviour Poisson

- Multiple impulse response

$$\begin{aligned} \mathcal{L}(\theta; T) \doteq & - \sum_{t_n \in \{\Omega_T, \Psi_T\}} \log \left(\sum_{t_i \in \Omega_T} \kappa \theta \sum_{\mathfrak{s}_z \in \Psi_T} e^{-\theta(t_n - t_i)} \mathbb{[}t_n - \mathfrak{s}_z \geq 0\mathbb{]} + \sum_{\mathfrak{s}} \delta(t_n - \mathfrak{s}_z) \right) \\ & + \frac{\kappa}{\kappa - 1} e^{(\kappa - 1)\theta(T - \bar{s})} - \frac{|\Psi_T|}{\kappa - 1} \end{aligned} \quad (62)$$

- Step response

$$\begin{aligned} \mathcal{L}(\theta; T) \doteq & - \sum_{t_n \in \{\Omega_T, \Psi_T\}} \log \left(\frac{\kappa}{\kappa - 1} e^{(\kappa - 1)\theta t_n} \mathbb{[}t_n \geq 0\mathbb{]} - \frac{1}{\kappa - 1} u(t_n) \right) \\ & + \frac{\kappa}{(\kappa - 1)^2 \theta} e^{(\kappa - 1)\theta T} - \frac{1}{\kappa - 1} \left(\frac{\kappa}{(\kappa - 1)\theta} + T \right) \end{aligned} \quad (63)$$

- Dassios response

$$\begin{aligned} \mathcal{L}(\theta; T) \doteq & - \sum_{t_n \in \{\Omega_T, \Psi_T\}} \log \left(\frac{\kappa\theta}{1-\kappa} + \left(u_0 - \frac{\kappa\theta}{1-\kappa}\right) e^{-(1-\kappa)\theta t_n} \right) \\ & + \frac{\kappa\theta T}{1-\kappa} + \left(\frac{u_0}{(1-\kappa)\theta} - \frac{\kappa}{(1-\kappa)^2} \right) (1 - e^{-(1-\kappa)\theta T}) \end{aligned} \quad (64)$$

For the MBP process, the objective function are not convex in k or θ . Usually, convexity is one of the method used to show uniqueness of minimum. There are other methods. One can show unique min. without convexity. For instance, $f(x) = -8(x+1)^2 + (x-1)^4$ has a unique min. at $x = 1$ (Note also that there are three stationary values 1, -1, 3)

In what follows we will present an independent proof of non-convexity. Let us first recall, the function f defined by $f(x) = -\ln x$ for $x > 0$ is convex as $f''(x) = \frac{1}{x^2} > 0$ for all $x > 0$. Suppose there is another function g is defined by $g(x) = -\ln(a+bx)$ with $b > 0$ and $x > 0$ then it is convex as $g''(x) = b^2/(a+bx)^2 > 0$.

Issue: Is the $\mathcal{L}(\theta, T)$ convex with respect to k, θ . As they are supposed to be log-likelihood functions which we want to maximize, it is concavity that is required (not convexity).

Let us now consider the multi impulse response exogenous function with a single impulse:

$$\mathcal{L}(\theta, T) = - \sum_{t_n \in \{\Omega_T, \Psi_T\}} \log \left(\kappa\theta e^{(\kappa-1)\theta t_n} u(t_n) + \delta(t_n) \right) + \frac{\kappa}{\kappa-1} e^{(\kappa-1)\theta T} - \frac{1}{\kappa-1}$$

First we rewrite above simply as

$$\mathcal{L}(\theta, T) = T_1 + T_2 + T_3 \quad (65)$$

$$\frac{\partial^2 T_3}{\partial \kappa^2} = -\frac{1}{(\kappa-1)^3} > 0 \quad \text{as } 0 < \kappa < 1$$

$$\left(\frac{1}{(\kappa-1)^3} - \frac{2\theta T}{(\kappa-1)} + \frac{\kappa(\theta T)^2}{(\kappa-1)} \right) e^{(\kappa-1)\theta T} < 0 \quad \text{if } 0 < \kappa < 1$$

Now we turn back to the first term. For brevity, Let $\kappa = x, u(t_n) = c$. Consider

$$\begin{aligned} x & \rightarrow -\ln x \equiv f(x) \quad \text{convex} \\ x & \rightarrow -\ln x \quad \text{is decreasing} \end{aligned}$$

$$x \rightarrow x\theta e^{(x-1)\theta t_n} \equiv g(x) \quad \text{is concave}$$

$$\frac{\partial^2}{\partial x^2} (\dots) = (2\theta^2 t_n + x\theta^3 t_n^2) e^{(x-1)\theta t_n}$$

$$x \rightarrow x\theta e^{(x-1)\theta t_n} \quad \text{is increasing}$$

$$\frac{\partial}{\partial x}(\dots) = (\theta + x\theta^2 t_n) e^{(x-1)\theta t_n}$$

Define the map

$$x \rightarrow -\ln(x\theta e^{(x-1)\theta t_n} c + d) \equiv G(x)$$

$$G(x) = f(g(x)c + d)$$

$$G'(x) = f'g'(x)c$$

$$G''(x) = f''[g'(x)c]^2 + f'g''(x)c$$

$$f''[g'(x)c]^2 \geq 0$$

$$f'g''(x)c \geq 0 \quad \text{as} \quad f'(x) < 0$$

So $-\ln(\dots)$ is convex in κ .

It is not possible to show that $\frac{\partial^2}{\partial \kappa^2}(T_2 + T_3) \geq 0$. For the convexity with respect to θ , note that $\frac{\partial^2 \mathcal{L}}{\partial \theta^2} \geq 0$ does not hold as $\theta \rightarrow -\ln(\kappa\theta e^{(\kappa-1)\theta t_n} u(t_n) + \delta(t_n))$ is convex but

$$\frac{\partial^2}{\partial \theta^2} \left(\frac{\kappa}{\kappa-1} e^{(\kappa-1)\theta T} \right) = \kappa(\kappa-1)T^2 e^{(\kappa-1)\theta T} < 0$$

as $0 < \kappa < 1$.

For the same reason, the multiple impulse response (62) objection function is also not convex with respect to the two parameters, due to the lack of convexity of second and third terms.

For (63), we could prove neither the convexity of objective function with respect to κ or θ .

Fortunately, convexity is not a strict requirement to get unique optimum. What one needs is some form of convexity in the neighbourhood of stationary points, then one can tell if there exists unique minimum or not.

Remark 16 *Recall our goal here is to minimize the negative log-likelihood. Due to the lack of convexity, we could not rely on any gradient based algorithm. The most appropriate substitute for gradient descent here would be the Nelder-Mead algorithm, which can be implemented with many languages (the methods L-BFGS-B in R and Python, nm in QuantLib C++ library)*

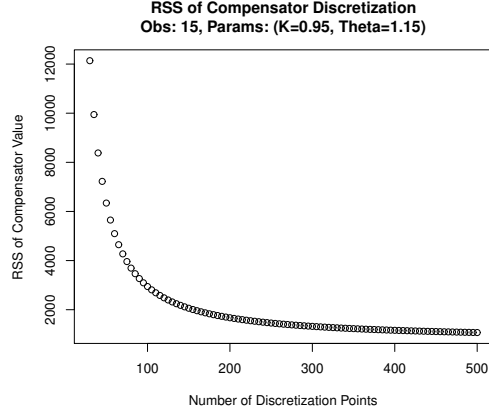


Figure 6: Compensator approximation error with respect to the number of discretization points.

E. Experiments

E.1 Number of Approximation Points

Appendix E.1 shows the RSS of the compensator values of the discrete compensator function versus the closed-form compensator function.

E.2 Other Non-endogenous Experiments

Appendix E.2 shows the parameter fittings resulting from different number of discretisation points.

Table 12: Non-endogenous synthetic experiments for Scenario F.

true True Params.	Loss Func.	Model	Number of Observation Intervals						
			5	10	15	30	60	100	
$\kappa = 0.6$ $\theta = 0.8$	SSE	Closed	κ	0.726 ± 0.004	0.682 ± 0.005	0.668 ± 0.005	0.642 ± 0.005	0.62 ± 0.005	0.612 ± 0.005
			θ	0.647 ± 0.021	0.641 ± 0.024	0.801 ± 0.031	0.995 ± 0.052	0.915 ± 0.052	0.865 ± 0.045
		Approx	κ	10 ± 0	0.621 ± 0.006	0.605 ± 0.006	0.601 ± 0.006	0.601 ± 0.006	0.601 ± 0.006
	IC-LL	Closed	κ	0.728 ± 0.004	0.69 ± 0.005	0.673 ± 0.005	0.644 ± 0.005	0.622 ± 0.005	0.613 ± 0.005
			θ	0.644 ± 0.019	0.67 ± 0.023	0.828 ± 0.031	1.014 ± 0.054	0.931 ± 0.05	0.876 ± 0.045
		Approx	κ	10 ± 0	0.618 ± 0.007	0.599 ± 0.006	0.594 ± 0.006	0.595 ± 0.006	0.596 ± 0.006
$\kappa = 0.95$ $\theta = 1.15$	SSE	Closed	κ	0.958 ± 0.002	1.496 ± 2.17	1.494 ± 2.171	0.95 ± 0.004	0.95 ± 0.004	0.95 ± 0.004
			θ	1.765 ± 0.098	1.362 ± 0.358	1.301 ± 0.344	1.283 ± 0.089	1.216 ± 0.08	1.19 ± 0.076
		Approx	κ	10 ± 0	1.139 ± 0.007	1.033 ± 0.005	0.958 ± 0.003	0.95 ± 0.004	0.95 ± 0.004
	IC-LL	Closed	κ	0.959 ± 0.002	0.953 ± 0.003	0.95 ± 0.003	0.949 ± 0.003	0.95 ± 0.004	0.95 ± 0.004
			θ	1.703 ± 0.086	1.52 ± 0.091	1.451 ± 0.096	1.314 ± 0.083	1.233 ± 0.075	1.202 ± 0.071
		Approx	κ	10 ± 0	1.161 ± 0.007	1.041 ± 0.005	0.958 ± 0.003	0.95 ± 0.004	0.95 ± 0.004
		θ	0.017 ± 0	9.767 ± 0.403	10 ± 0	10 ± 0	1.776 ± 0.163	1.433 ± 0.102	

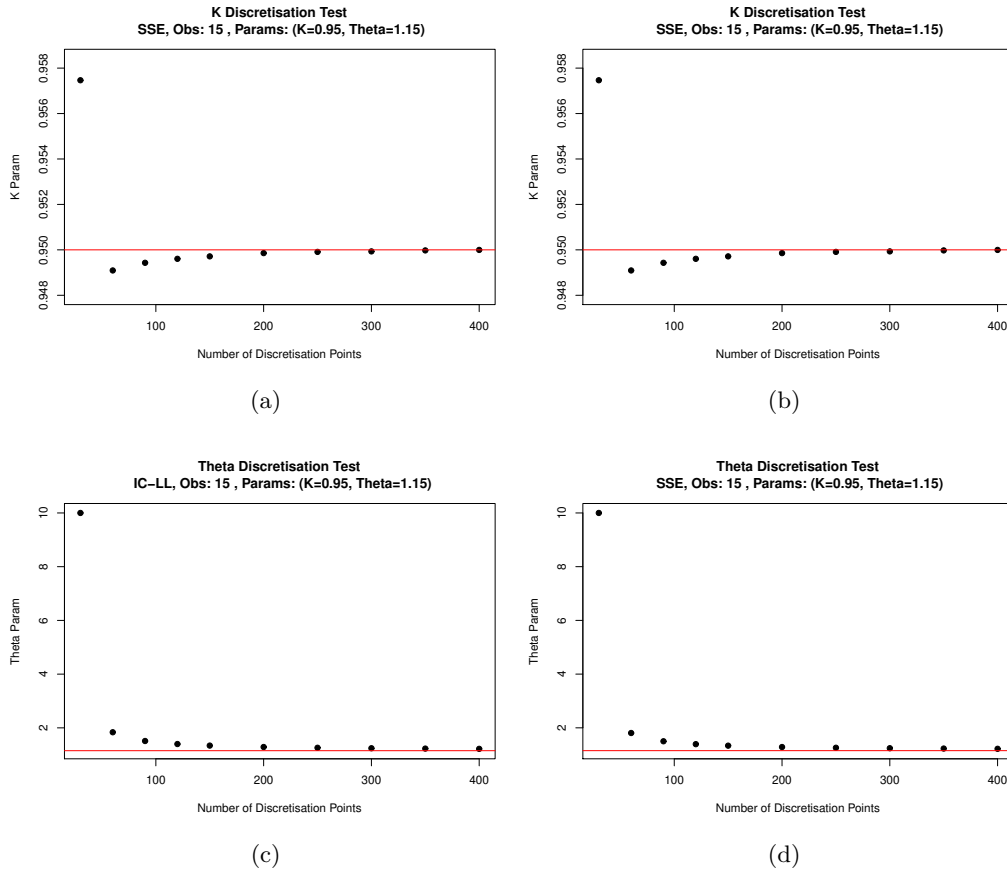


Figure 7: Plots detailing the parameter fits of synthetic data in setting D with varying numbers of discretization points. The plots are taken over 15 observation intervals, using $\kappa = 0.95$ and $\theta = 1.15$ parameters. The red line indicates these true parameters of the synthetic data.